ORIENTATION OF LIGO RECEIVERS

WRITTEN BY: Yekta Gürsel and Massimo Tinto December 29, 1988

I. Introduction

Ligo receivers will be Laser Interferometric Gravitational Wave Detectors. These detectors consist of three or more suspended masses which are free to move in the horizontal plane tangent to the earth at the receiver location. These masses are arranged in two perpendicular "arms" and their relative displacements are measured with a laser interferometer. The quadrupolar arrangement described above has a different sensitivity for each incoming wave direction and polarization. A ligo observatory will have at least two of such receivers separated by a large distance.

For this reason, the receiver patterns will have to be aligned in such a way to maximize the likelihood of coincidence between these receivers and to minimize area of the "dead regions" which give poor reception in one or more antennae of the LIGO observatory. In this memorandum, we analyze the reception patterns of receivers located on the candidate sites for the LIGO observatory. We consider different orientations on each site as well as different polarization states of the incoming gravitational radiation.

I. The Theoretical Antenna Pattern

The response of a laser interferometric gravitational wave detector can be written in the following form:

$$\frac{\delta l(t)}{l_0} = F_+(\theta\,,\phi\,,\alpha\,,\beta\,,\gamma)\,h_+(t) + F_\times(\theta\,,\phi\,,\alpha\,,\beta\,,\gamma)\,h_\times(t) \qquad (1)$$

where the functions F_+ and $F_\times$ are linear combinations of spin-weighted spherical harmonics in the angles $(\theta\,,\phi)$, which locate the source in the sky, and in the parameters $(\alpha\,,\beta\,,\gamma)$ which are the geographic orientation, latitude and longitude of the detector respectively. The orientation α of the receiver is measured from the local East-West direction and it is the angle between the bisector of the two arms of the receiver and the reference direction. The location of the source in the sky is referred to a coordinate system with an origin at the center of the Earth and with a z-axis coinciding with axis of revolution of the Earth. The remaining two axes are chosen to lie in the equatorial plane of the Earth. The angles $\theta\,,\phi$ are the Euler angles for the source direction in this coordinate system.

II. Maximizing the Mean Coincidence Probabilities

As shown by Tinto (Ph. D. Thesis, University of Wales, Cardiff, UK (1987)) there are optimal orientations of a pair of receivers that maximize the "mean coincidence probability" of detection for any polarization of the incoming radiation.

The term "mean coincidence probability" refers to the average of the coincidence probability of detection over all possible thresholds set in the receivers with respect to the incoming

amplitude of the radiation. For likely values of the signal-to-noise ratio at a given pair of detectors it turns out that the coincidence probability (not the mean probability) is not significantly reduced by orientations which differ from the optimal orientation significantly.

This result is derived by averaging over all possible polarizations of the incoming signal. In the case of purely linear polarization of the input signal, the result given above does not hold. There is a reduction by a approximately factor of two and a half in the observed number of events detected in coincidence if the detectors deviate from the optimal orientation by 45 degrees. The optimal orientations for arbitrary polarizations do not significantly differ from the optimal orientations for the linear polarization case.

In the reference mentioned above there are contour plots of the mean coincidence probability as a function of the orientations of several pairs of detectors in the United States of America and in Europe. In this memorandum, we include similar contour plots for the California and Louisiana sites (Figures 1 and 2).

Unfortunately the contour plotting program we used does not label the contours it plots. We labeled the maximum and the minimum regions on the plot and indicated the values corresponding to the extrema as well as their location on the side of the plot. Figure 1 shows the mean coincidence probability for sources located in the Virgo cluster of galaxies. Figure 2 shows the mean coincidence probability for randomly distributed source locations in the sky.

III. Geometric Antenna Patterns

Since each detector has a reception pattern which is a function of its orientation as well as its geographic location, it is also desirable to minimize the fraction of the sky that is invisible to a given set of detectors. This issue is extremely relevant when the location of the source is to be deduced from the detector data. As shown by Gürsel and Tinto (Proceedings of the Fifth Marcel Grossmann meeting in Perth, 1988) and Gürsel and Tinto (in preparation) a simultaneous signal-to-noise ratio of about 6 in three detectors is enough to determine the location of the source within about 12 arc minutes.

The shape and the size of the regions in the sky which are invisible to a given detector depends on the polarization of the incoming gravitational radiation as well as on the orientation and the location of the detector. In sets of figures 3 to 6, we show the antenna patterns for the Edwards site in California. The set 3 is for an orientation of 12 degrees from the East-West line, the set 4 is for an orientation of 67 degrees from the East-West line, the set 5 is for an orientation of 40 degrees from the East-West line and the set 6 is for an orientation of 85 degrees from the East-West line.

In each set we consider different polarizations of the incoming radiation which is assumed to have a sinusoidal form. The figures are arranged with respect to the polarization from (a) to (e) which correspond to circular and linear polarizations respectively. We considered a range of (1.0, 0.8, 0.5, 0.2, 0.0) for the polarization parameter. Note that in the circular case (1.0, which is denoted by $h_\times = h_+$) the "dark" regions are the areas centered around four points denoted by "-" on the graphs. The areas labeled by 1/2 are the regions which result in a reception of half the maximum amplitude. As the polarization changes from circular to linear in the figures (a) to (e)

the dark regions distort into the "bands" shown in figure (e).

In sets 7 and 8 we show the antenna patters for a receiver located on the Louisiana site. In set 7 the pattern for an orientation of 27.5 degrees from the East-West line is shown. This orientation optimizes the mean coincidence probability with a receiver on the California site with an orientation of 40 degrees from the East-West line. The pattern in set 8 is for an orientation (72.5 degrees) which maximizes the mean coincidence probability with a receiver on the California site with an orientation of 85 degrees from the reference line.

In the set 9 we show the antenna pattern located on the Maine site with an orientation of 72 degrees from the local East-West line. We did not consider other orientations because of the geographic constraints in this site.

In sets 10, 11, 12, 13 we show the reception patterns of the detectors located in Germany, Italy, Japan and Australia respectively. The orientations of these detectors are such that they optimize the mean coincidence probability with a detector on the California site with an orientation of 12 degrees from the local East-West line.

IV. Realistic Skymaps

Finally, we wondered what the sky would look like to these detectors if the sources were uniformly distributed across the sky with varying random pulse durations. We assumed a detector with a band-width of 500 to 2500 Hz, with a rms signal-to-noise ratio of 10 and digitization rate of 10 KHz.

In sets 14, 15, 16, 17, 18, 19 we show the skymaps done by detectors located in California, Maine, Germany, Italy, Japan, and Australia respectively. In a given set, the figures (a) to (c) show the skymaps for circular (1.0), highly elliptical (0.2) and linear (0.0) polarizations of the sources. The orientations of the California and the Maine detectors are chosen to optimize the mean coincidence probability and the orientations of the other detectors were chosen to optimize the mean coincidence probability with the California and the Maine receivers.

If one compares the circular polarization skymaps with those in the geometric case one sees that the dead regions can be easily recognized. The regions of maximum amplitude are "flattened" by the noise, but they are still distinguishable.

V. Conclusion

We produced skymaps which should aid the site selection committee in choosing the sites and the orientations of the detectors located on the sites. In a future memorandum, we will describe the effect of the detector locations and orientations on the uncertainities in the determination of the source direction.

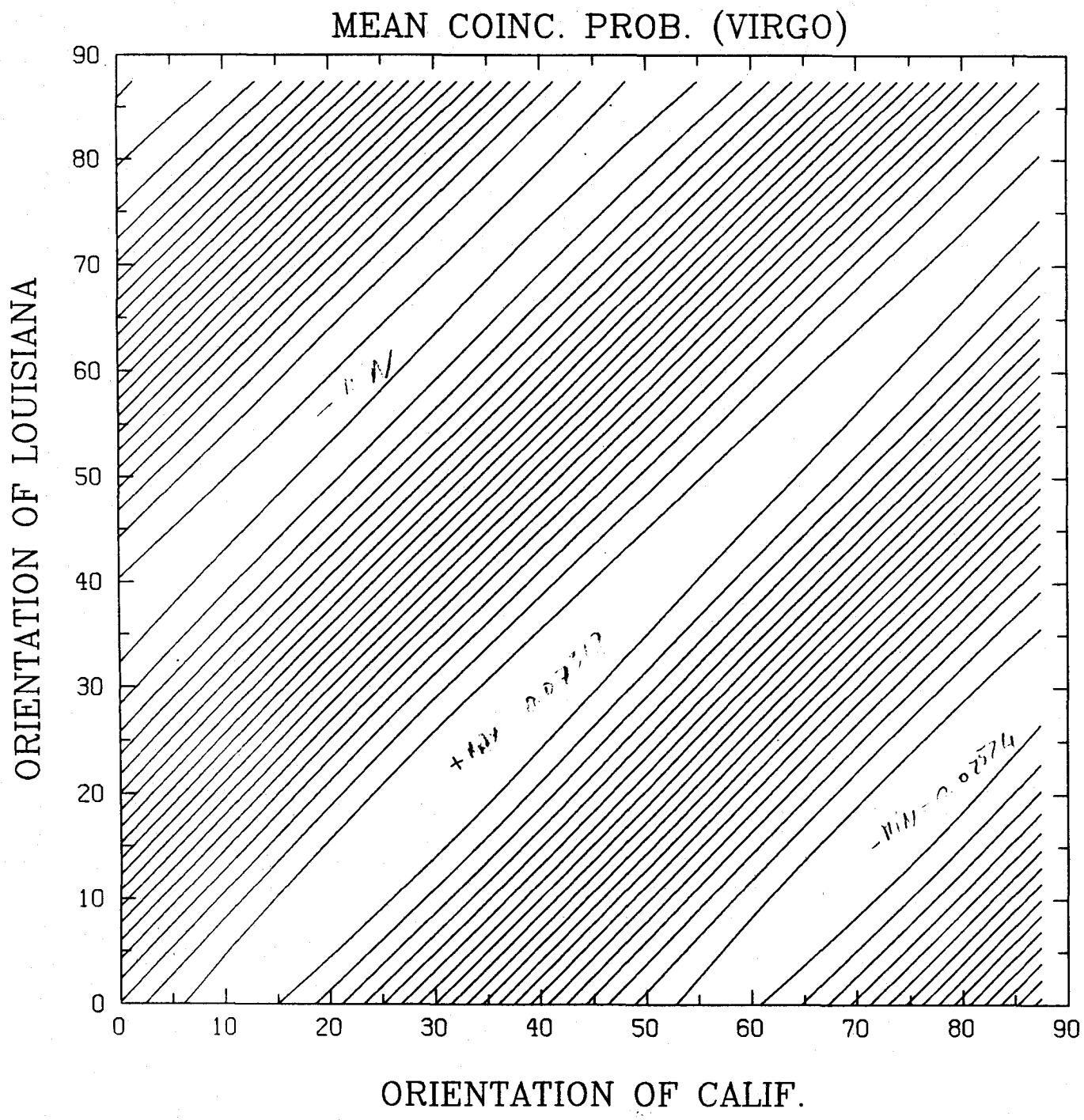
MEAN COINC. PROB. (VIRGO)
ORIENTATION OF LOUISIANA
ORIENTATION OF CALIF.
0
10
20
30
40
50
60
70
80
90

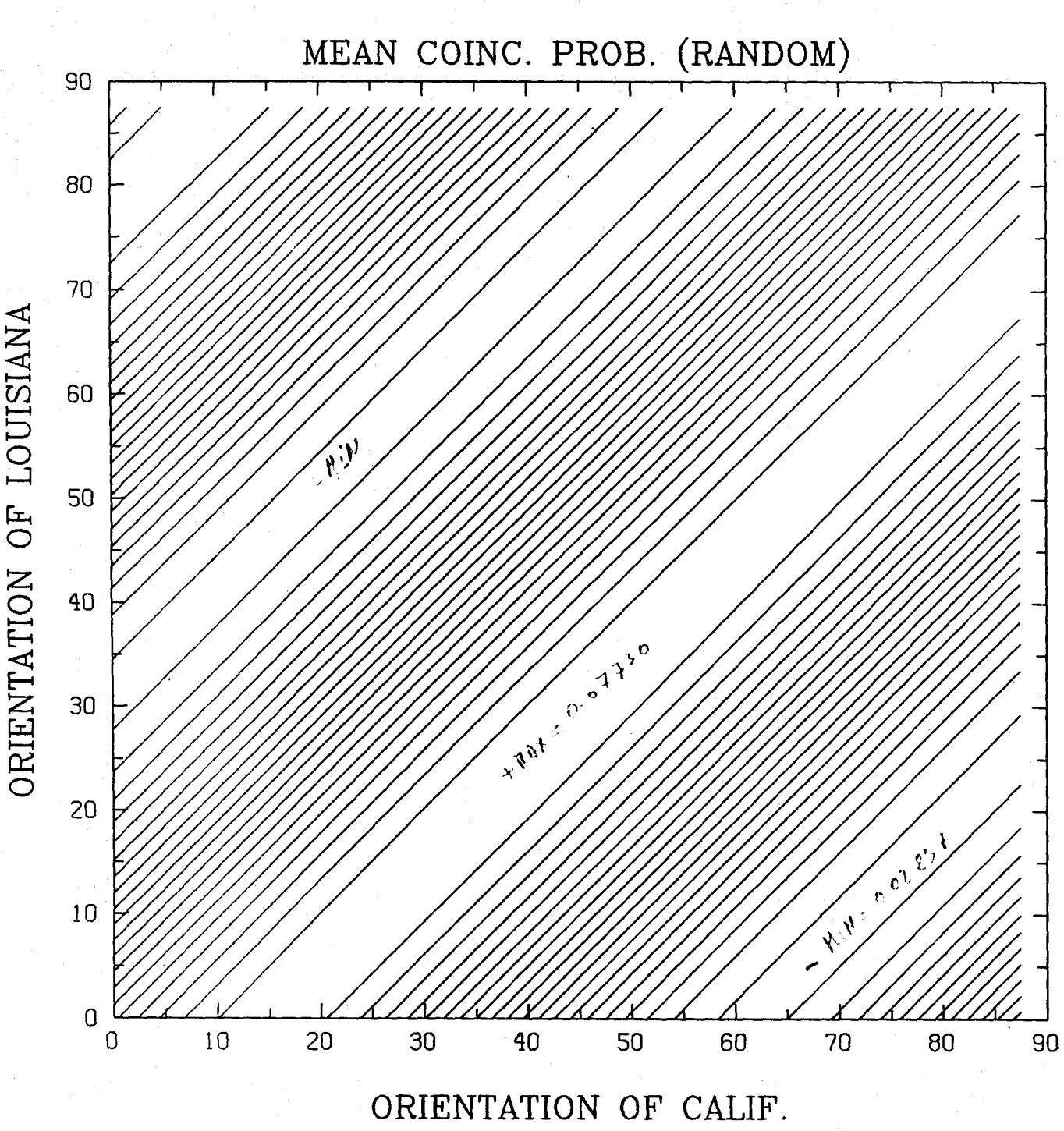
MEAN COINC. PROB. (RANDOM)
ORIENTATION OF LOUISIANA
ORIENTATION OF CALIF.
0
10
20
30
40
50
60
70
80
90

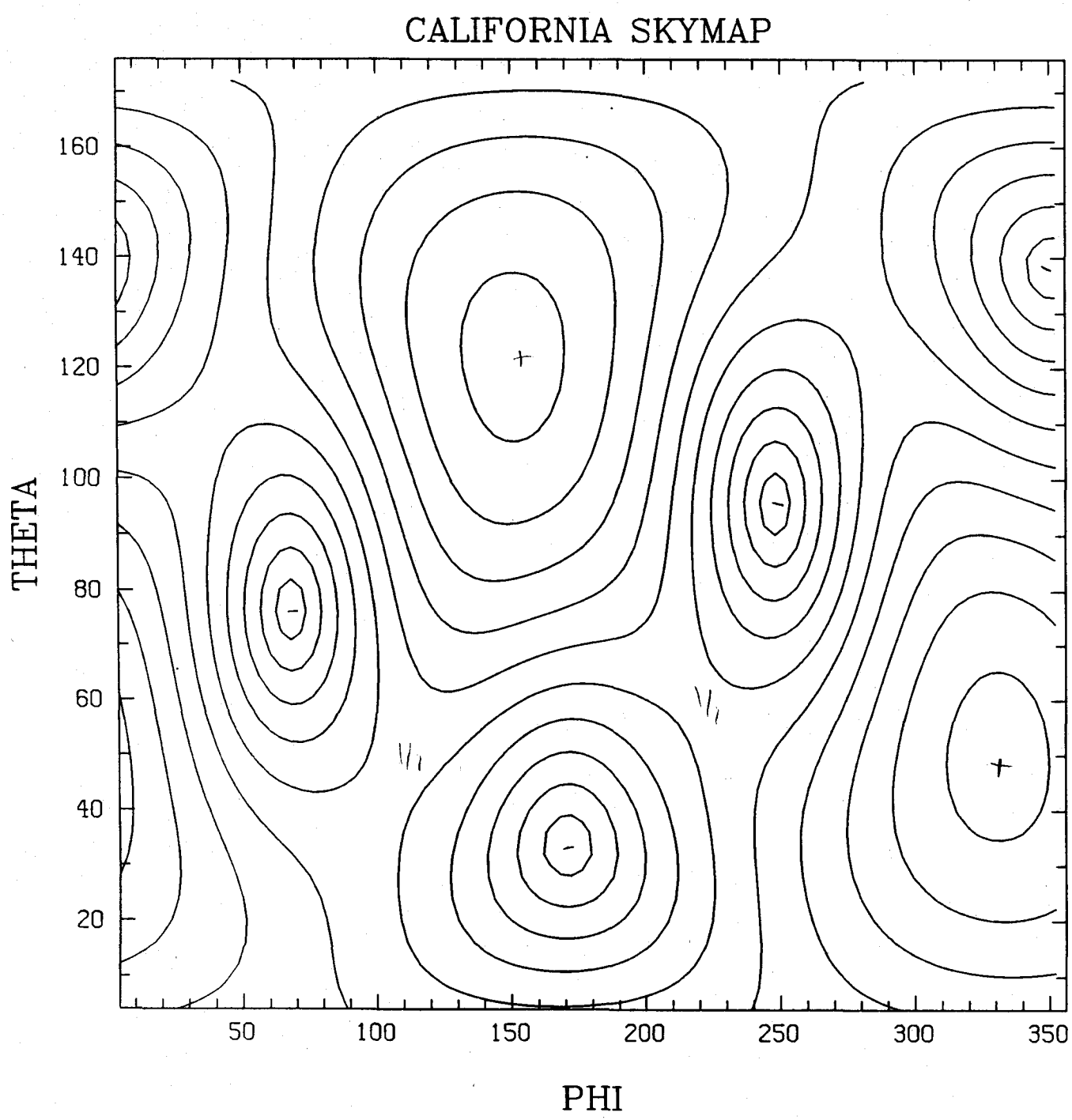

GEOMETRICAL

$h_+ = h_\times$

χ = ORIENTATION =

11.7° of binaries

with EAST-WEST

$T_{ij} \leq 10^{-1}$

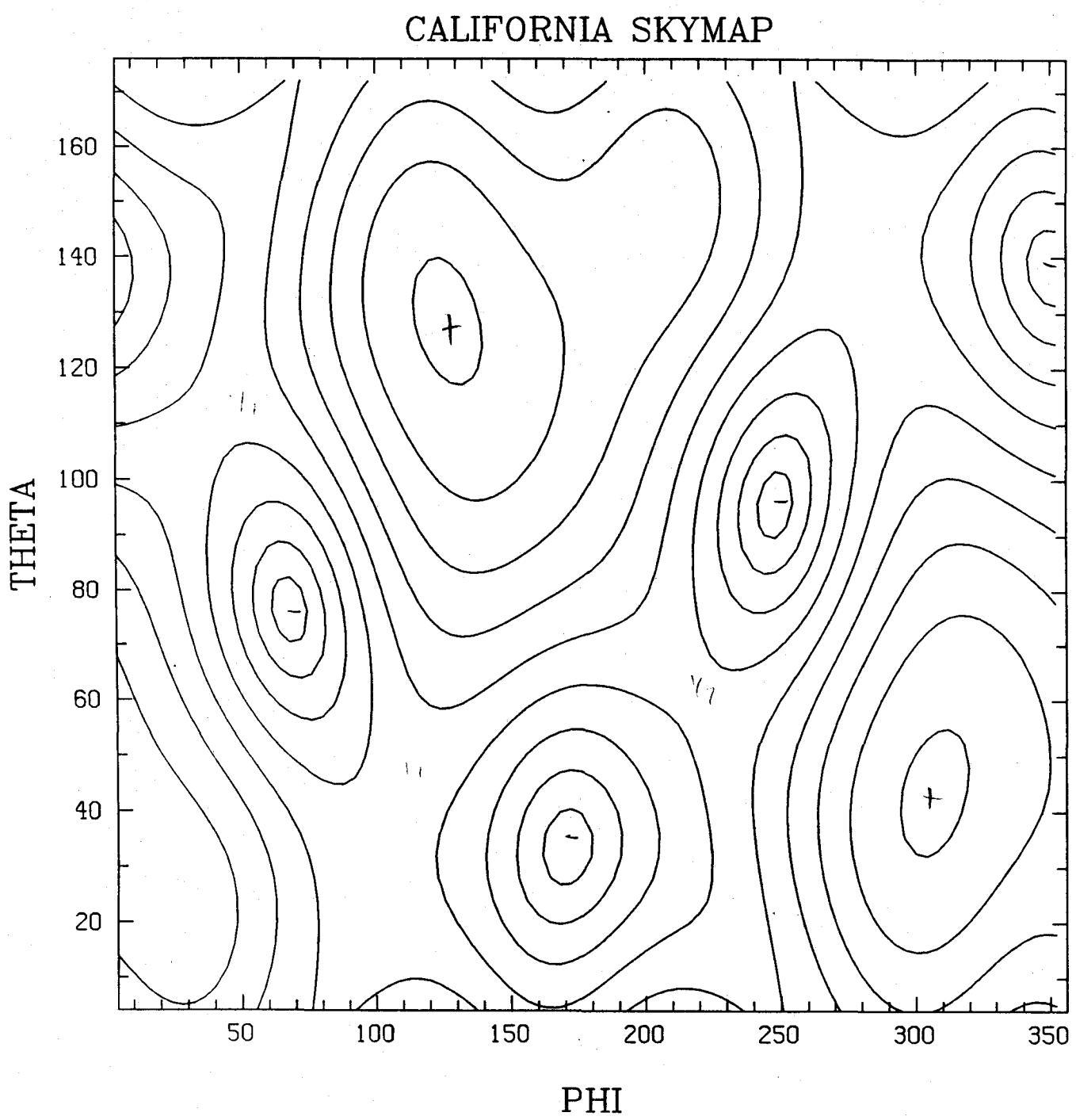

GEOMETRICAL

$h_X = 0.8\, h_T$

α = ORIENTATION = 11.97° of location with FAST-WEST

Figure 3(b)

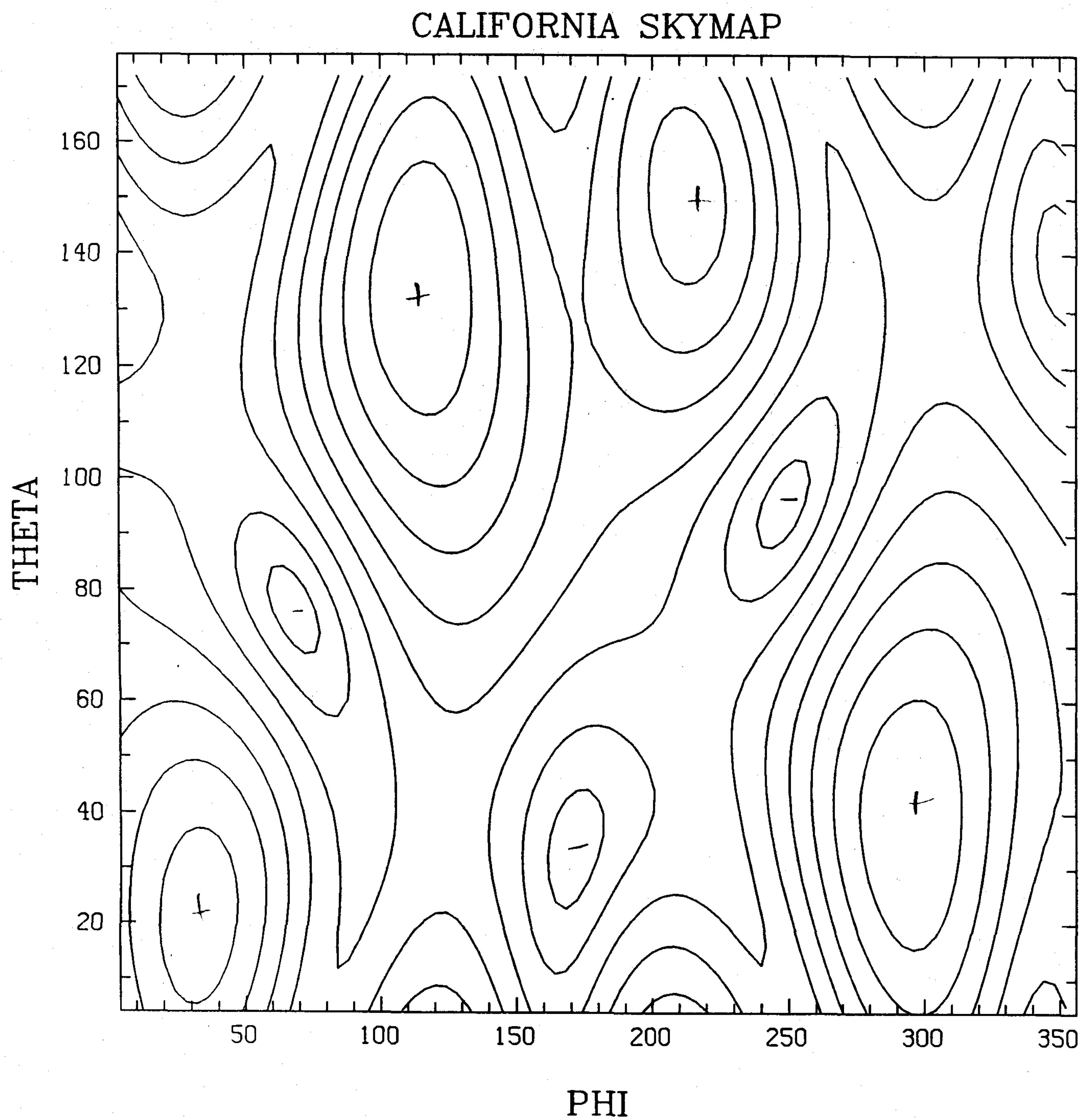

GEOMETRICAL

kx = 0.5 kt

θ = rotation ≈ 11.97°

Fig 2(a)

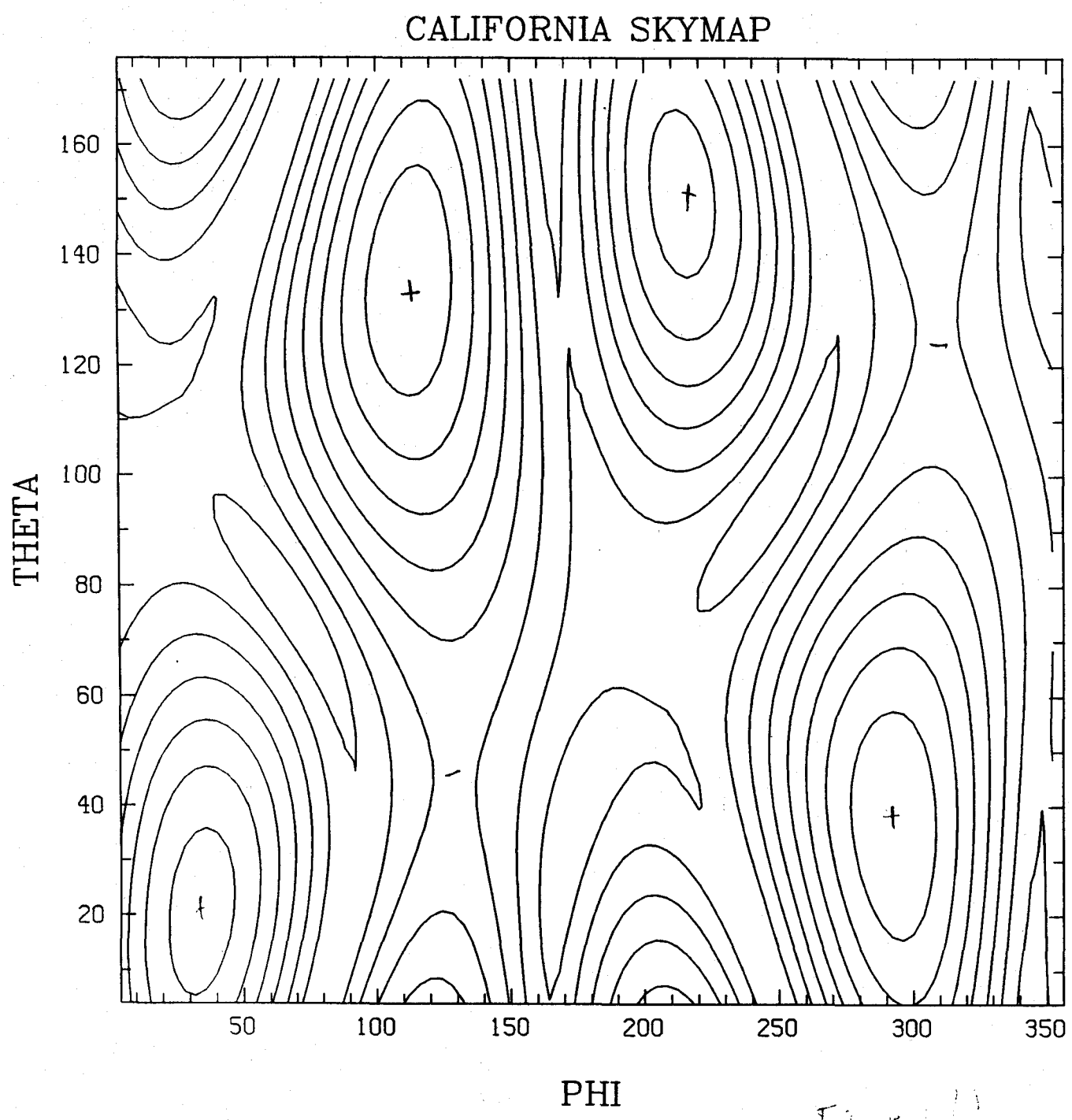

GEOMETRICAL

$h_x = 0.2 h_t$.

$\alpha \equiv$ orientation $=$

11.97° of location

with EAST-WEST

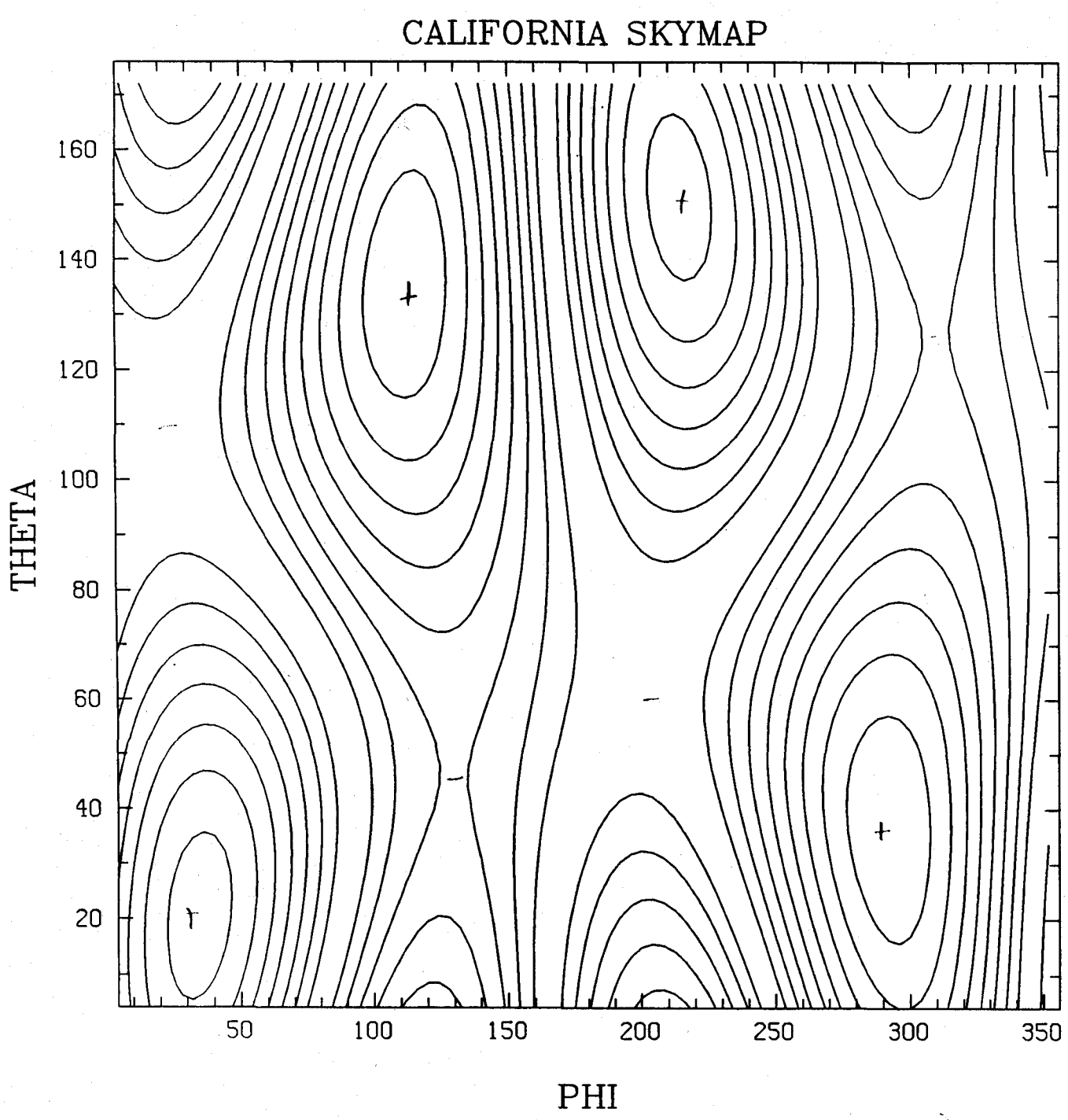

GEOMETRICAL

$h_x = 0$

NE ORIENTATION =

11.97° of Latitude with

FAST NEST

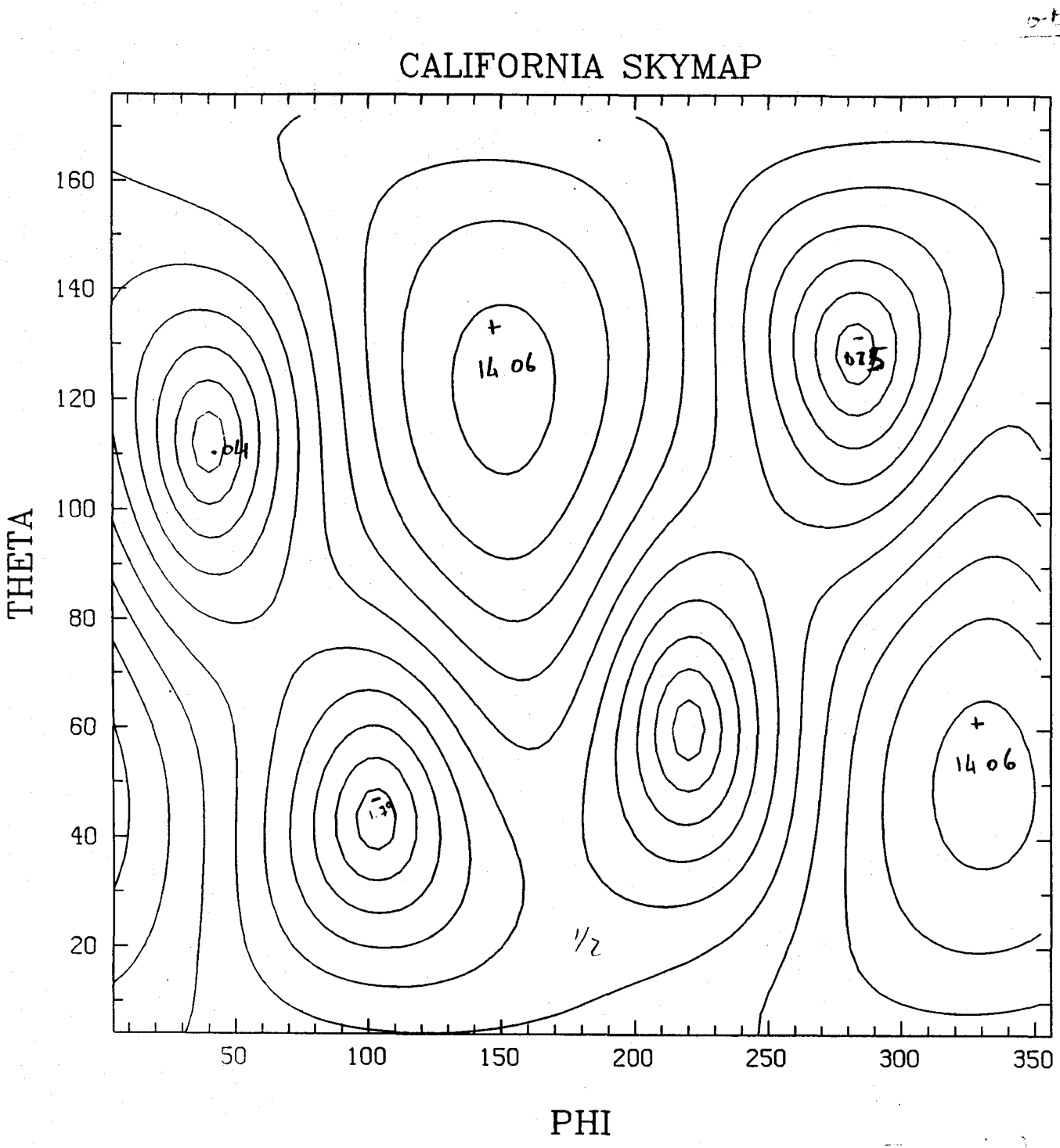
CALIFORNIA SKYMAP
THETA
PHI
160
140
120
100
80
60
40
20
50
100
150
200
250
300
350
+
14 06
.04
1/2

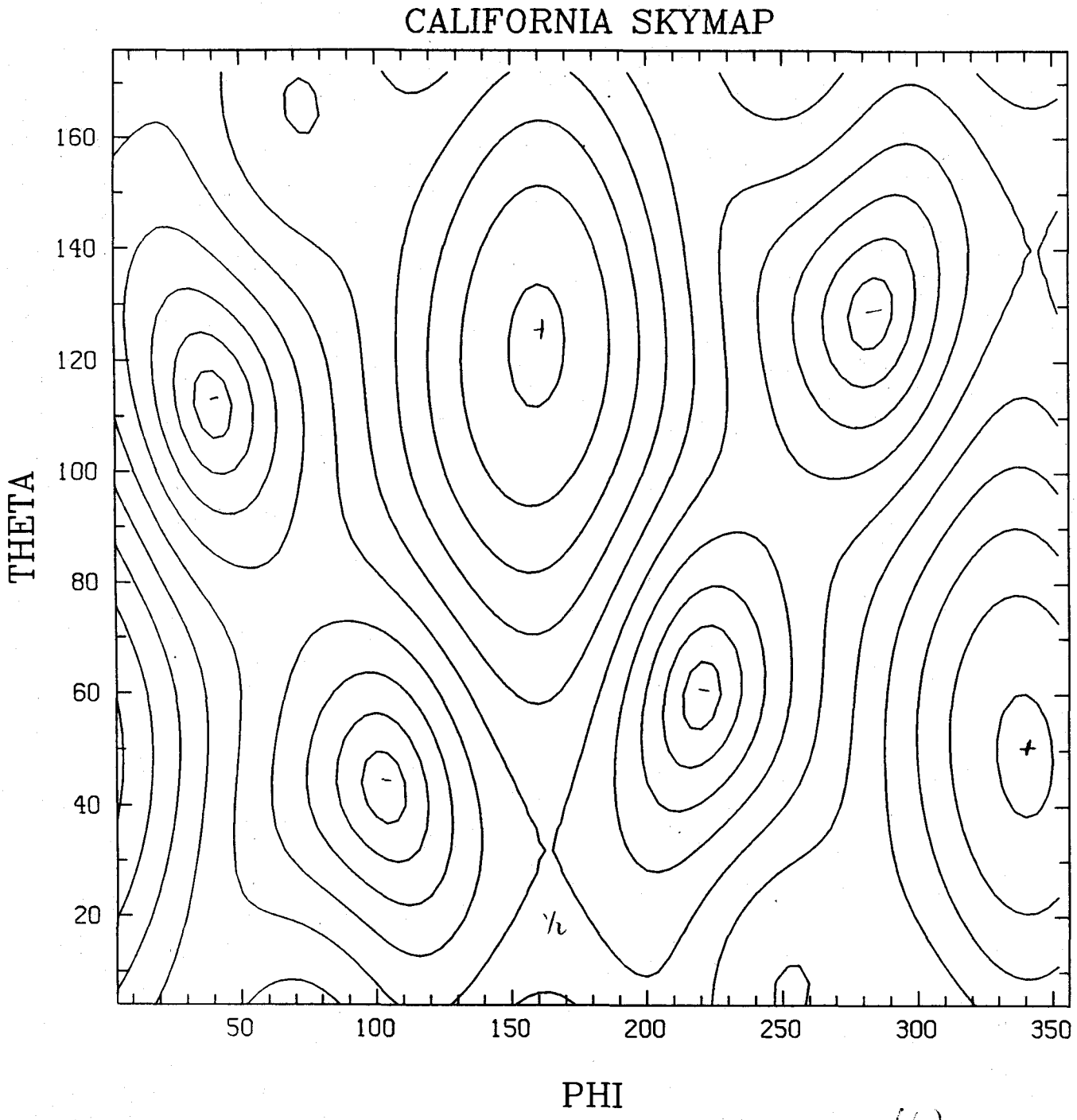
CALIFORNIA SKYMAP
THETA
PHI
160
140
120
100
80
60
40
20
50
100
150
200
250
300
350
+
-
-
+
-
-
+

GEOM

$h_x = 0.5\, h_+$

$\alpha = 11.97° + 4.5°$

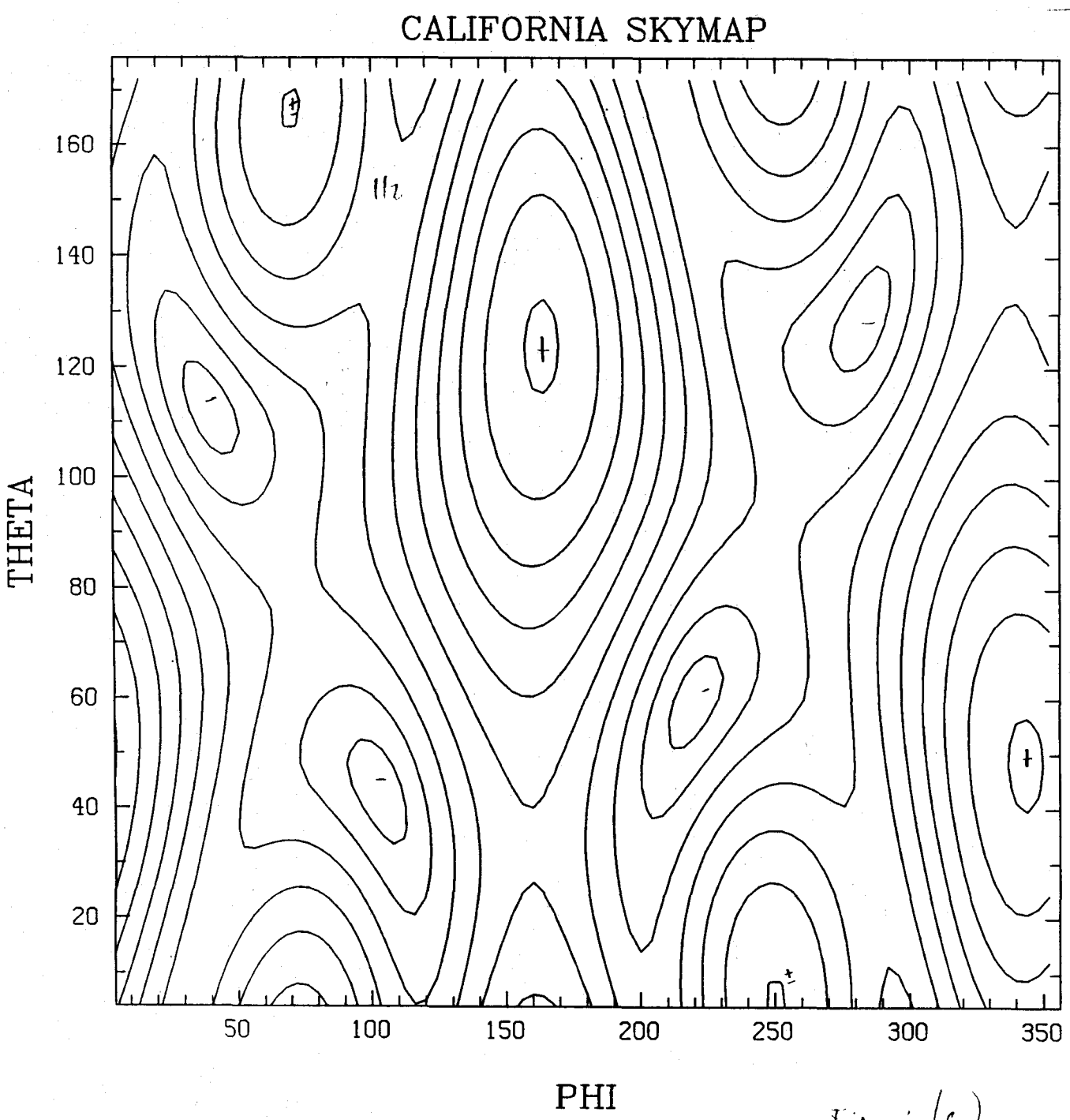

Fig. 1(c)

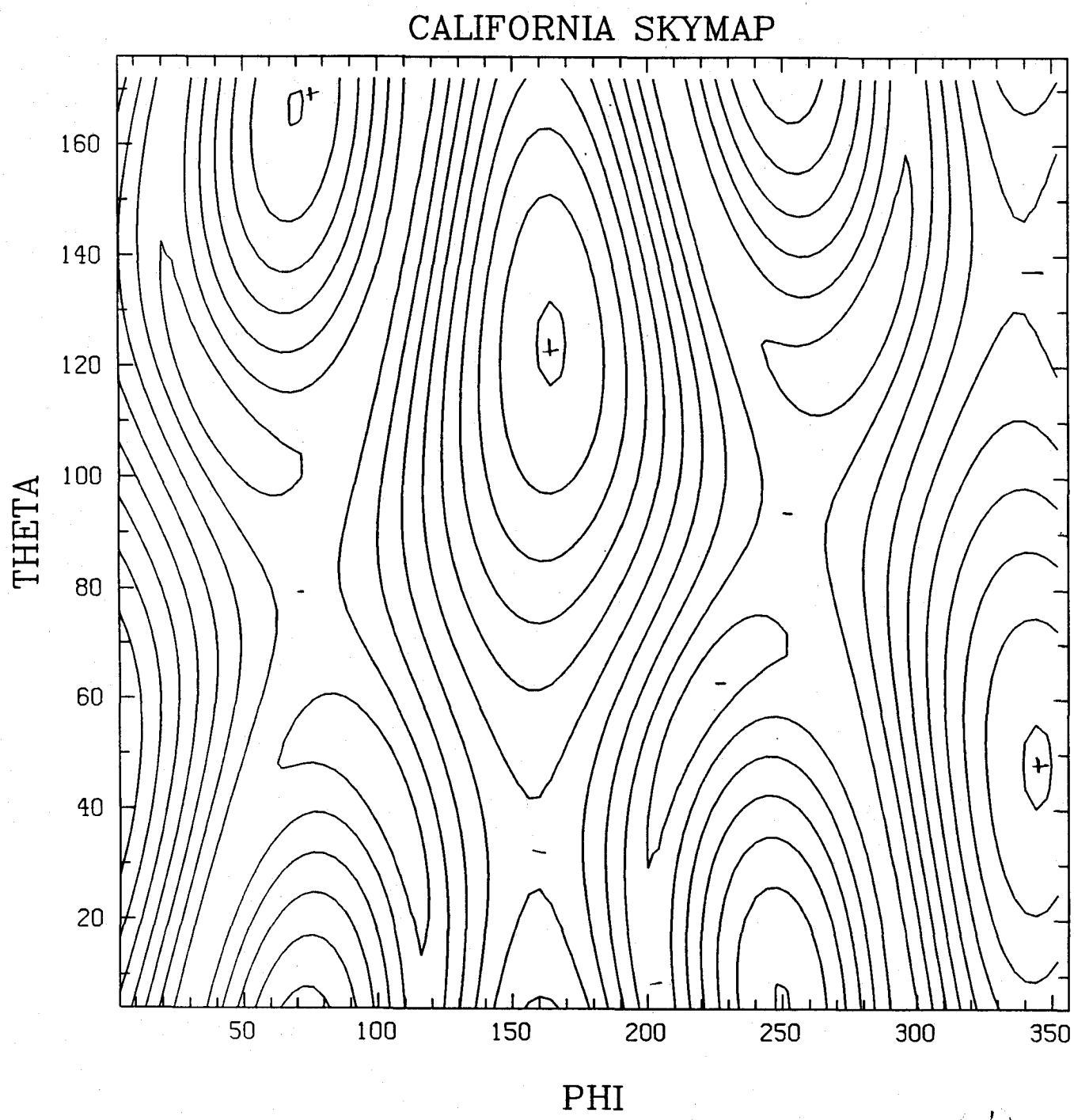
CALIFORNIA SKYMAP
THETA
PHI
160
140
120
100
80
60
40
20
50
100
150
200
250
300
350
0+
+
-
-
-
-
+
-

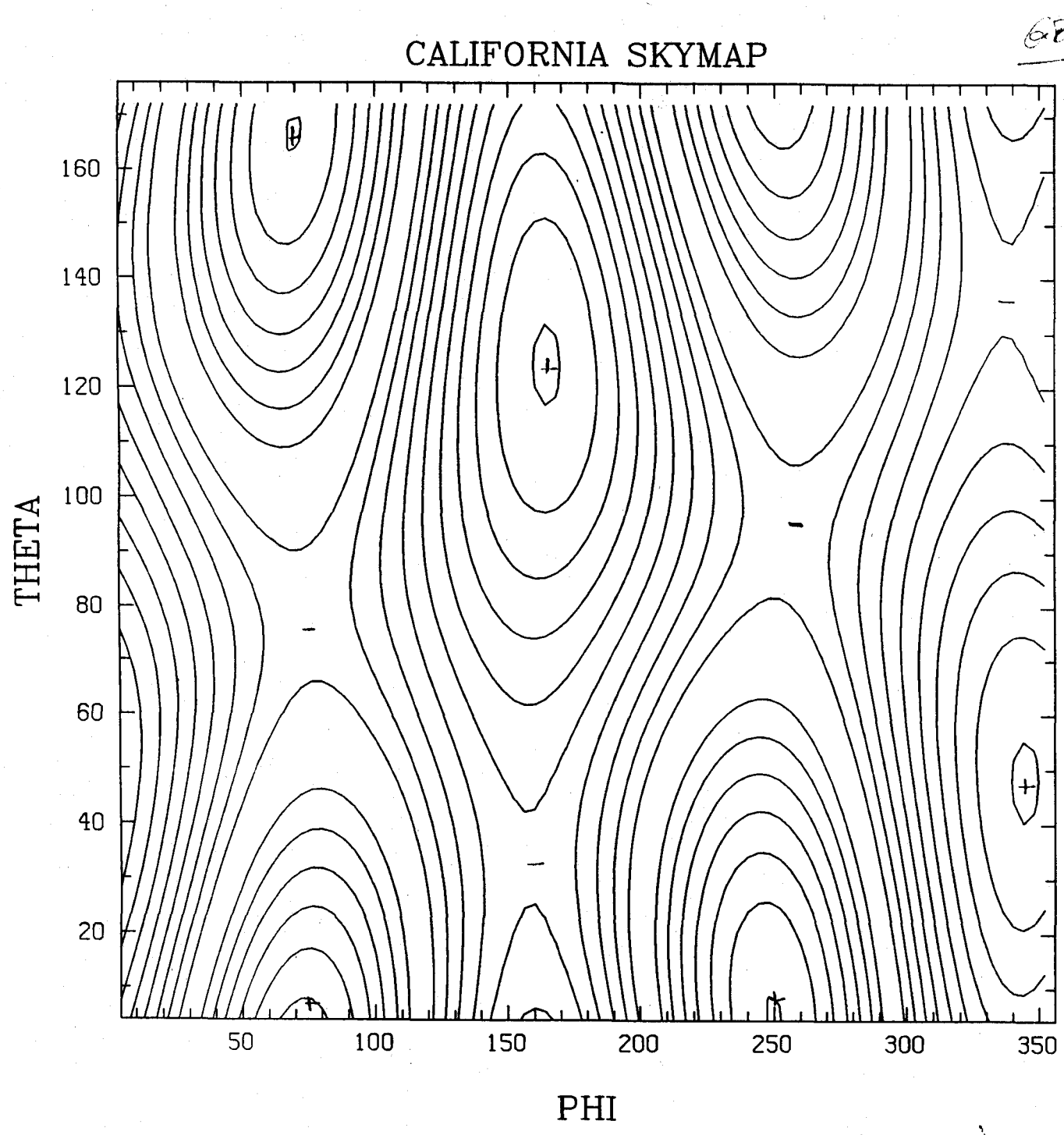
CALIFORNIA SKYMAP
THETA
PHI
160
140
120
100
80
60
40
20
50
100
150
200
250
300
350

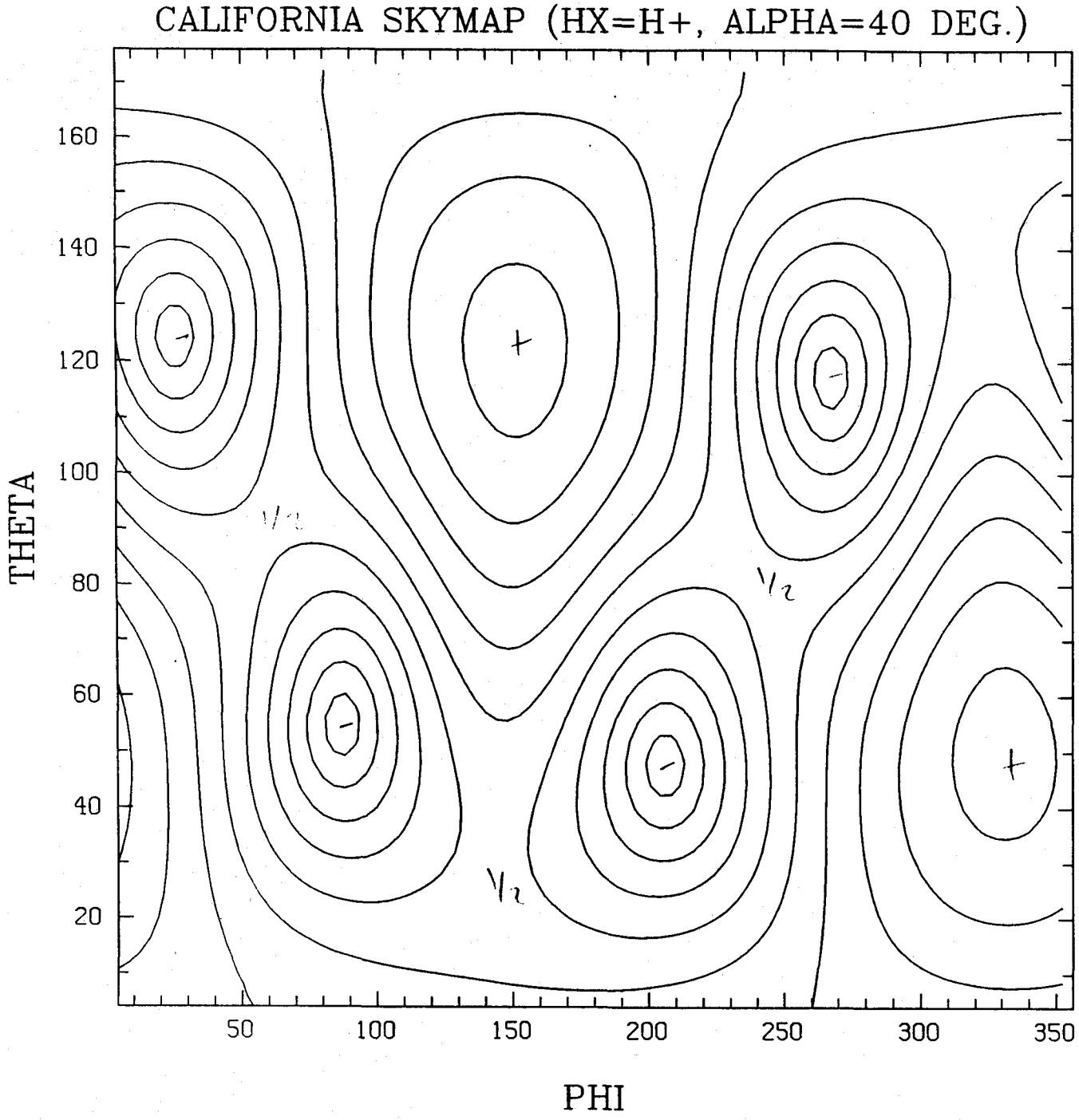
CALIFORNIA SKYMAP (HX=H+, ALPHA=40 DEG.)
THETA
160
140
120
100
80
60
40
20
50
100
150
200
250
300
350
PHI
+
-
+
-
-
+
1/2
1/2
1/2

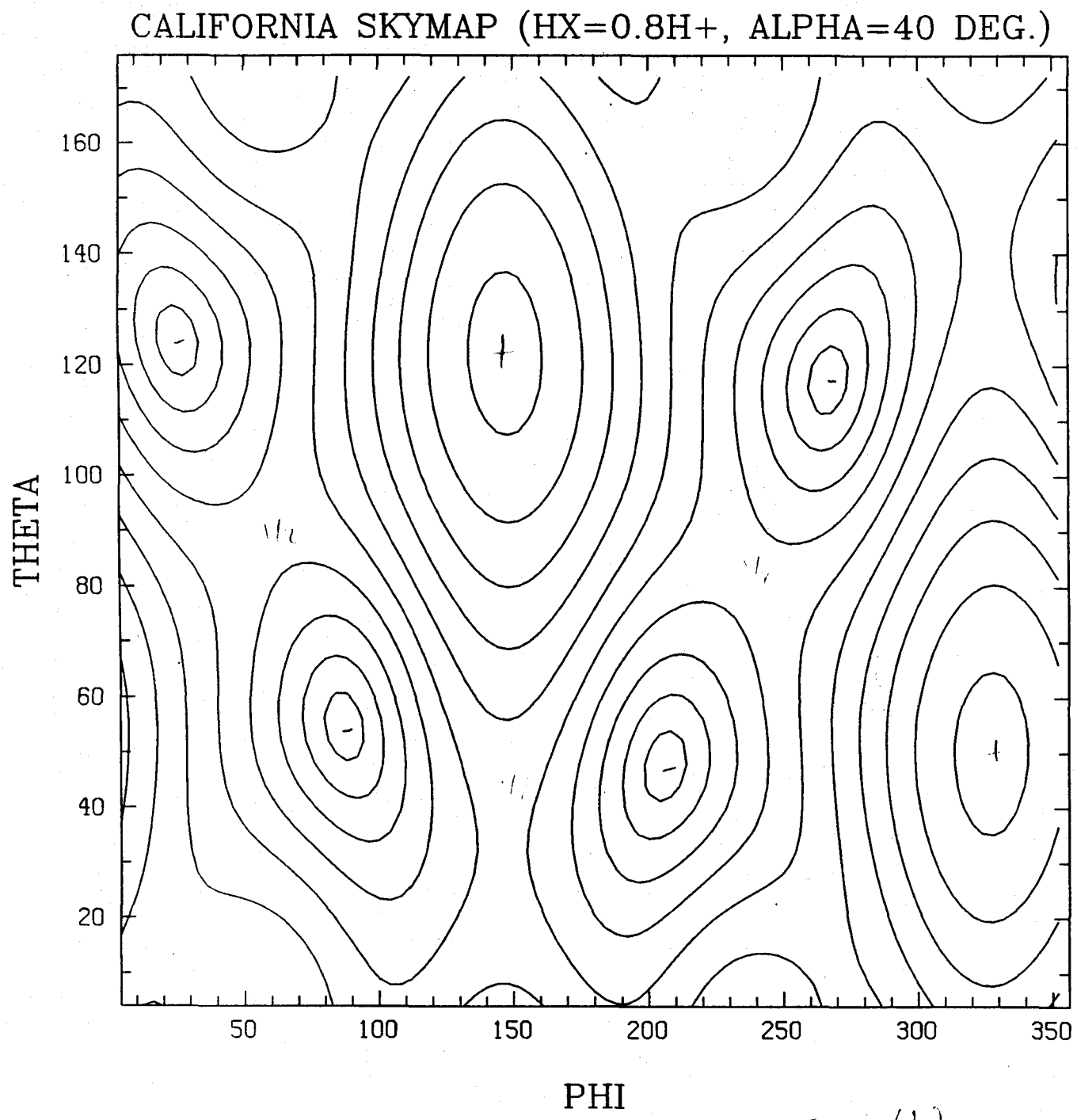
CALIFORNIA SKYMAP (HX=0.8H+, ALPHA=40 DEG.)
THETA
160
140
120
100
80
60
40
20
50
100
150
200
250
300
350
PHI

Fig 3(b)

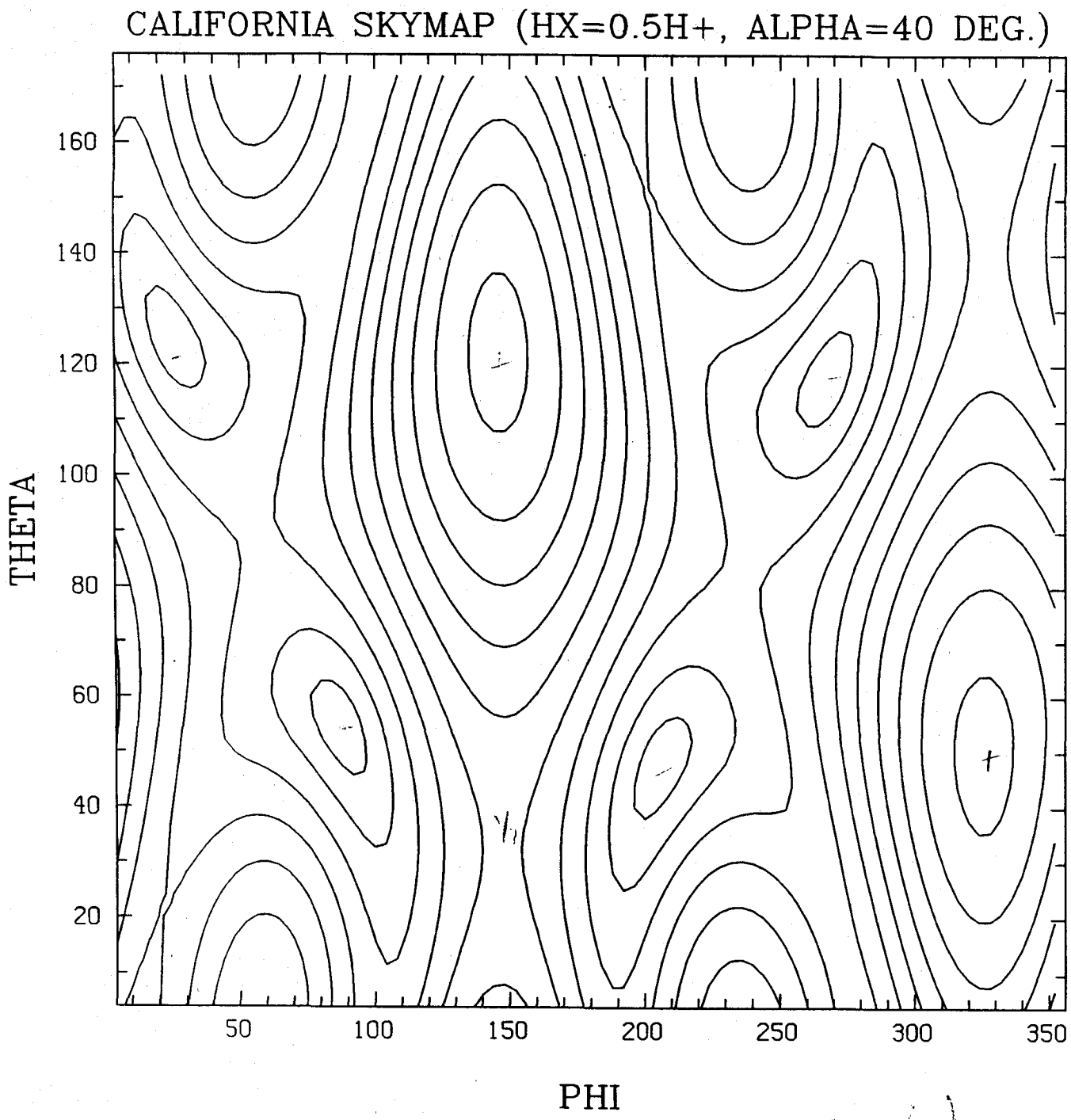
CALIFORNIA SKYMAP (HX=0.5H+, ALPHA=40 DEG.)
THETA
160
140
120
100
80
60
40
20
50
100
150
200
250
300
350
PHI

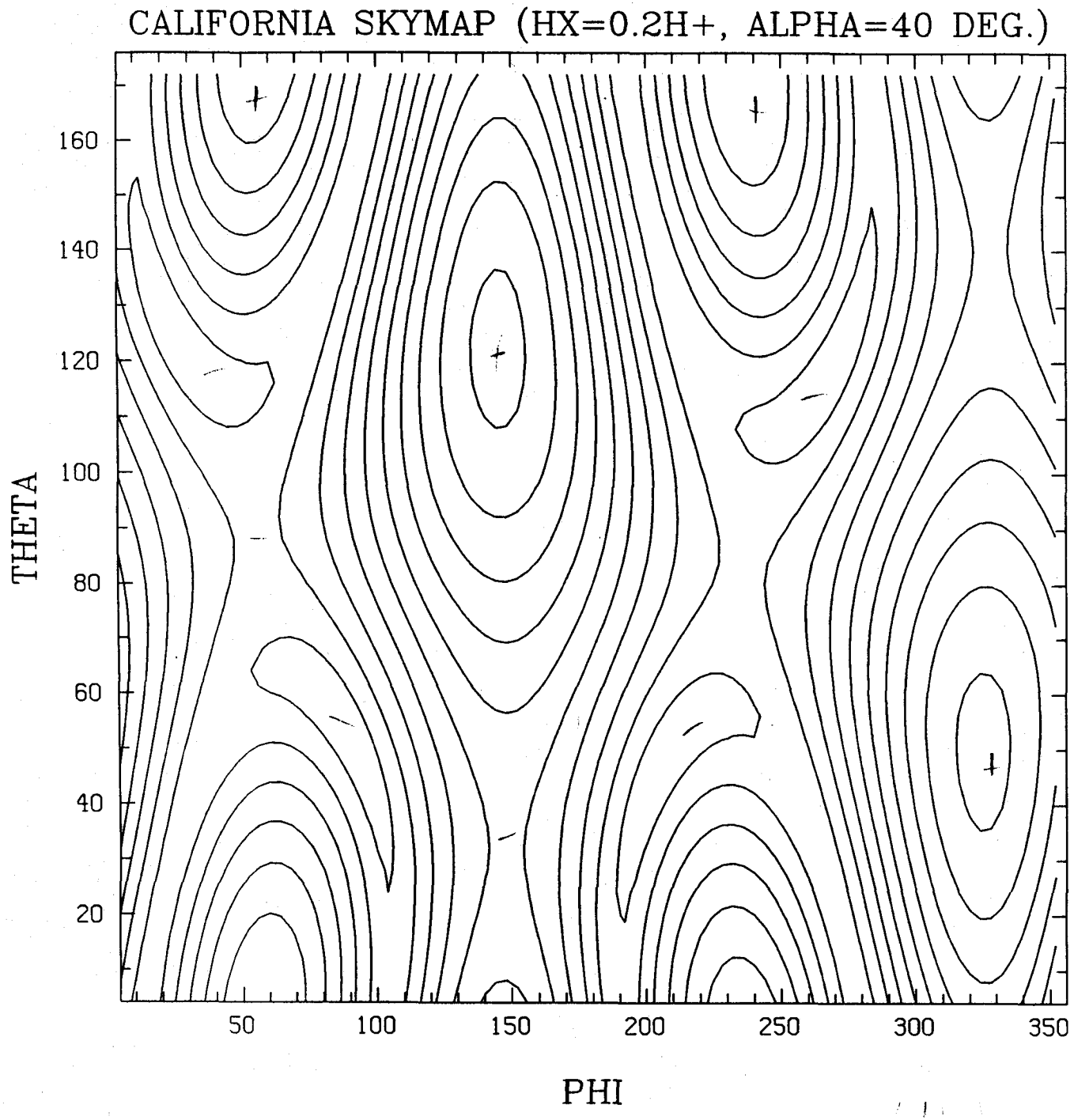
CALIFORNIA SKYMAP (HX=0.2H+, ALPHA=40 DEG.)
THETA
160
140
120
100
80
60
40
20
50
100
150
200
250
300
350
PHI

Fig. 1b

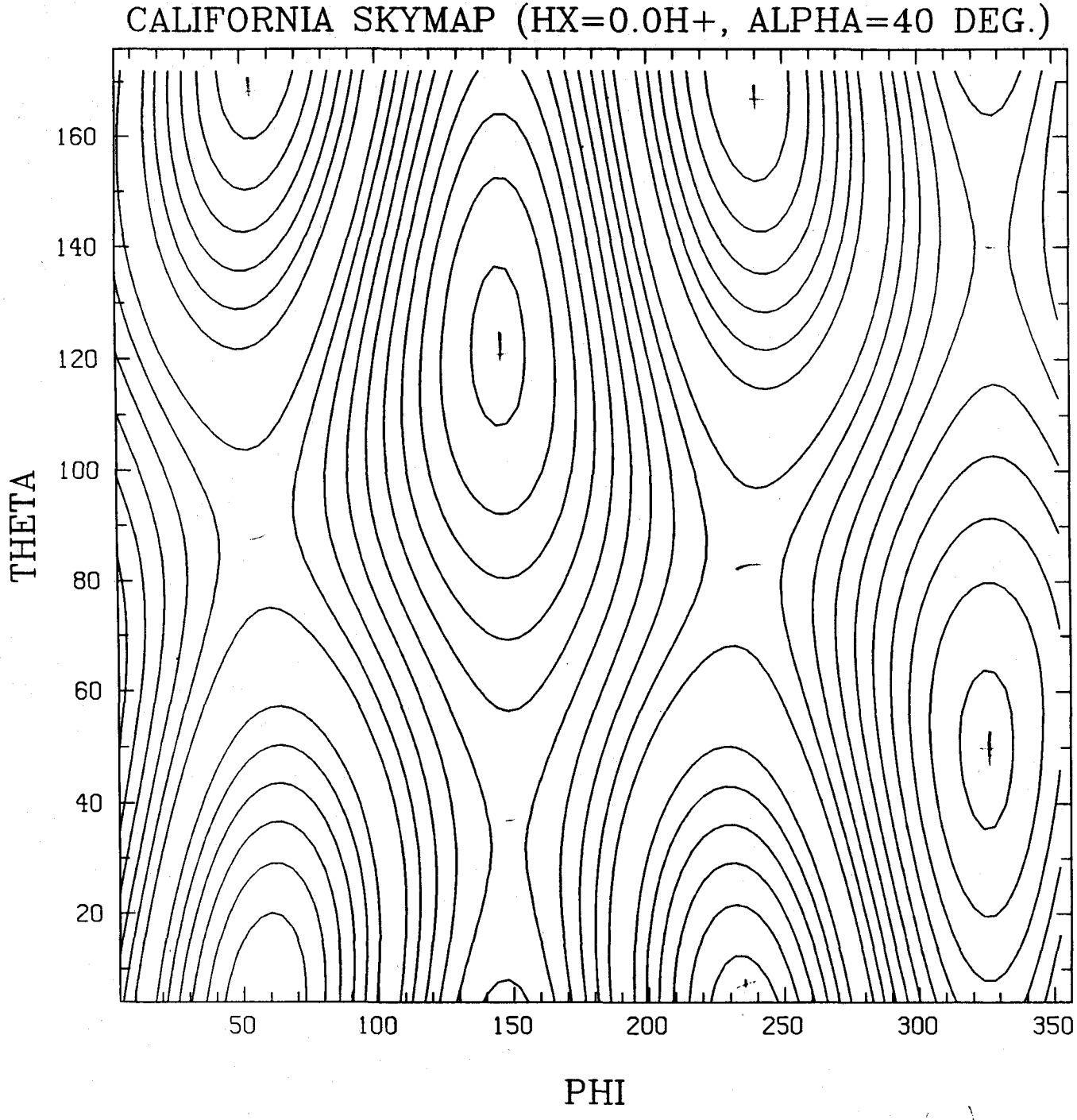
CALIFORNIA SKYMAP (HX=0.0H+, ALPHA=40 DEG.)
THETA
160
140
120
100
80
60
40
20
50
100
150
200
250
300
350
PHI

Fig. 4.1(a)

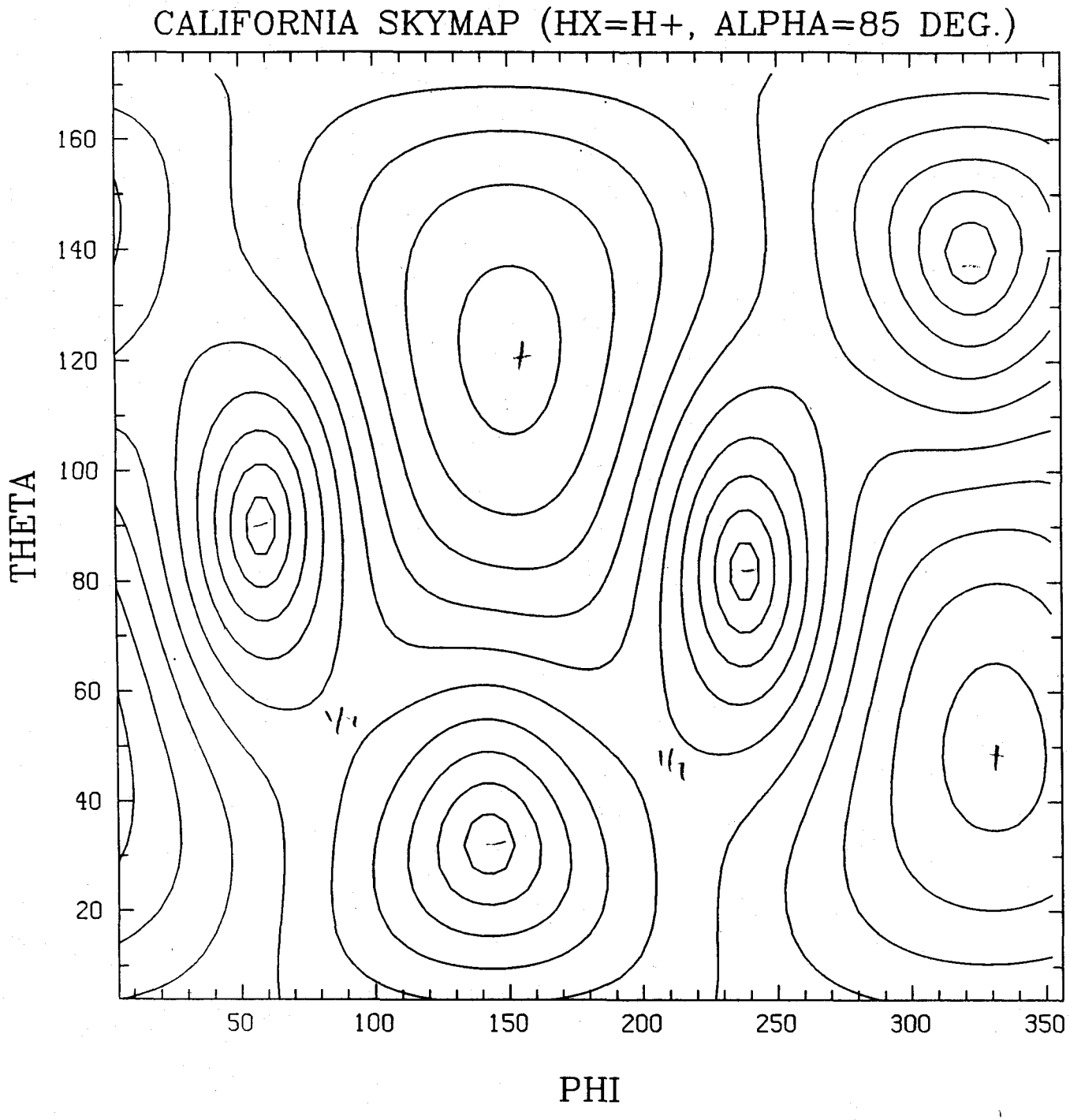
CALIFORNIA SKYMAP (HX=H+, ALPHA=85 DEG.)
THETA
160
140
120
100
80
60
40
20
50
100
150
200
250
300
350
PHI

Fig 6

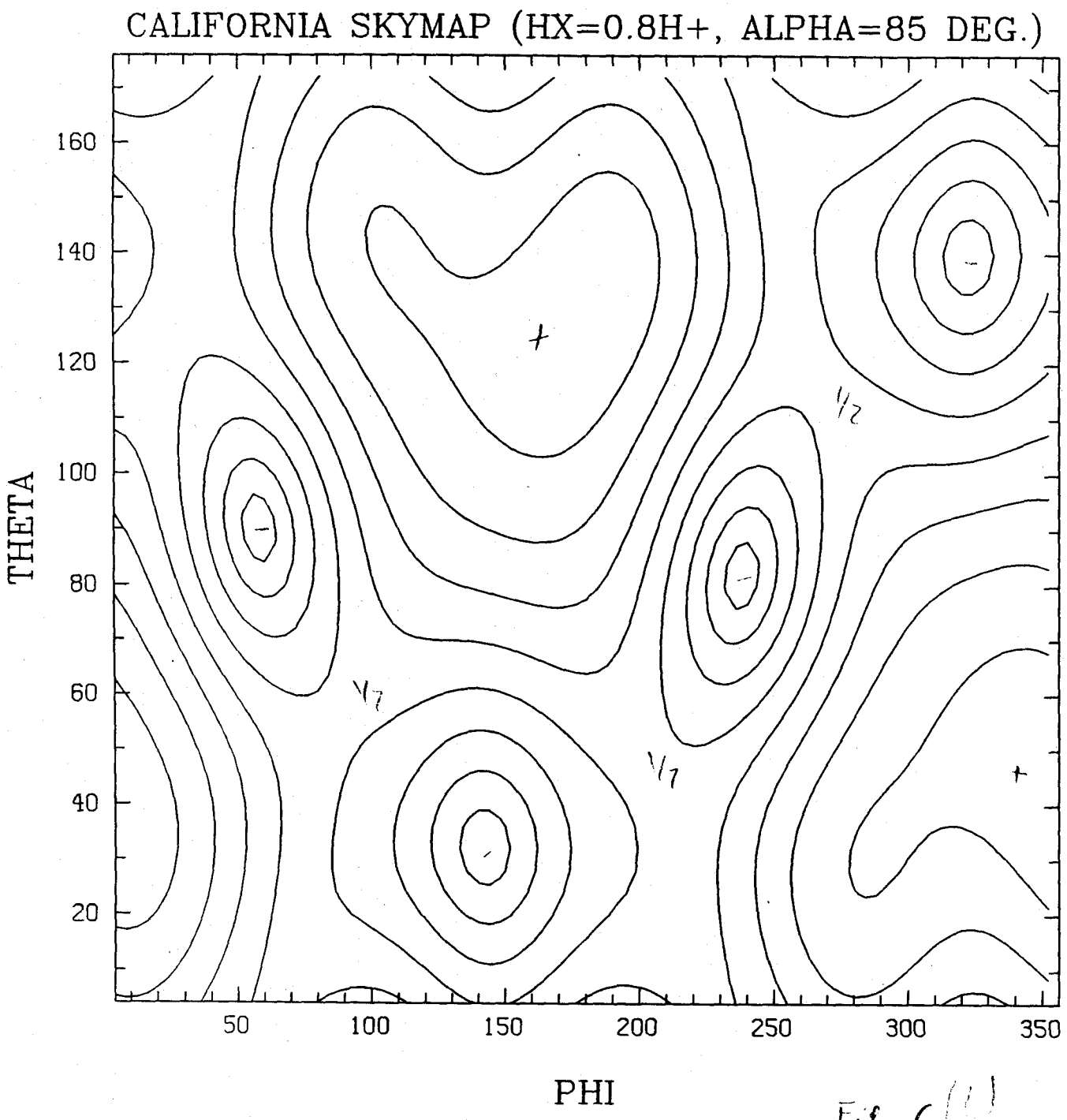
CALIFORNIA SKYMAP (HX=0.8H+, ALPHA=85 DEG.)
THETA
160
140
120
100
80
60
40
20
50
100
150
200
250
300
350
PHI
1/2
1/7
1/7
+
+
-
-
-

Fig 6(b)

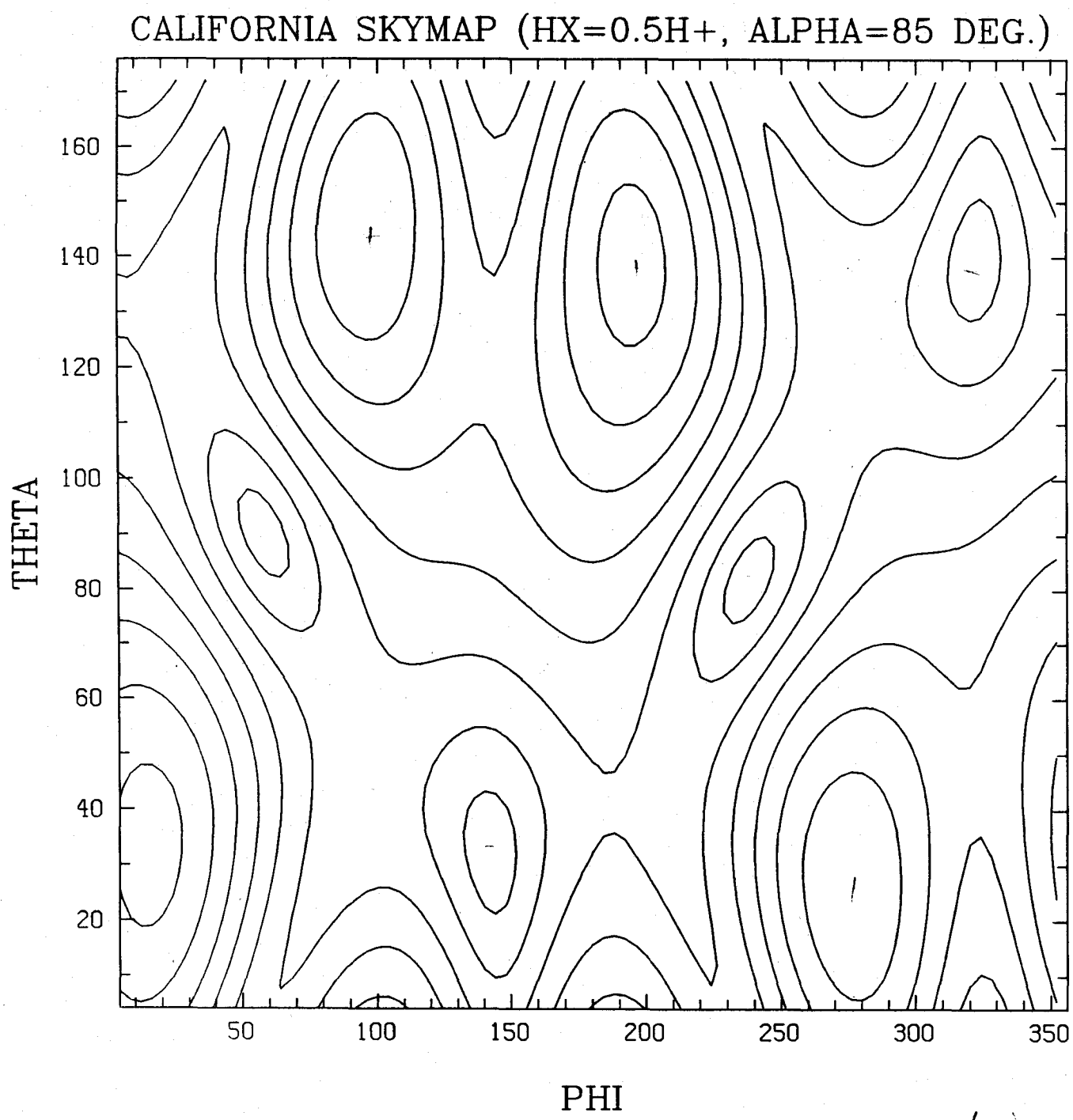
CALIFORNIA SKYMAP (HX=0.5H+, ALPHA=85 DEG.)
THETA
160
140
120
100
80
60
40
20
50
100
150
200
250
300
350
PHI

Fig 6(c)

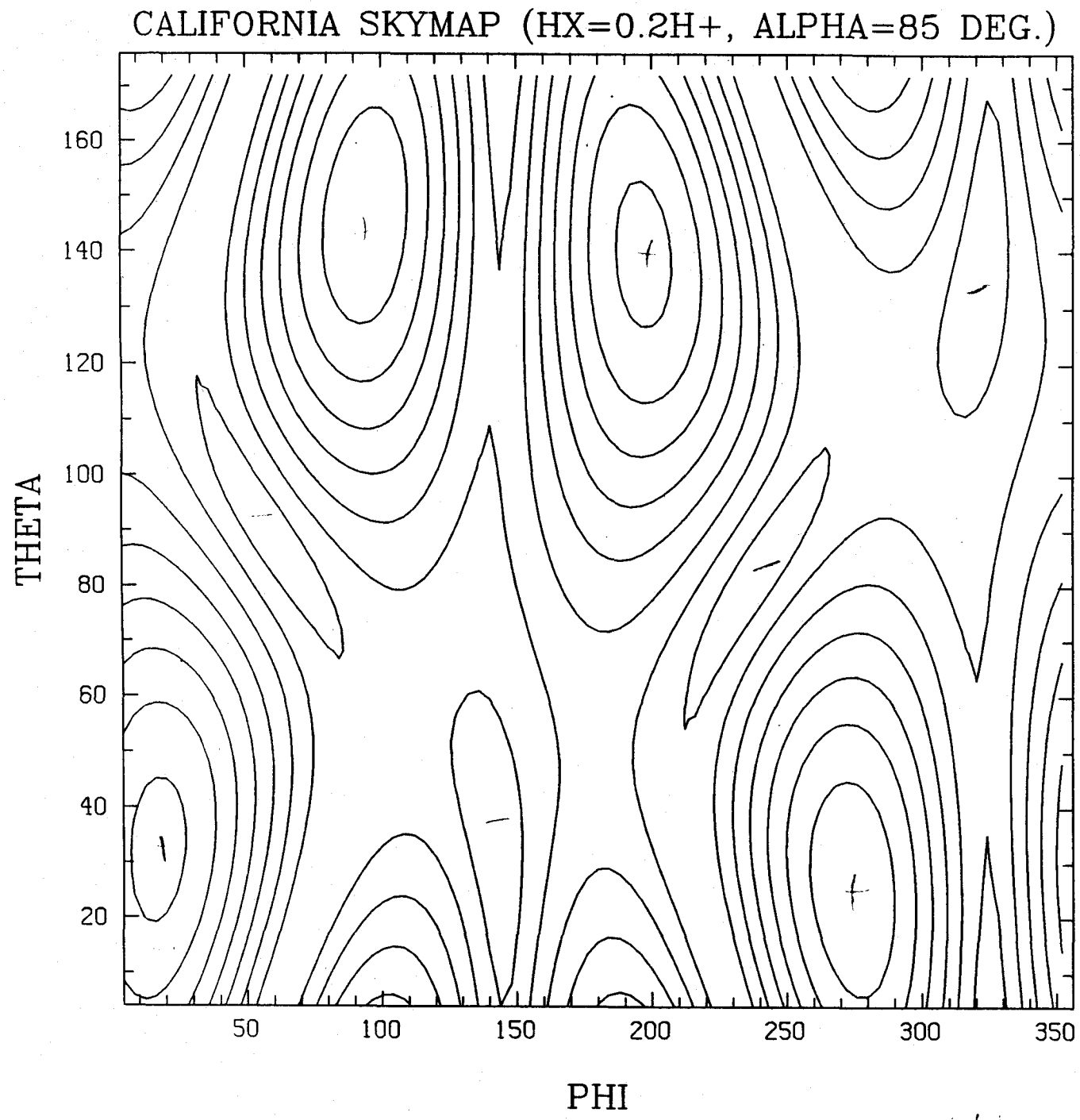
CALIFORNIA SKYMAP (HX=0.2H+, ALPHA=85 DEG.)
THETA
160
140
120
100
80
60
40
20
50
100
150
200
250
300
350
PHI

Fig. 6 (cont'd)

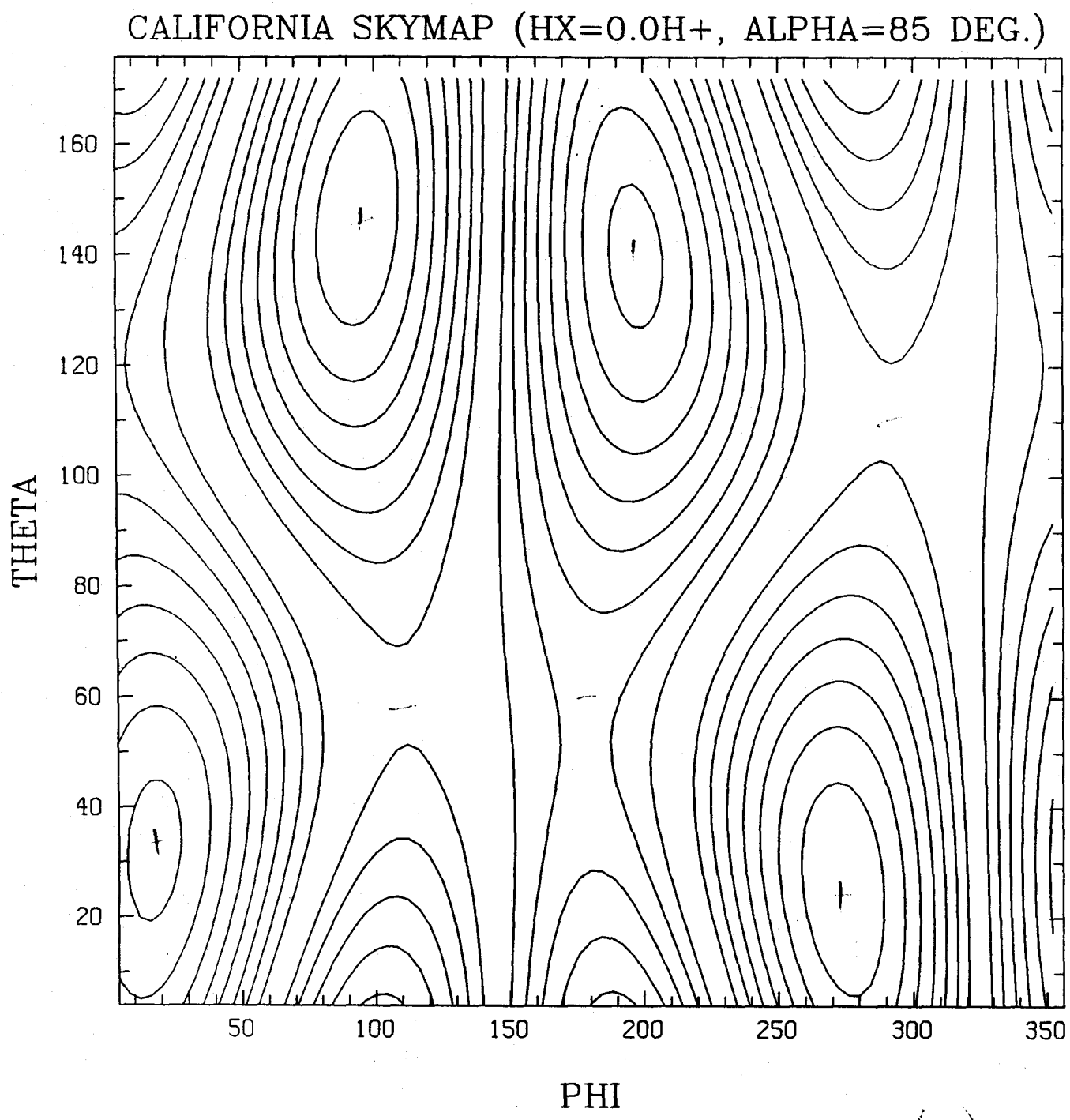
CALIFORNIA SKYMAP (HX=0.0H+, ALPHA=85 DEG.)
THETA
160
140
120
100
80
60
40
20
50
100
150
200
250
300
350
PHI

Fig 2(e)

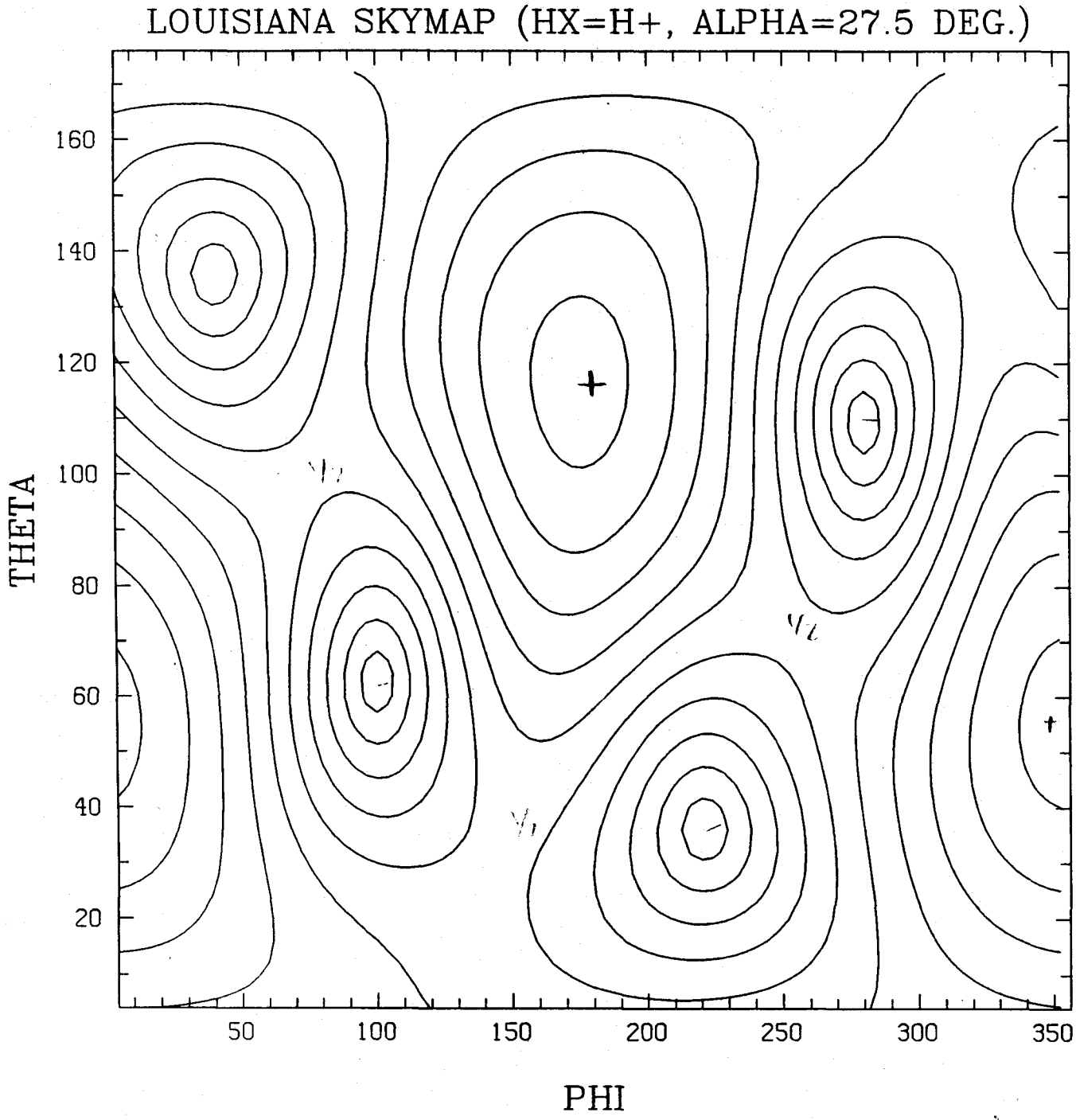
LOUISIANA SKYMAP (HX=H+, ALPHA=27.5 DEG.)
THETA
160
140
120
100
80
60
40
20
50
100
150
200
250
300
350
PHI

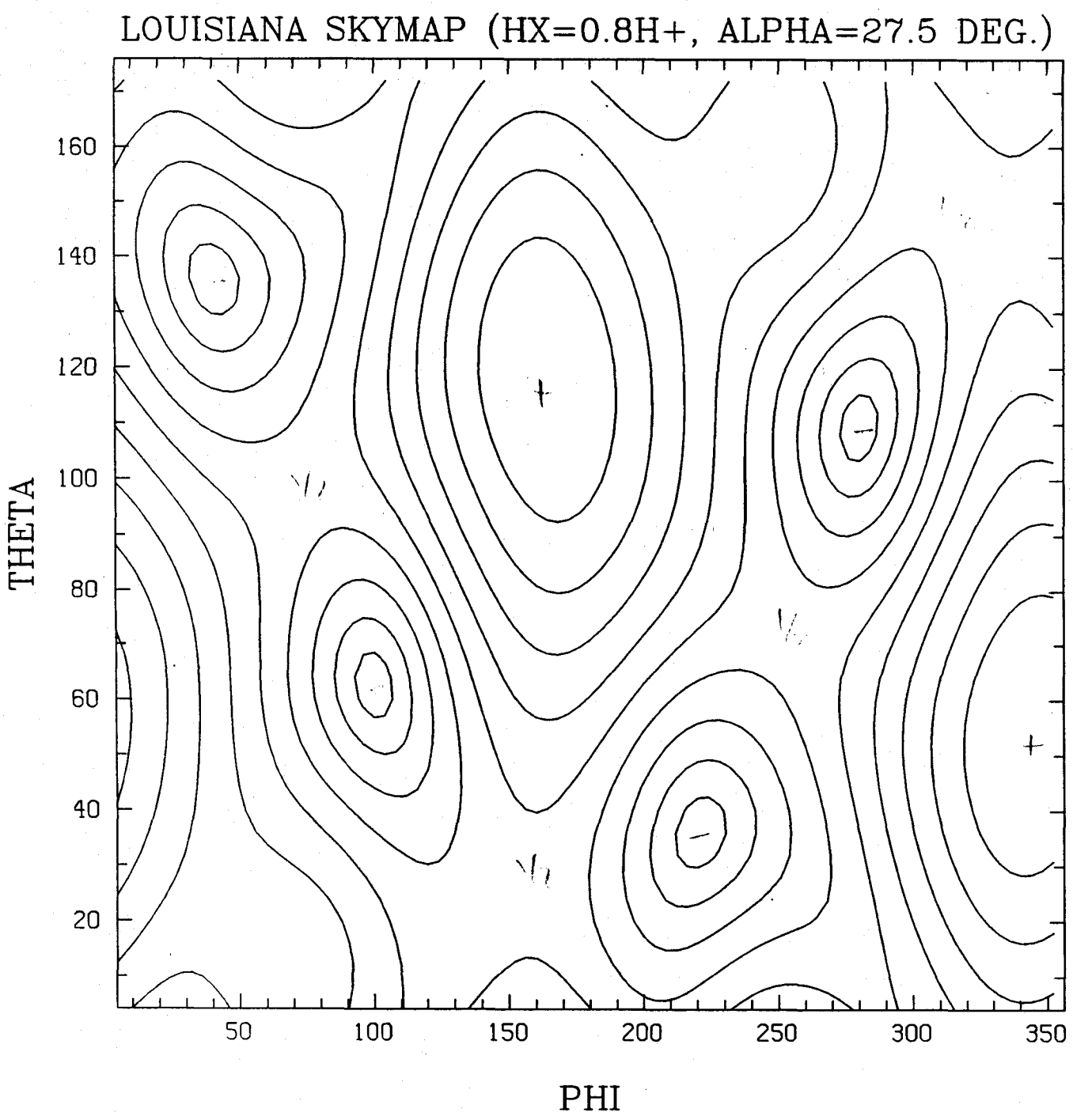
LOUISIANA SKYMAP (HX=0.8H+, ALPHA=27.5 DEG.)
THETA
160
140
120
100
80
60
40
20
50
100
150
200
250
300
350
PHI

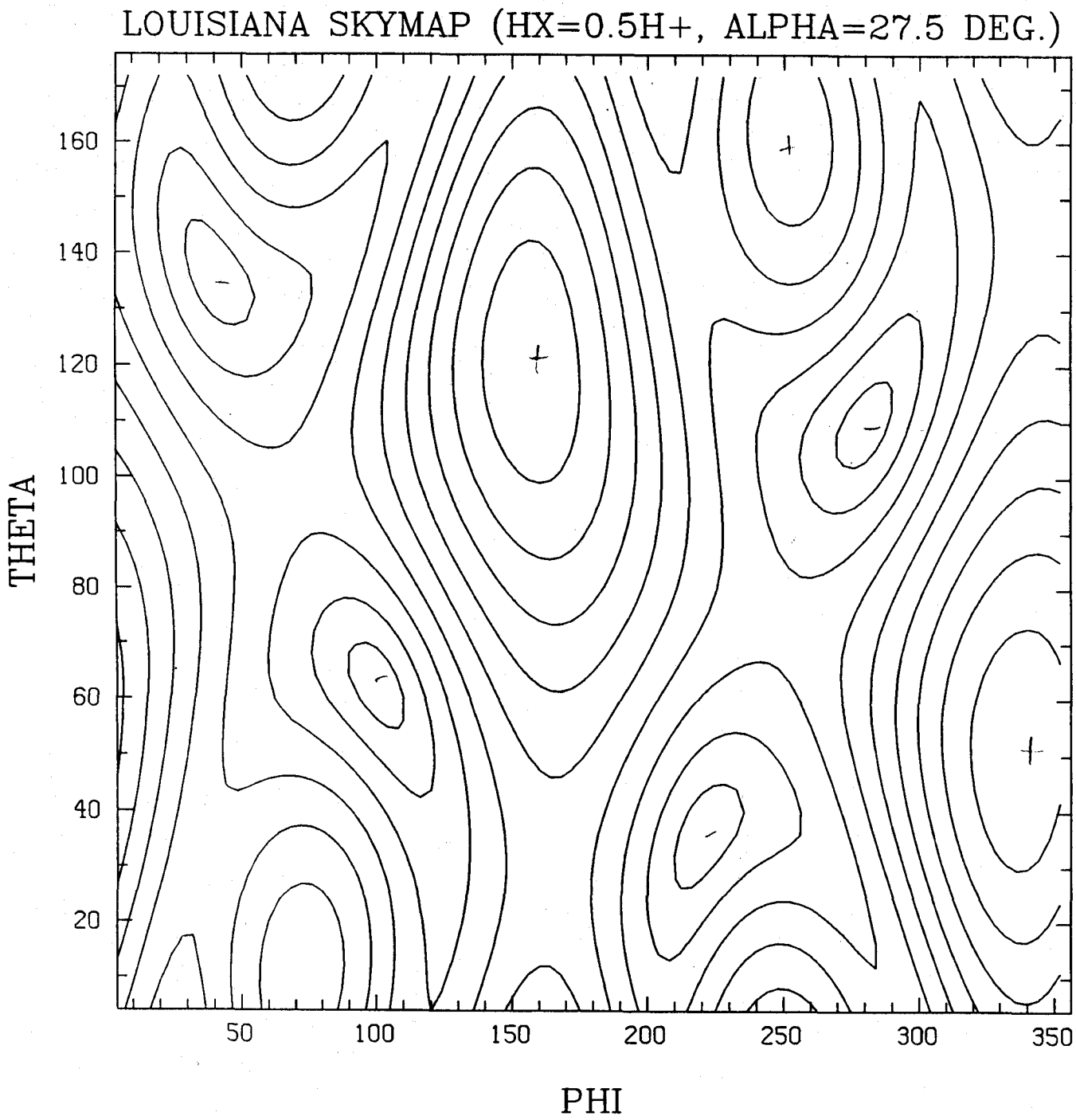
LOUISIANA SKYMAP (HX=0.5H+, ALPHA=27.5 DEG.)
THETA
160
140
120
100
80
60
40
20
50
100
150
200
250
300
350
PHI

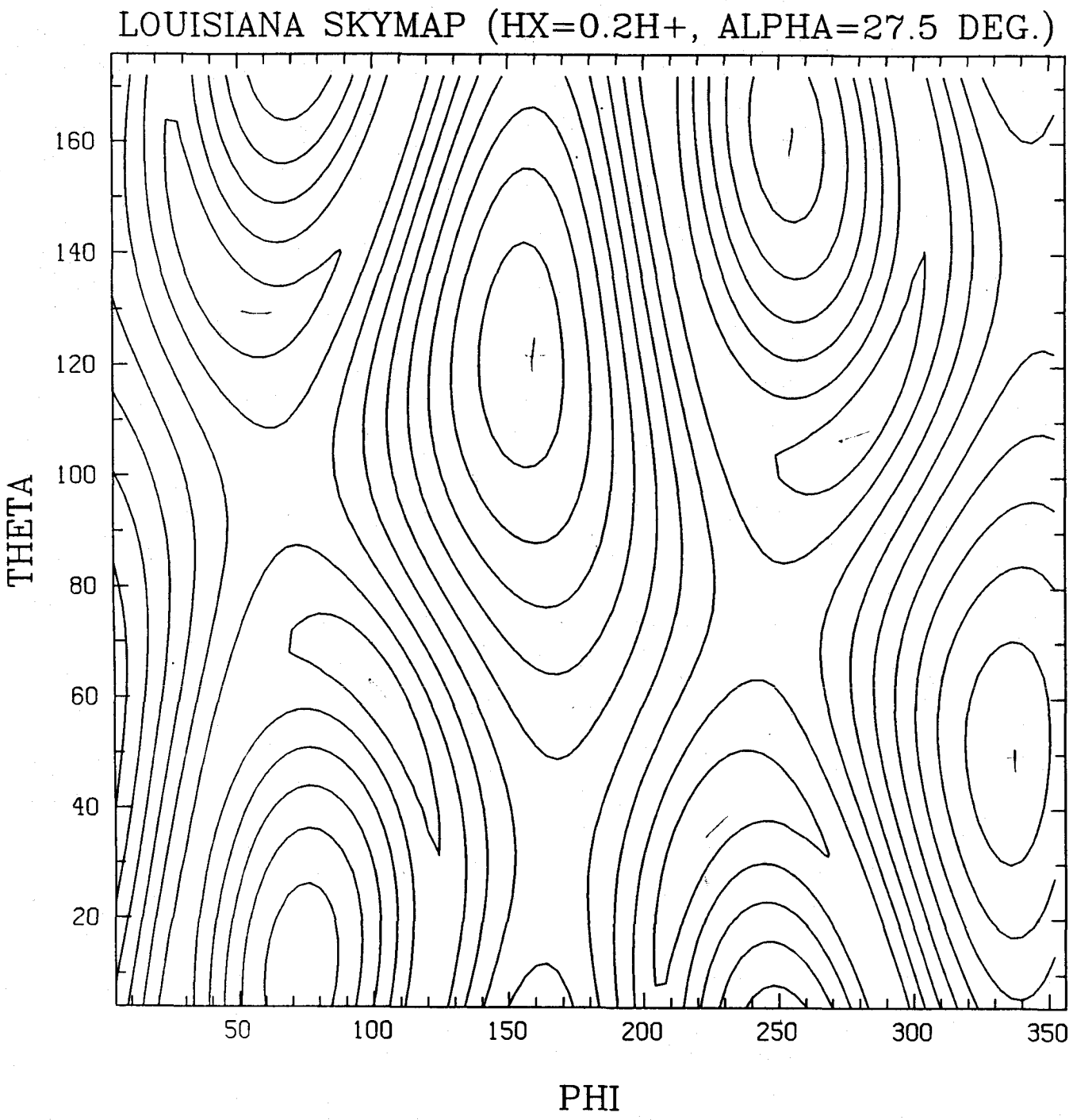
LOUISIANA SKYMAP (HX=0.2H+, ALPHA=27.5 DEG.)
THETA
160
140
120
100
80
60
40
20
50
100
150
200
250
300
350
PHI

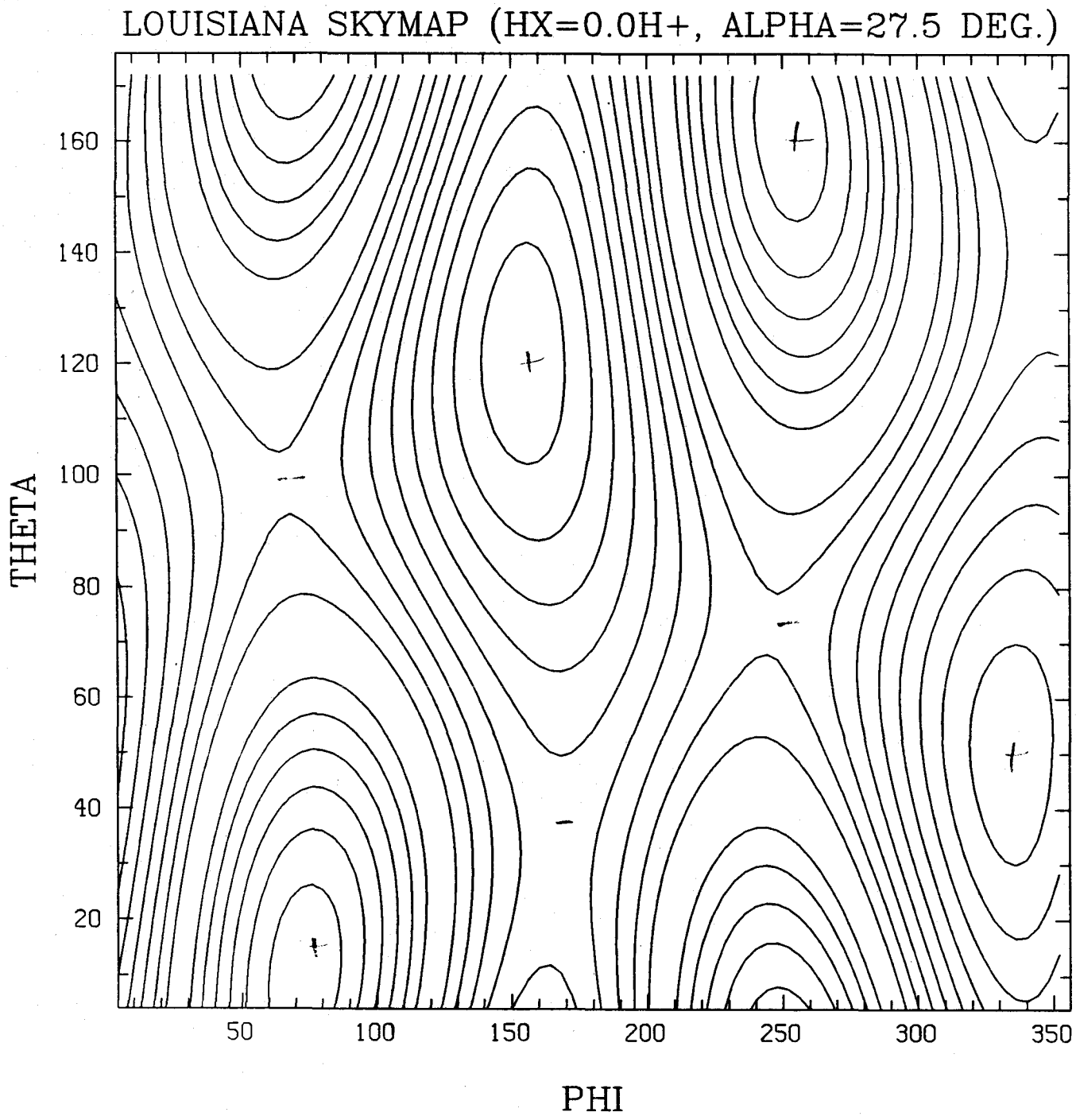
LOUISIANA SKYMAP (HX=0.0H+, ALPHA=27.5 DEG.)
THETA
160
140
120
100
80
60
40
20
50
100
150
200
250
300
350
PHI

Fig. (e)

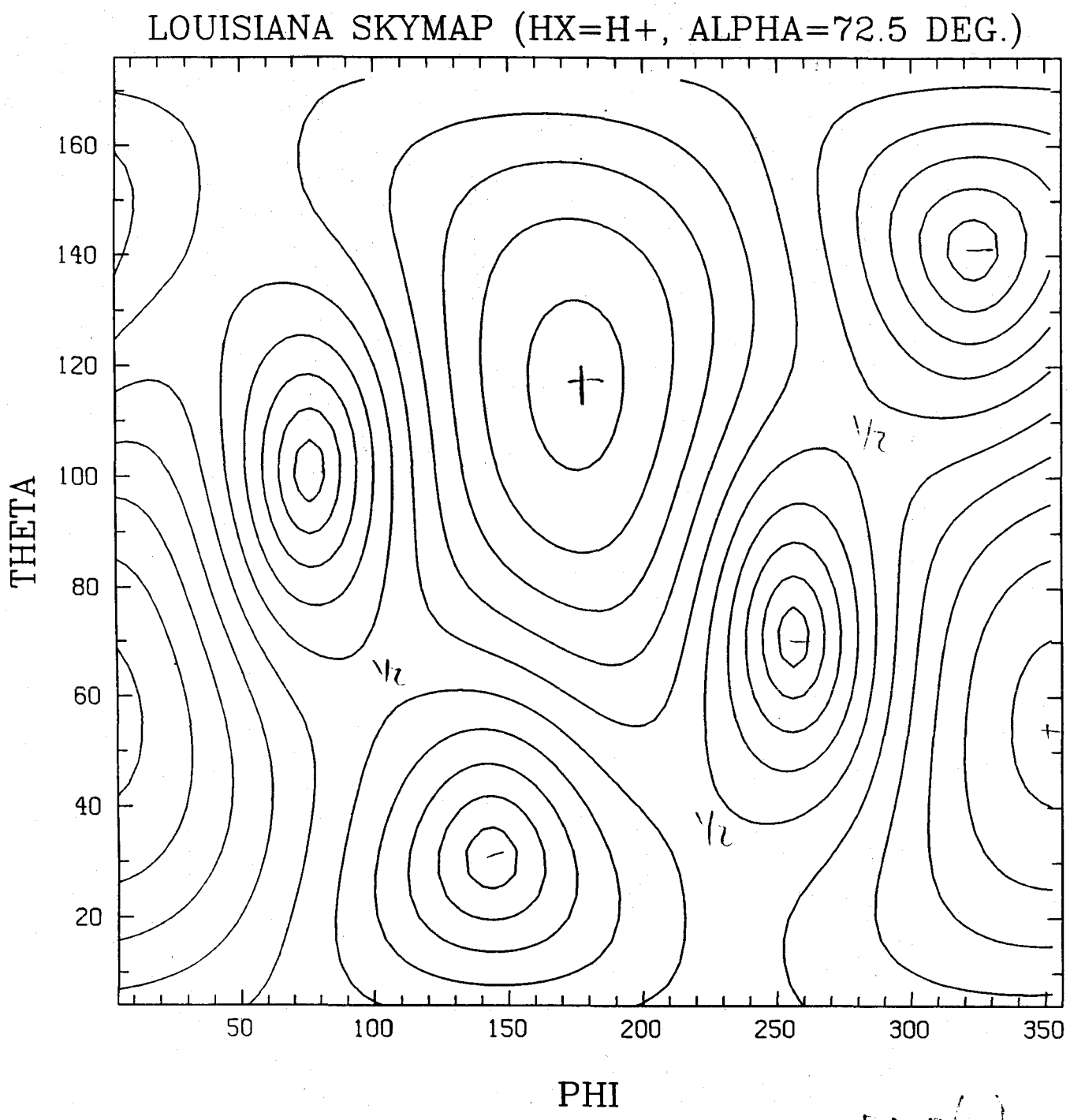
LOUISIANA SKYMAP (HX=H+, ALPHA=72.5 DEG.)
THETA
160
140
120
100
80
60
40
20
50
100
150
200
250
300
350
PHI
+
−
+
−
+
1/2
1/2
1/2

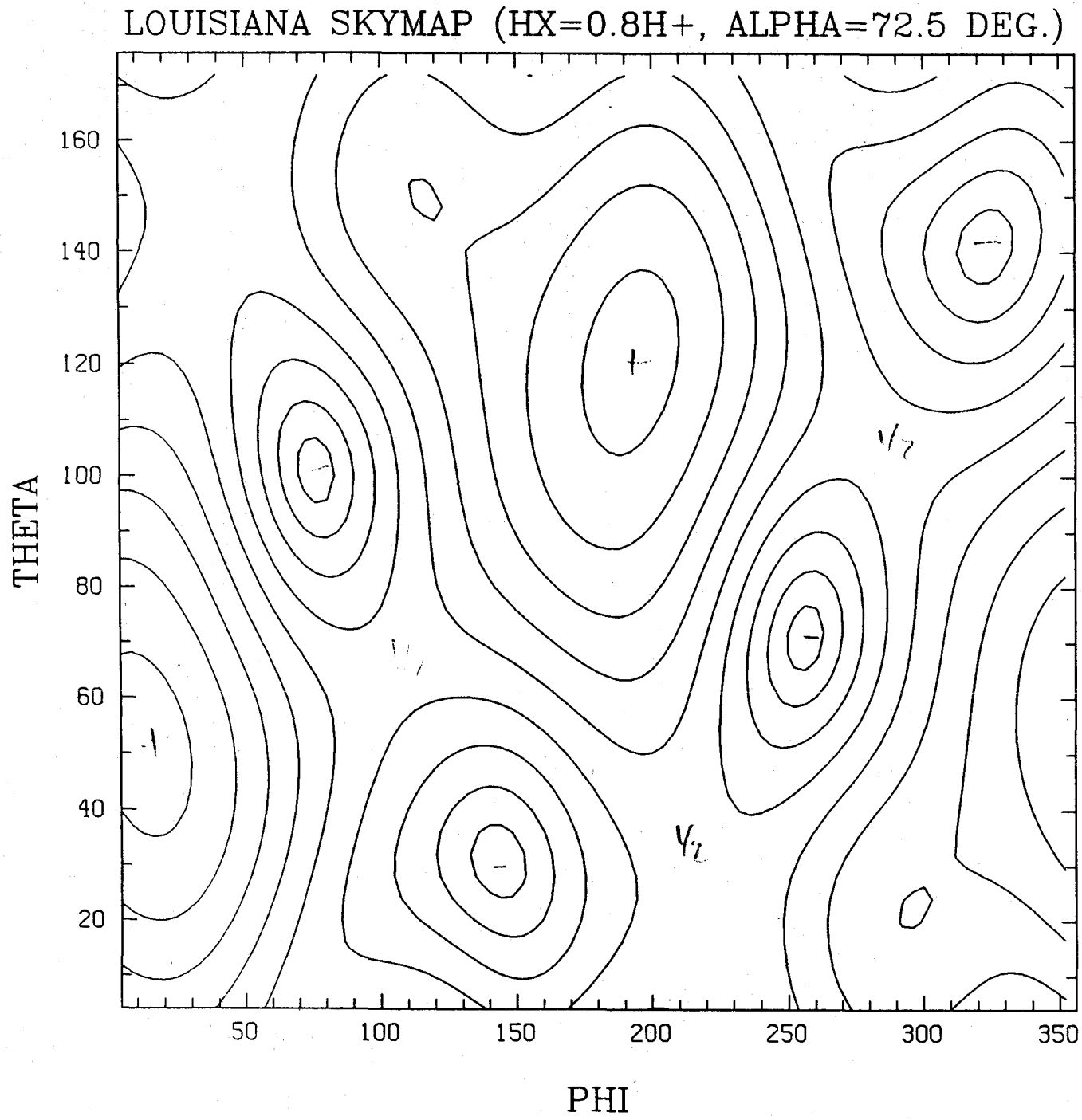
LOUISIANA SKYMAP (HX=0.8H+, ALPHA=72.5 DEG.)
THETA
160
140
120
100
80
60
40
20
50
100
150
200
250
300
350
PHI

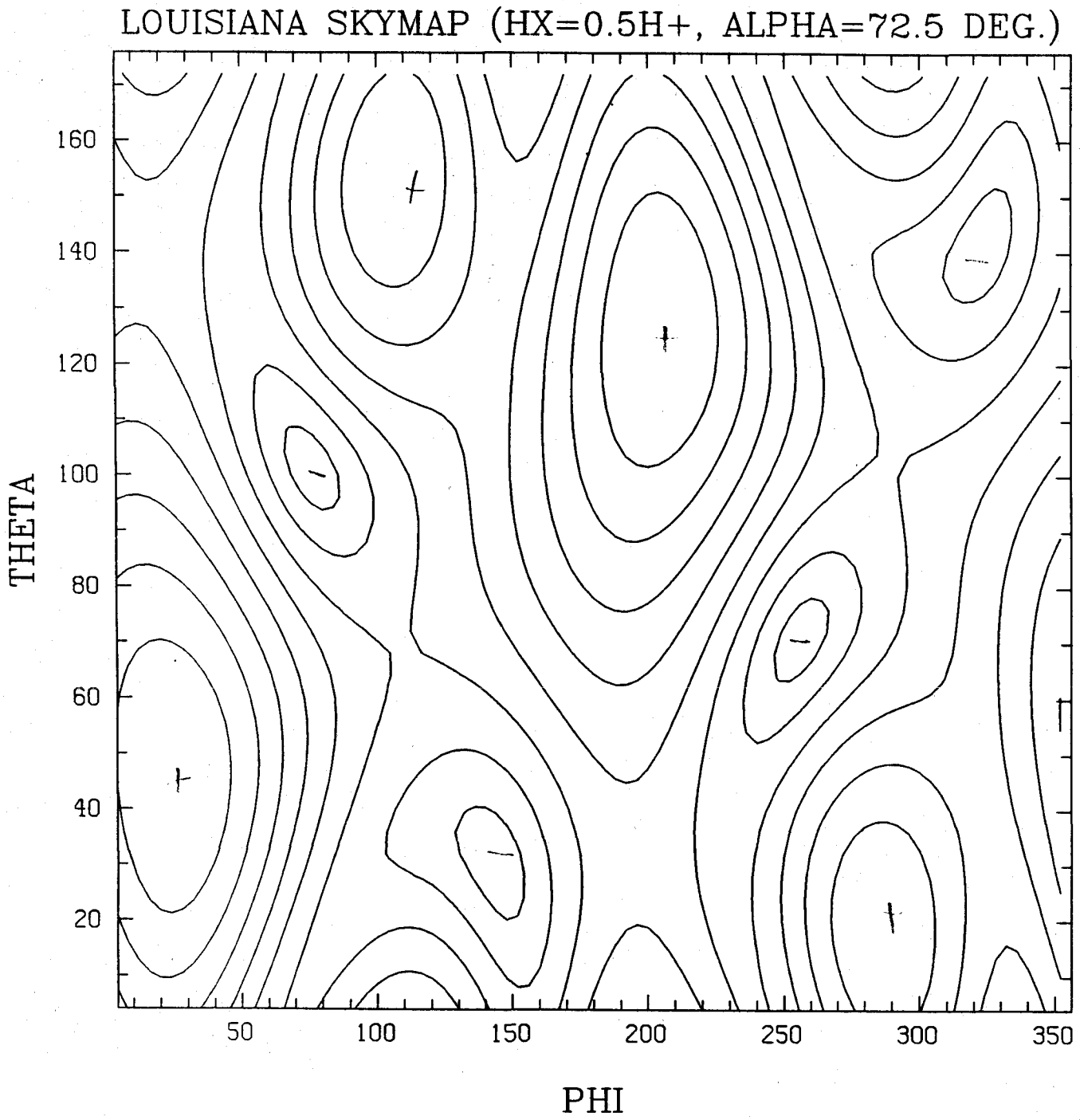
LOUISIANA SKYMAP (HX=0.5H+, ALPHA=72.5 DEG.)
THETA
160
140
120
100
80
60
40
20
50
100
150
200
250
300
350
PHI

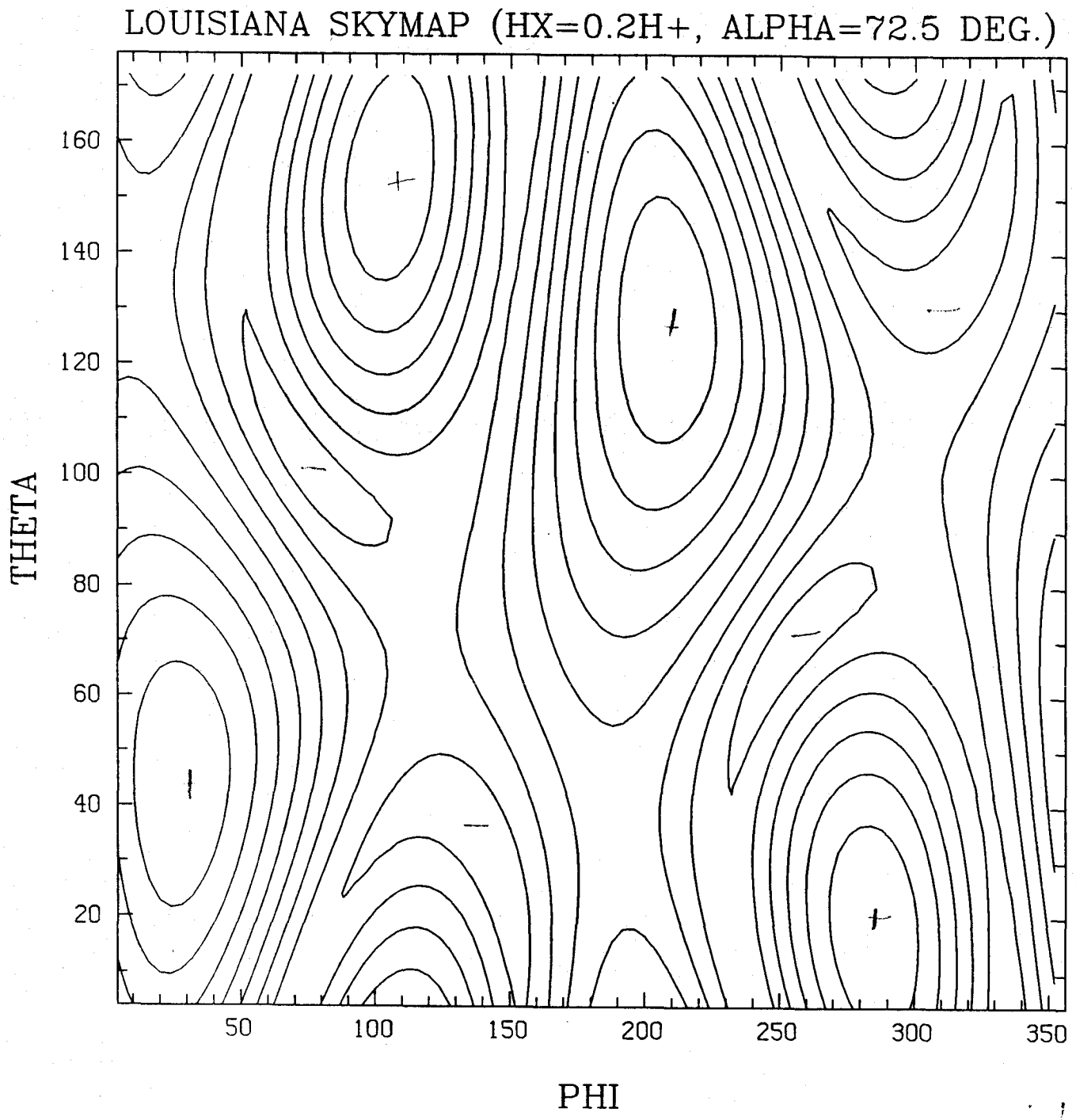
LOUISIANA SKYMAP (HX=0.2H+, ALPHA=72.5 DEG.)
THETA
160
140
120
100
80
60
40
20
50
100
150
200
250
300
350
PHI

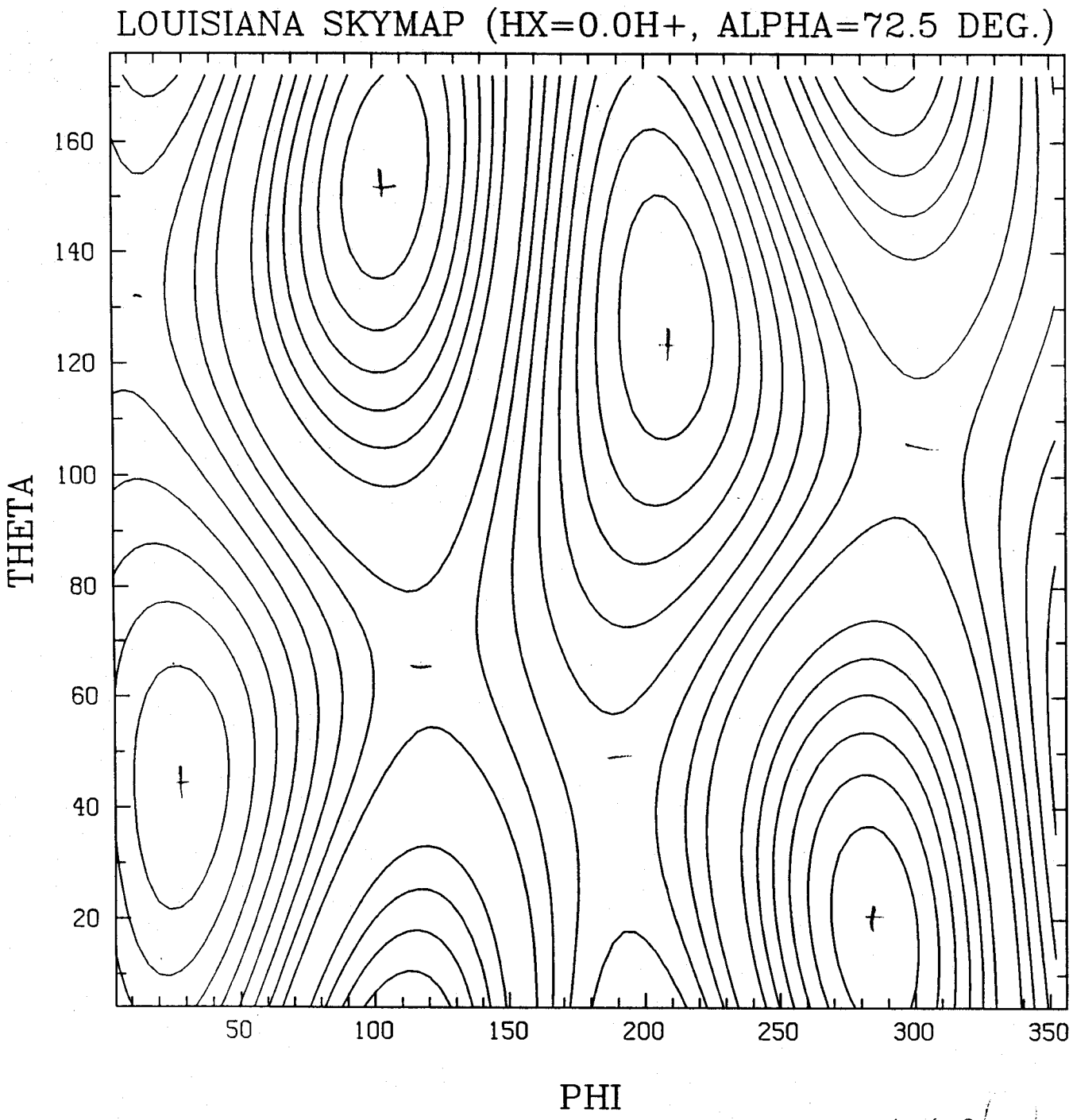
LOUISIANA SKYMAP (HX=0.0H+, ALPHA=72.5 DEG.)
THETA
160
140
120
100
80
60
40
20
50
100
150
200
250
300
350
PHI

GEOMETRICAL

$h_+ = h_\times$

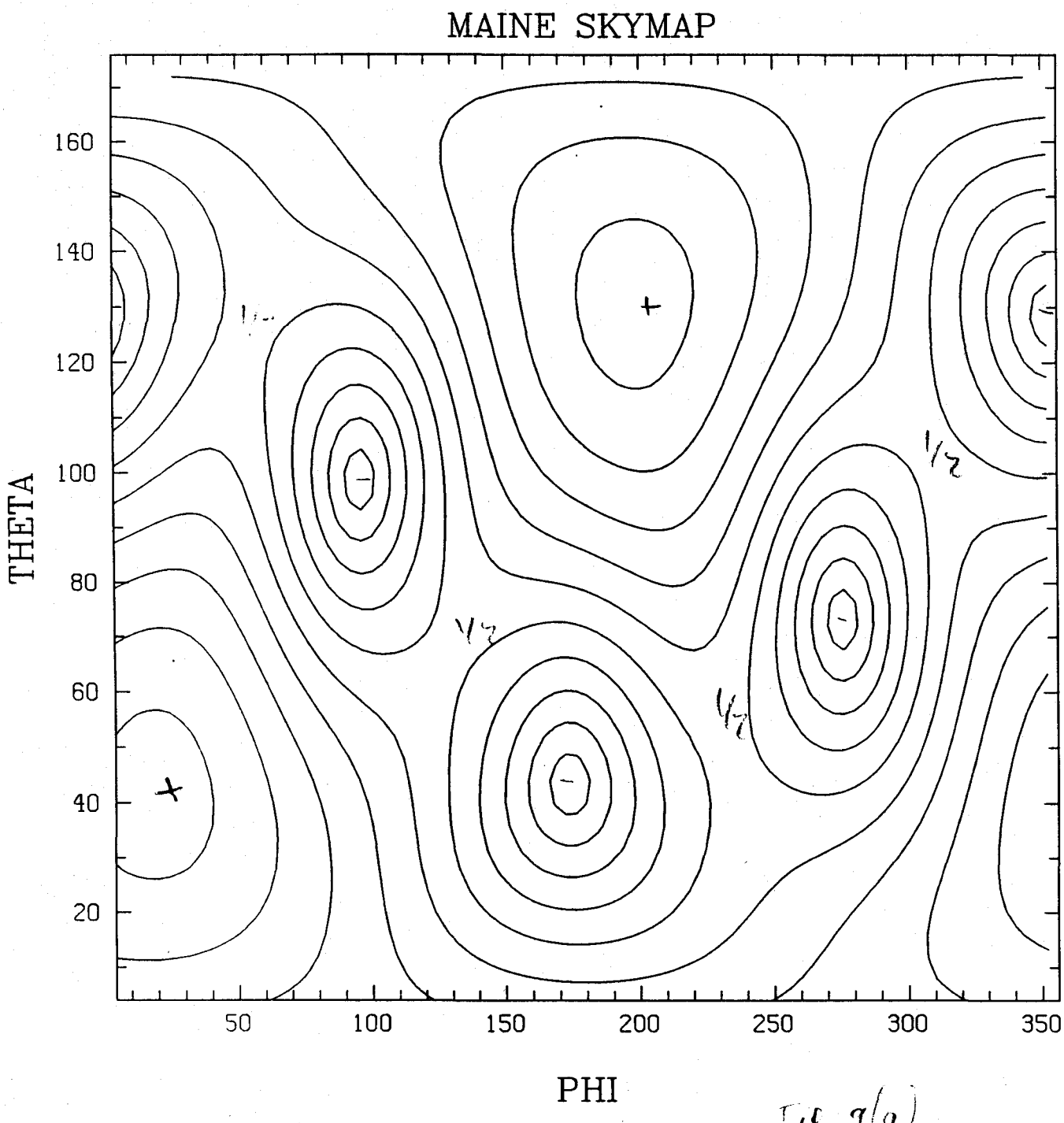

Fig 9(a)

GEOMETRICAL

$h_x = 0.8\, h_+$

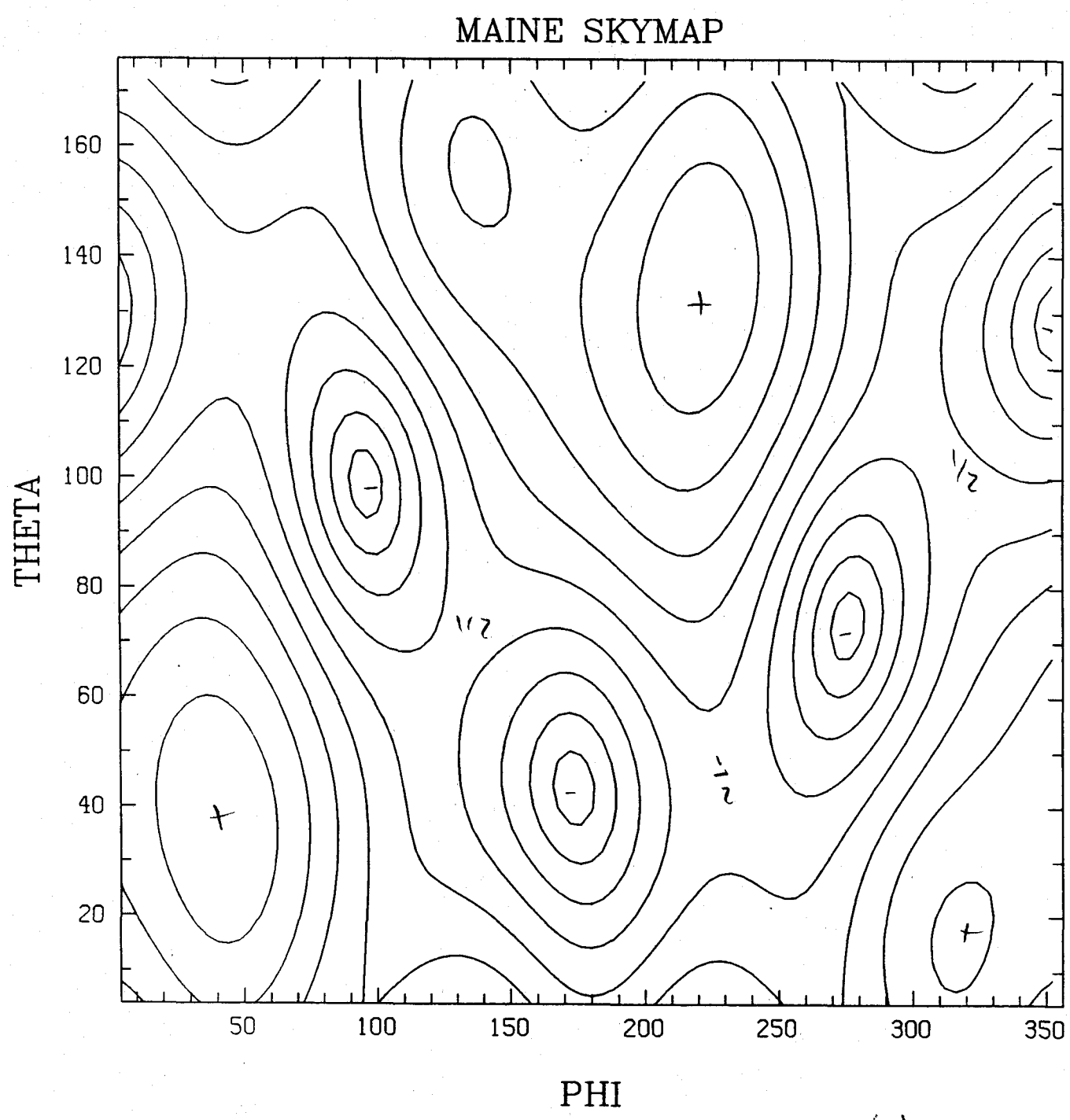

Fig 9(c)

GEOMETRICAL

$h_x = 0.5\, h_+$

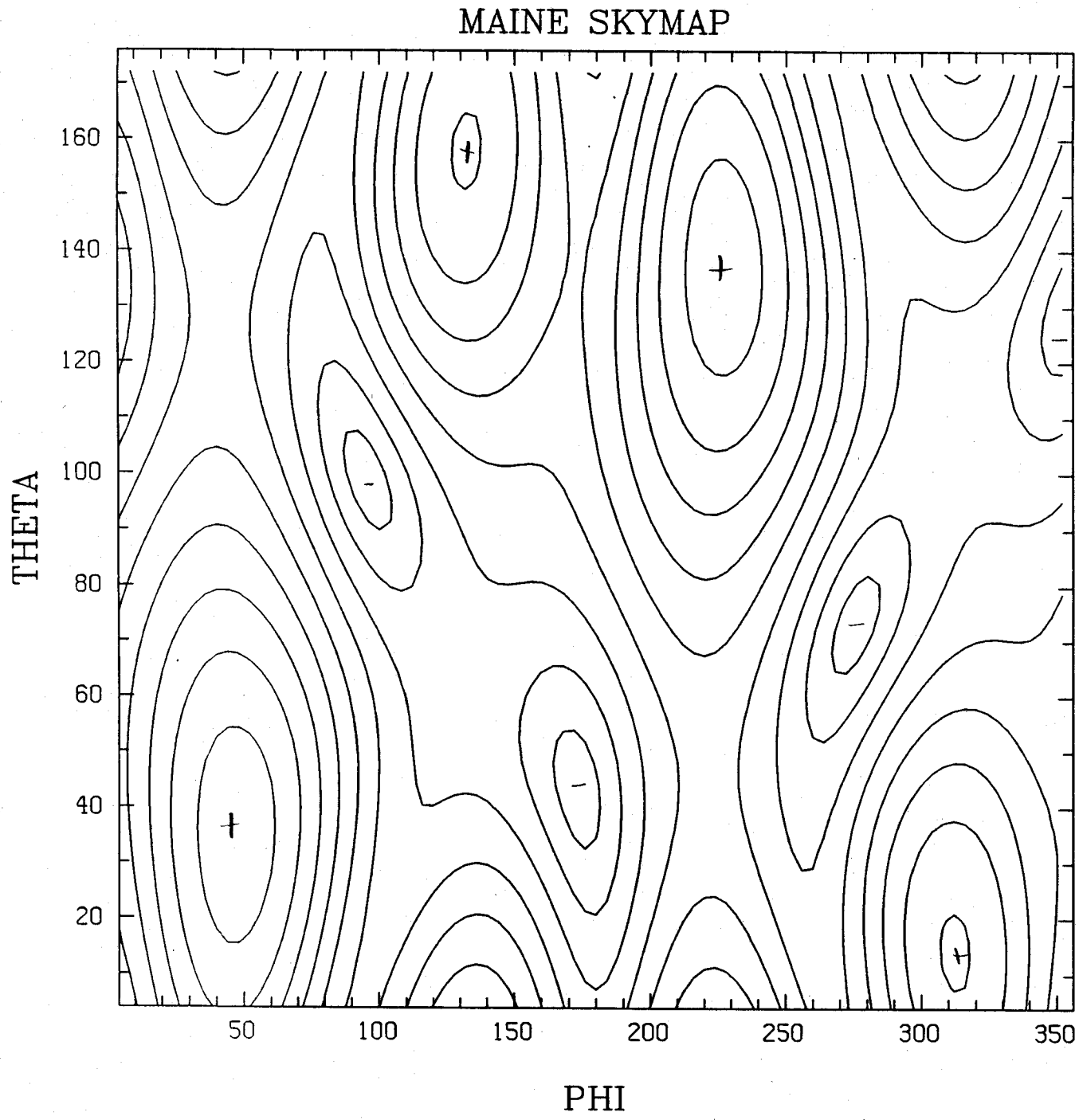

Fig 9(c)

GEOMETRICAL

$h_x = 0.2\, h_t$.

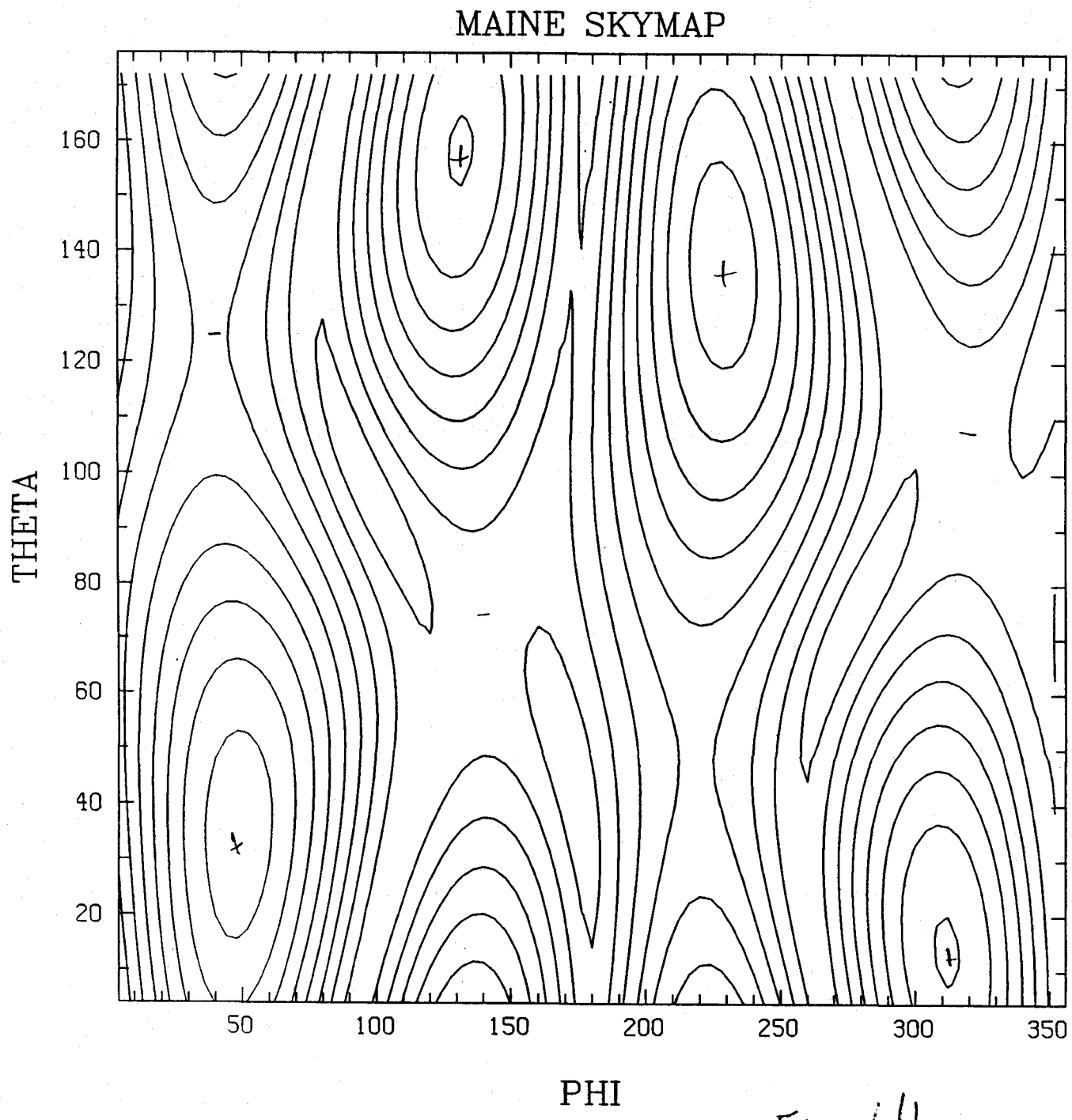

Fig 9 of 11

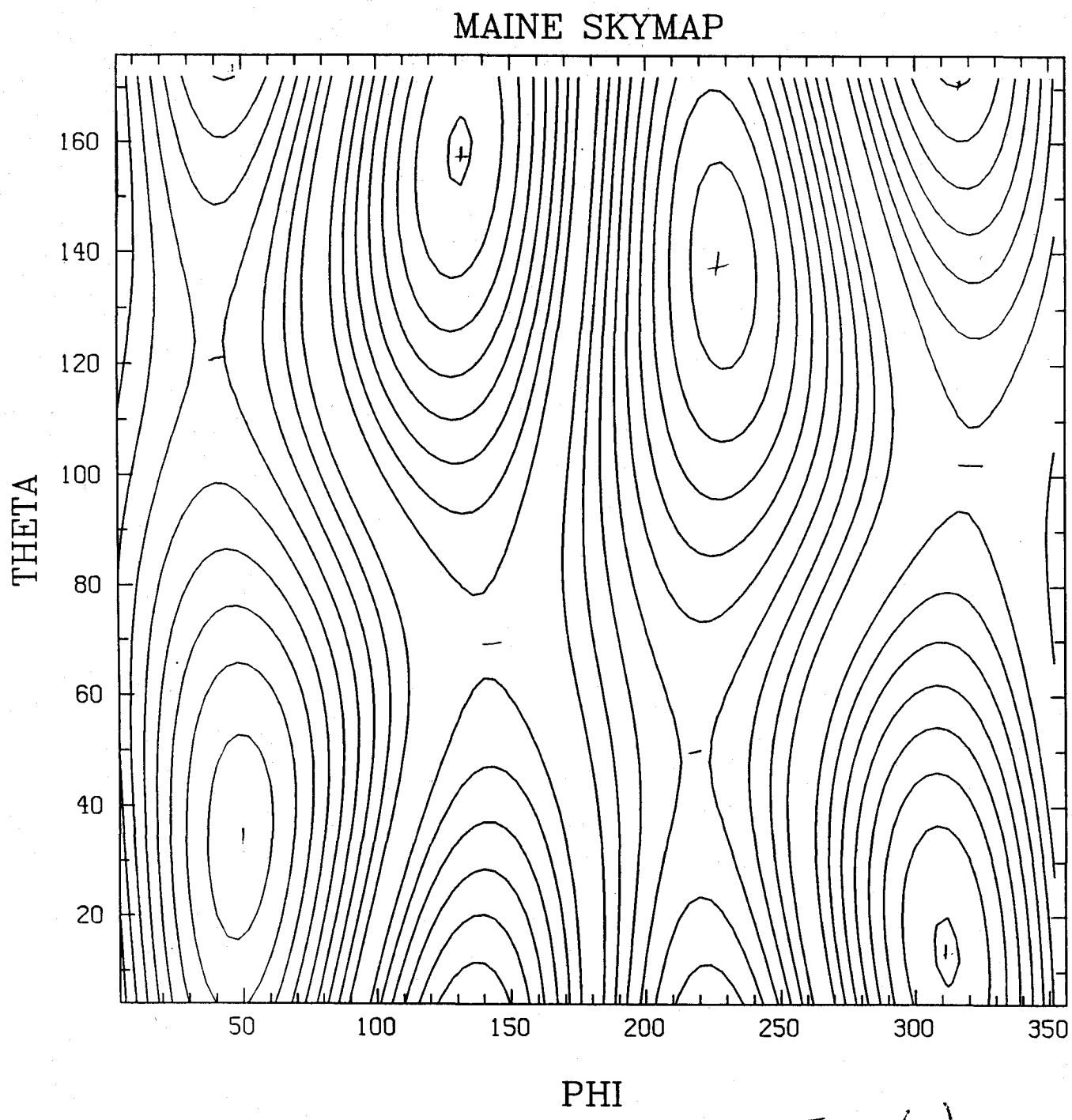

GEOMETRICAL

$h_x = 0$

Fig 9(e)

GEOMETRICAL

$h_+ = h_\times$

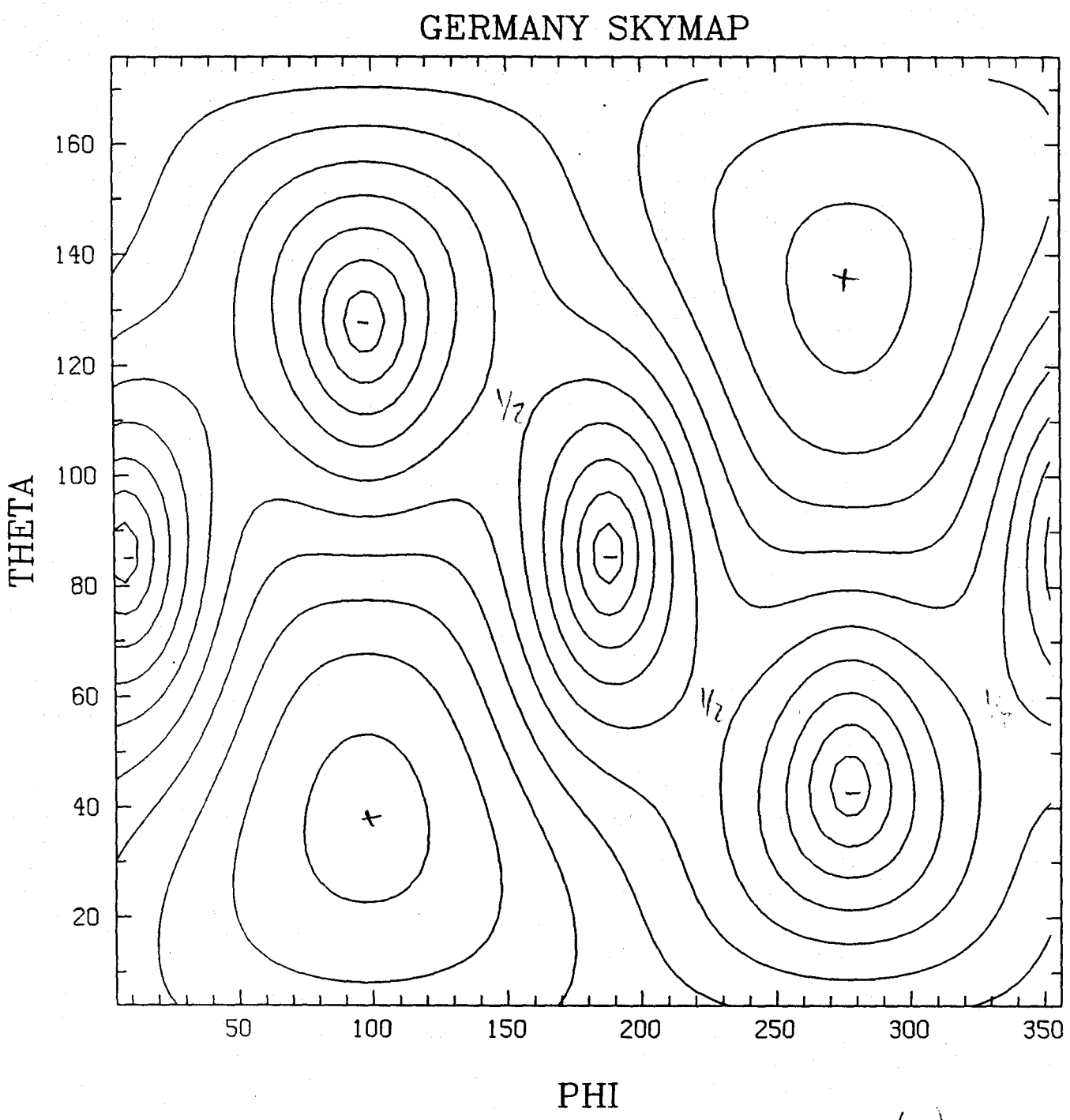

Fig 10(a)

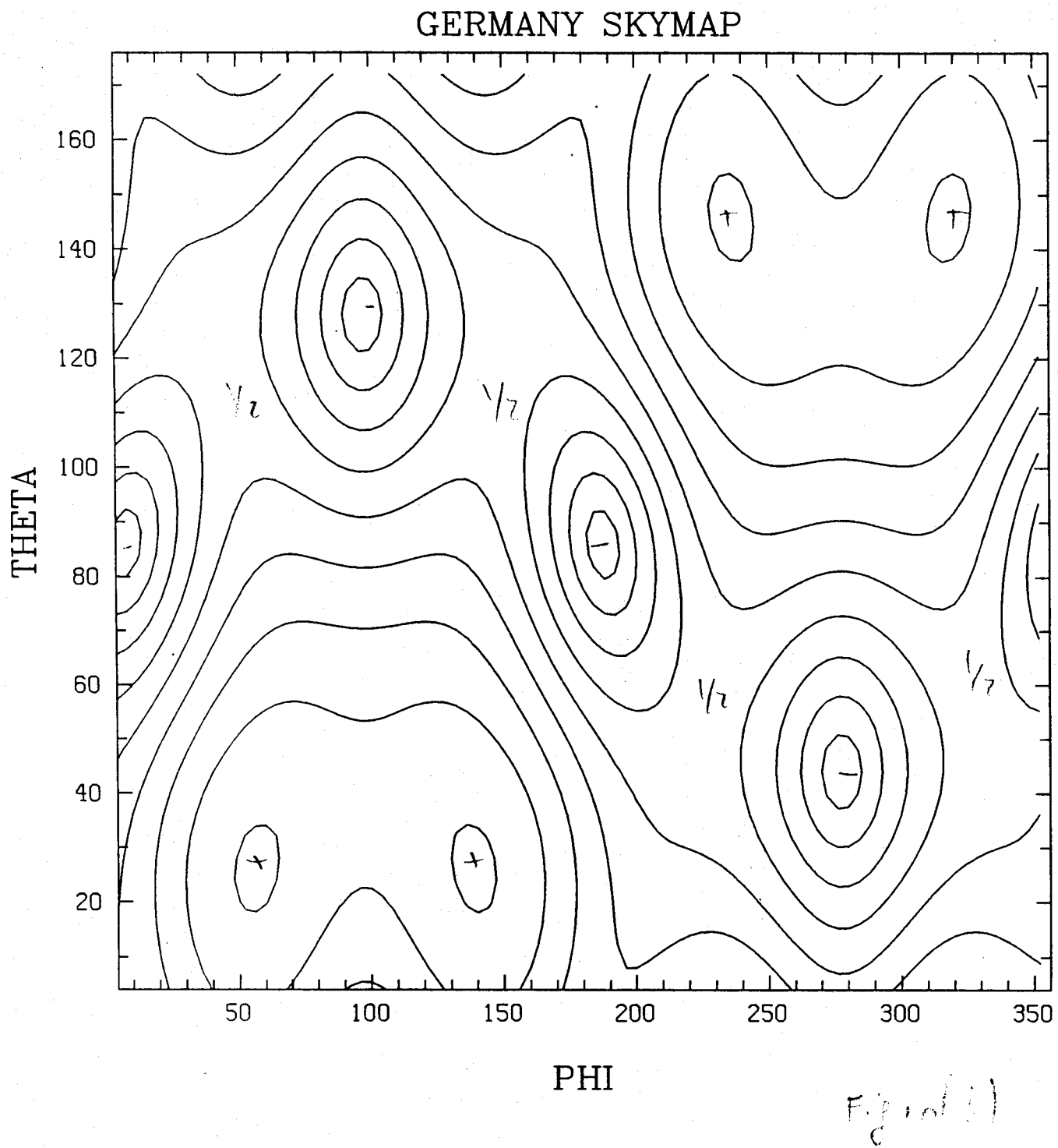

GEOMETRICAL

$h_X = 0.8\, h_+$

Figure 1

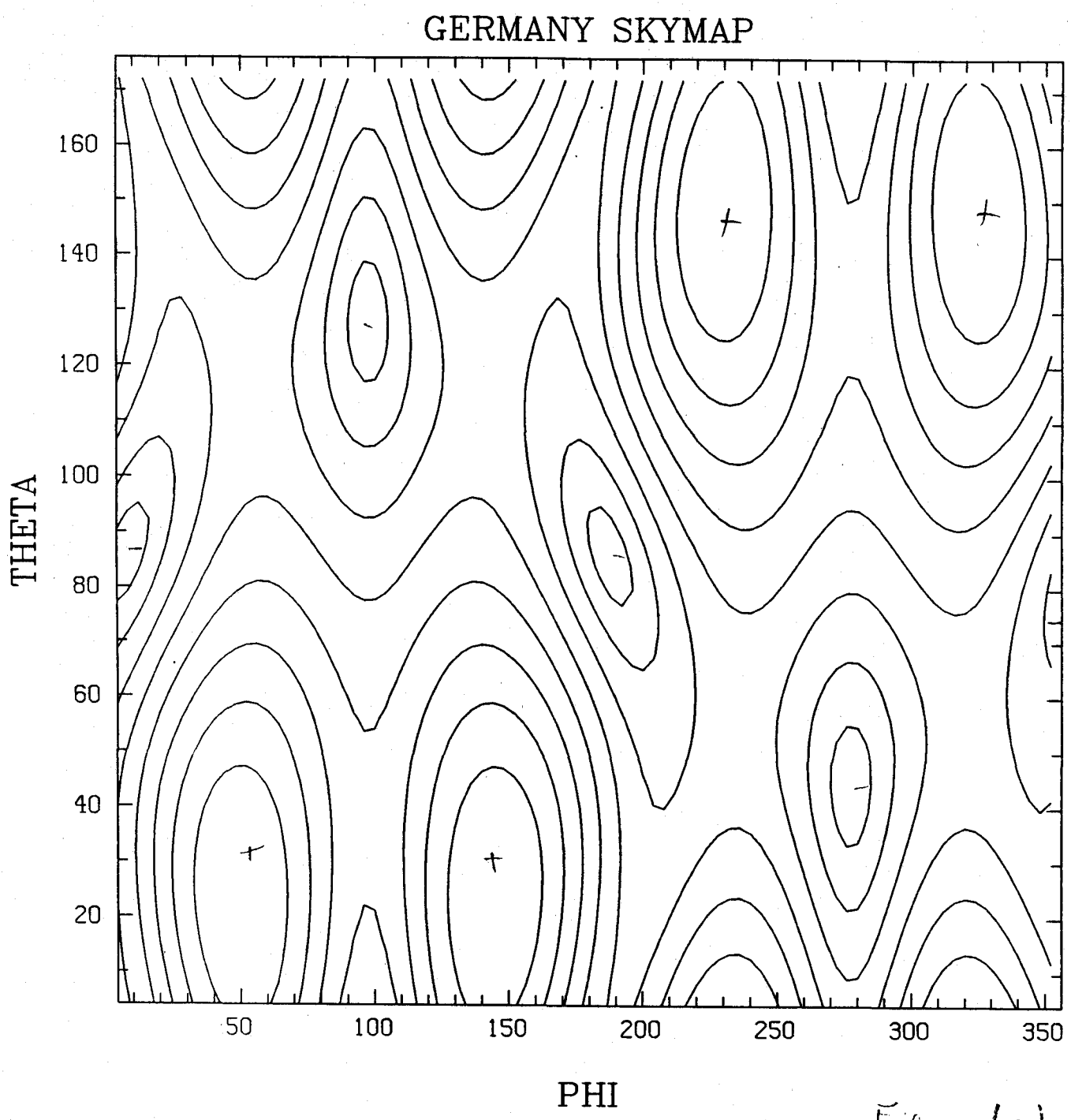

GEOMETRICAL

$h_x = 0.5\,h_t$.

Fig 10(c)

GEOMETRICAL

$h_x = 0.2\ h_t$.

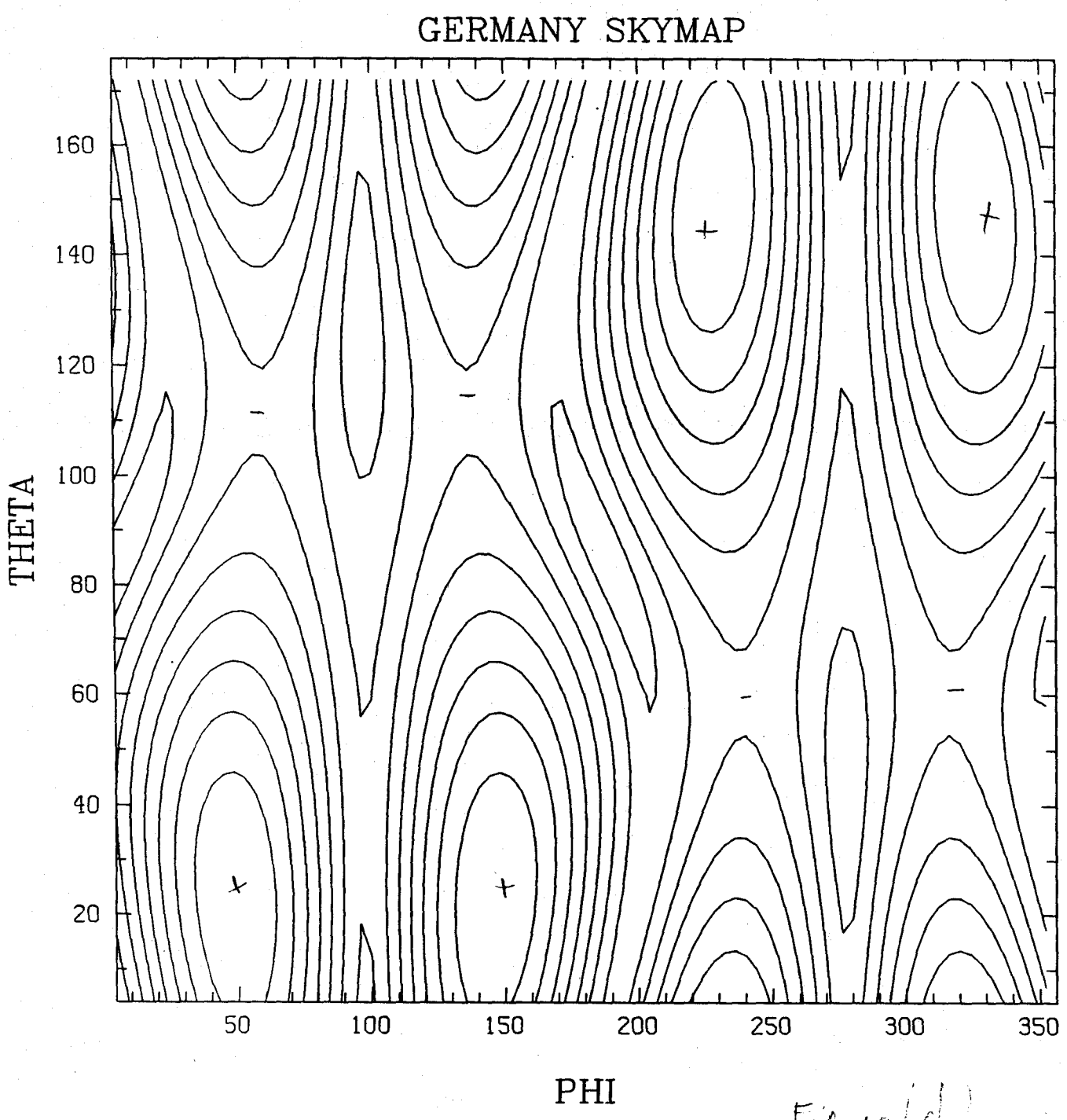

Fig. 1 of [illegible]

GEOMETRICAL

$h_x \simeq 0$

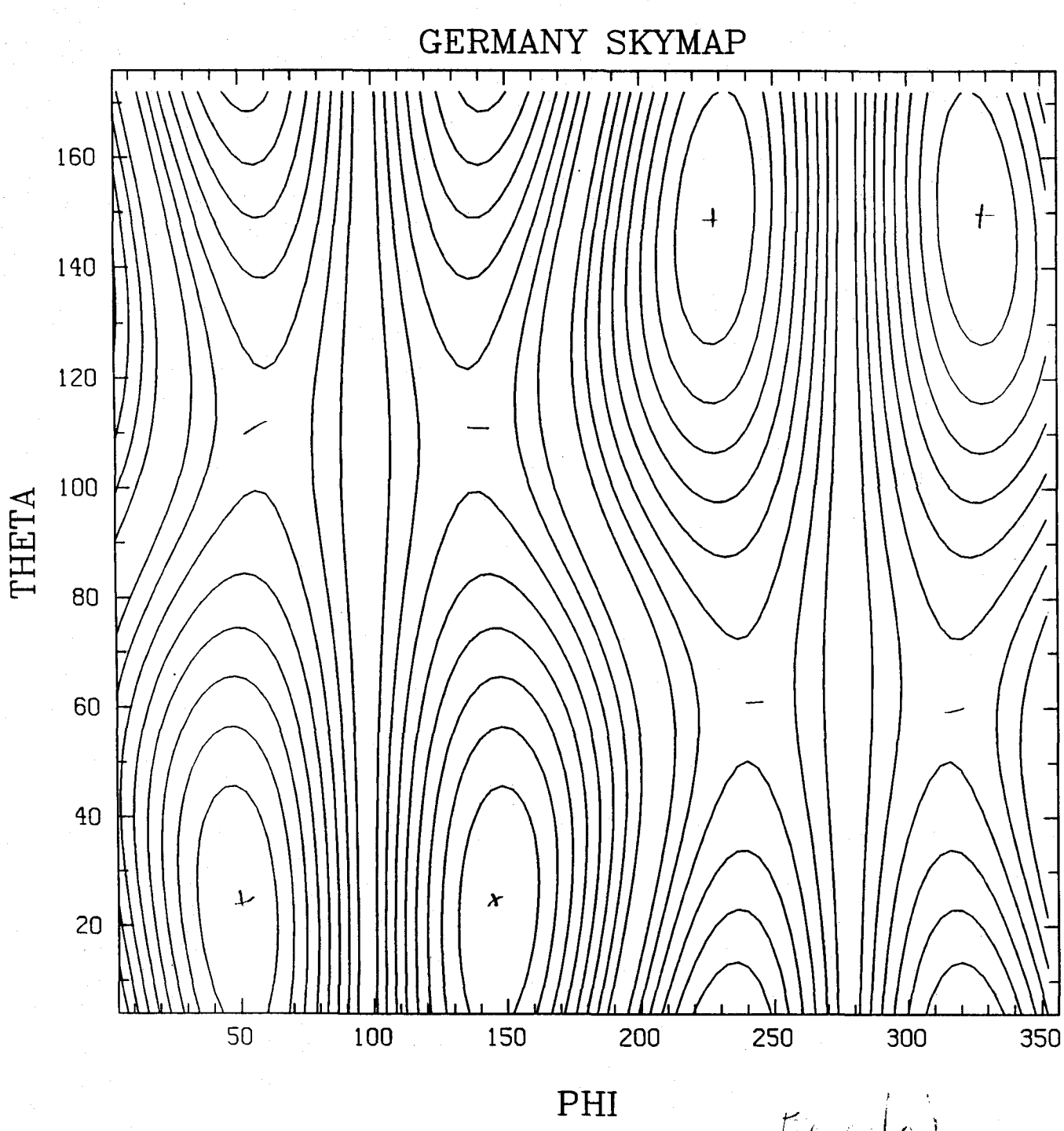

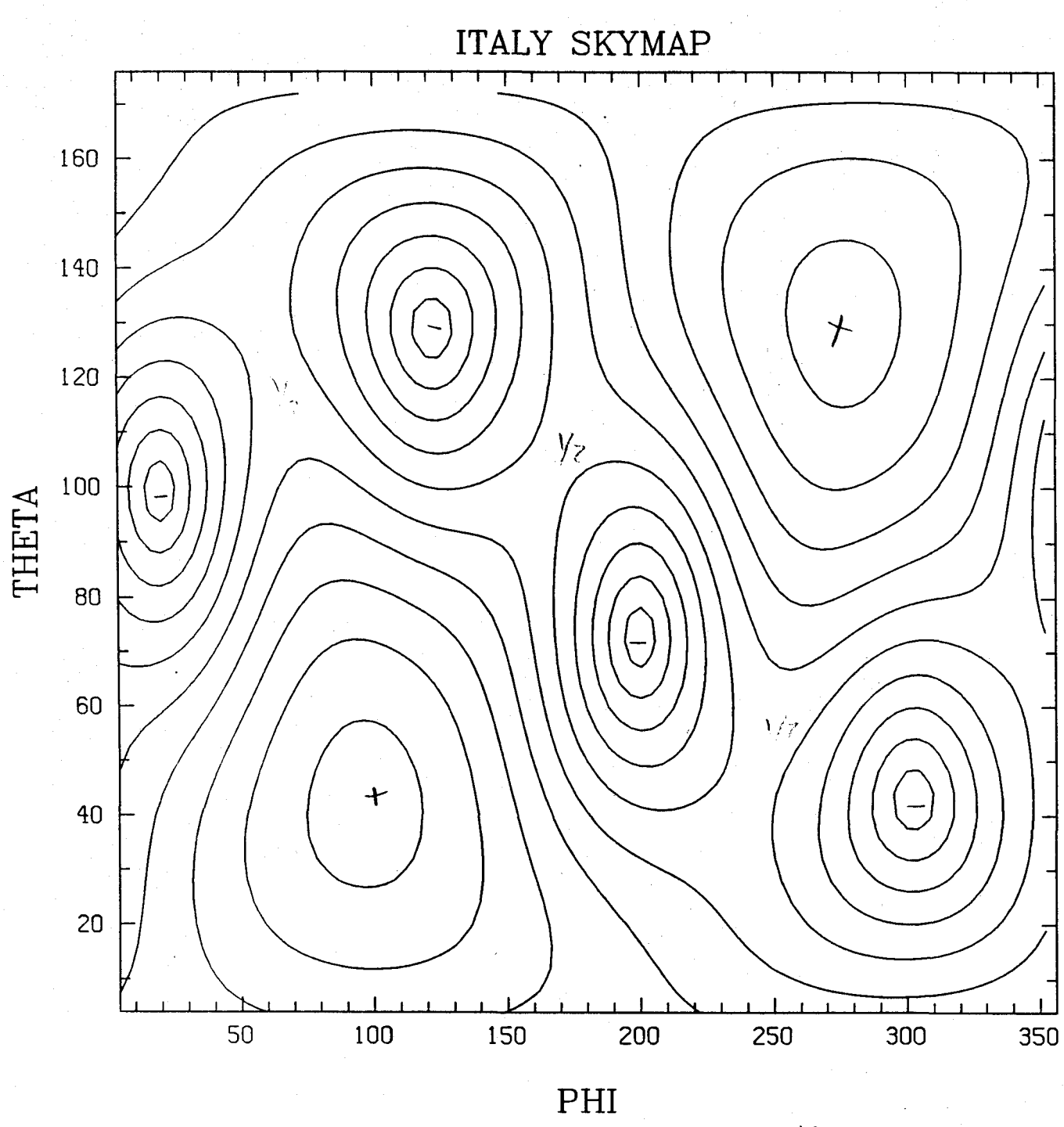
ITALY SKYMAP
THETA
PHI
160
140
120
100
80
60
40
20
50
100
150
200
250
300
350
+
−
−
+
−

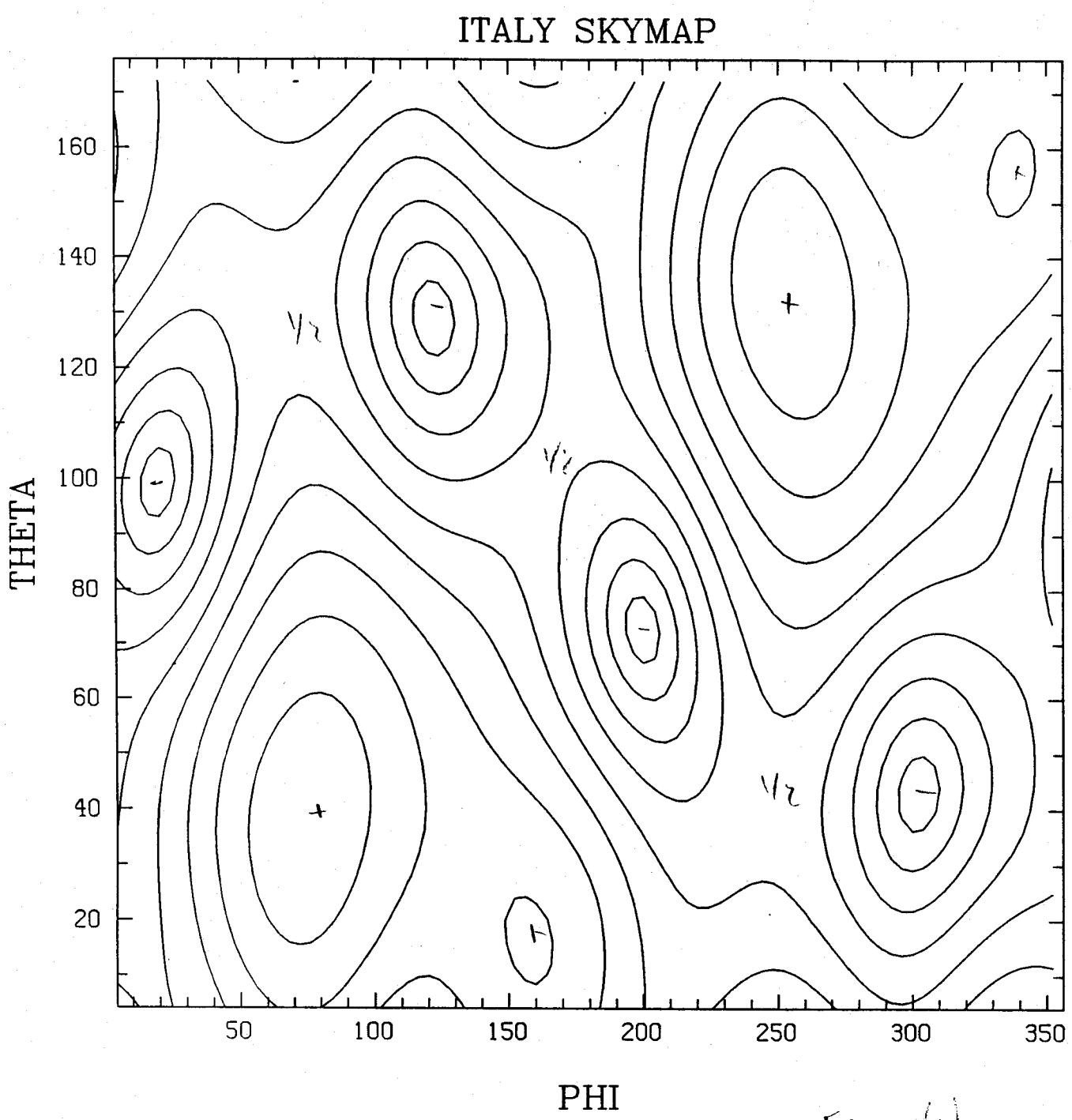

GEOMETRICAL

$\Delta x = 0.8 h t$

Fig. n/g

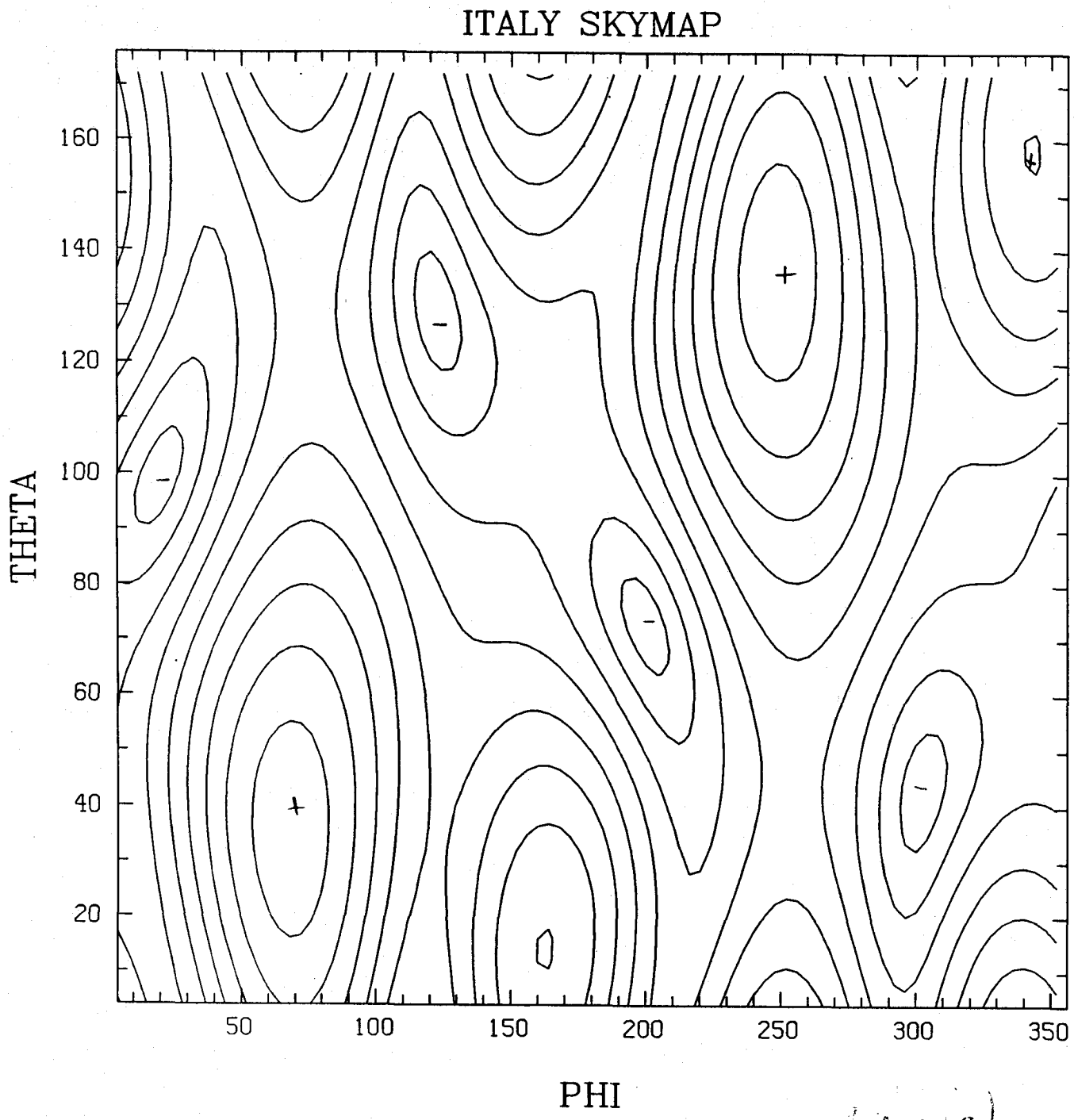

GEOMETRICAL

$h_x = 0.5\, h_t$

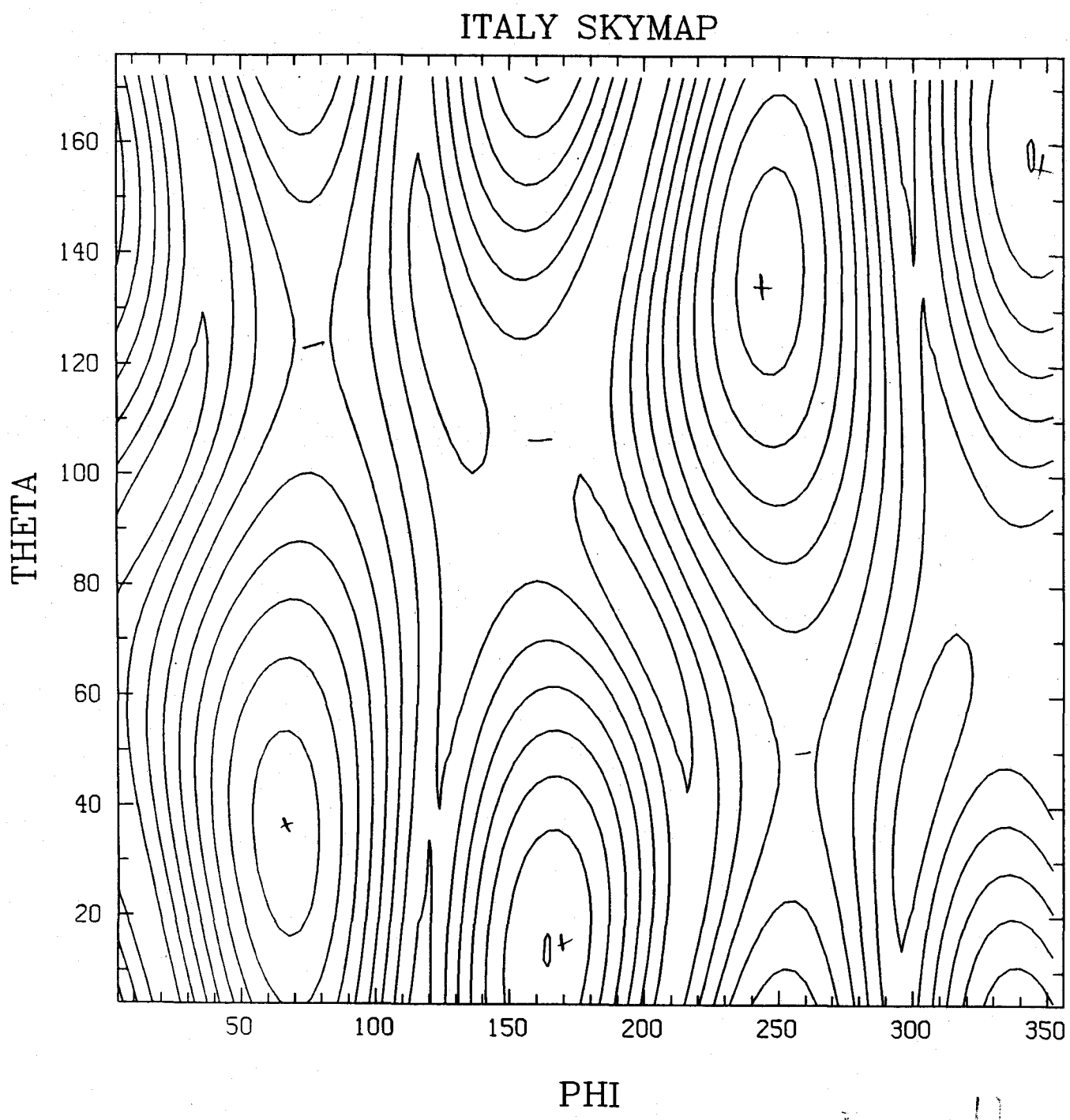

GEOMETRICAL

$\Delta x = 0.2\,\Delta t$.

GEOMETRICAL

$h_X = 0$

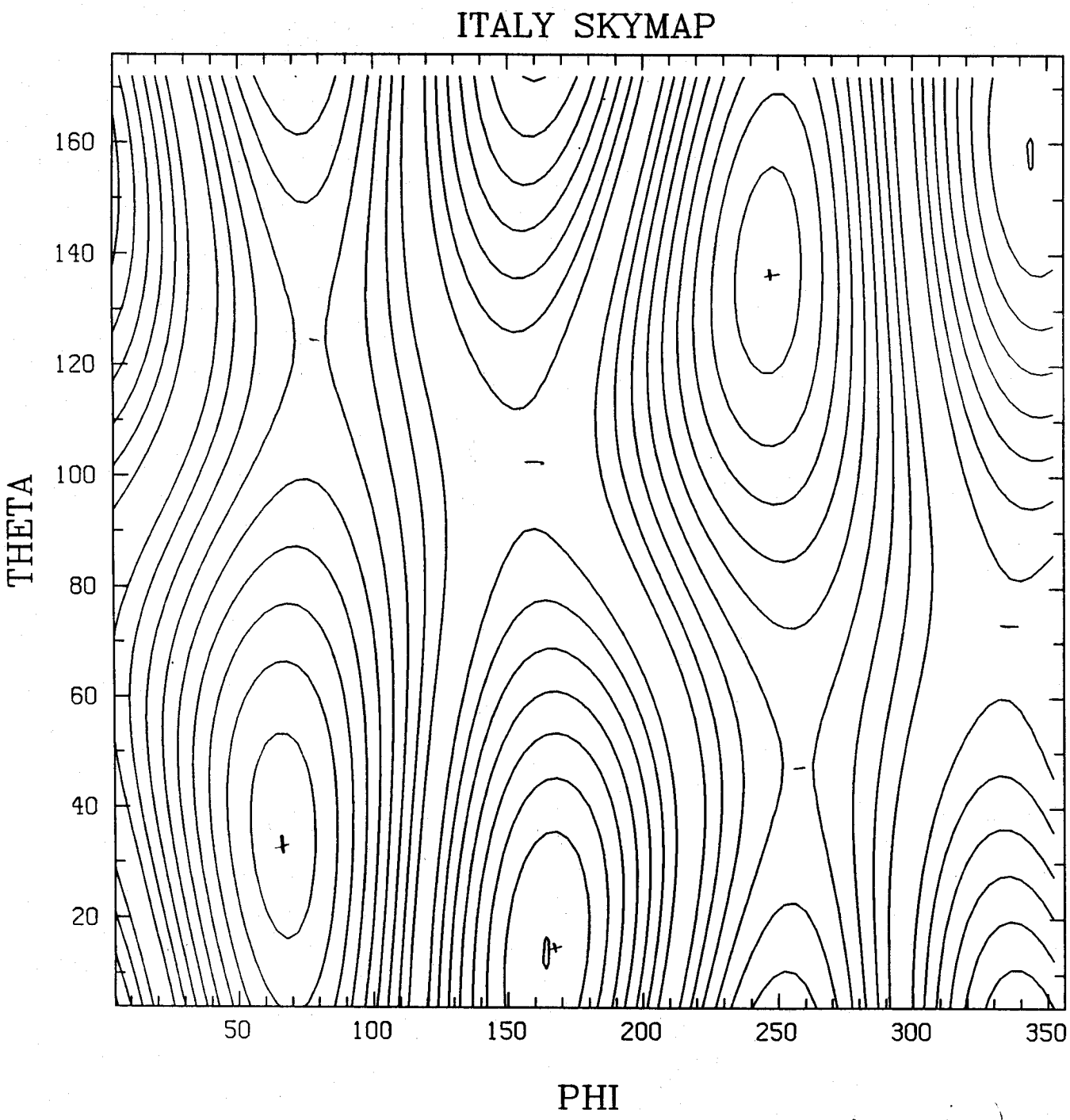

Figure 6)

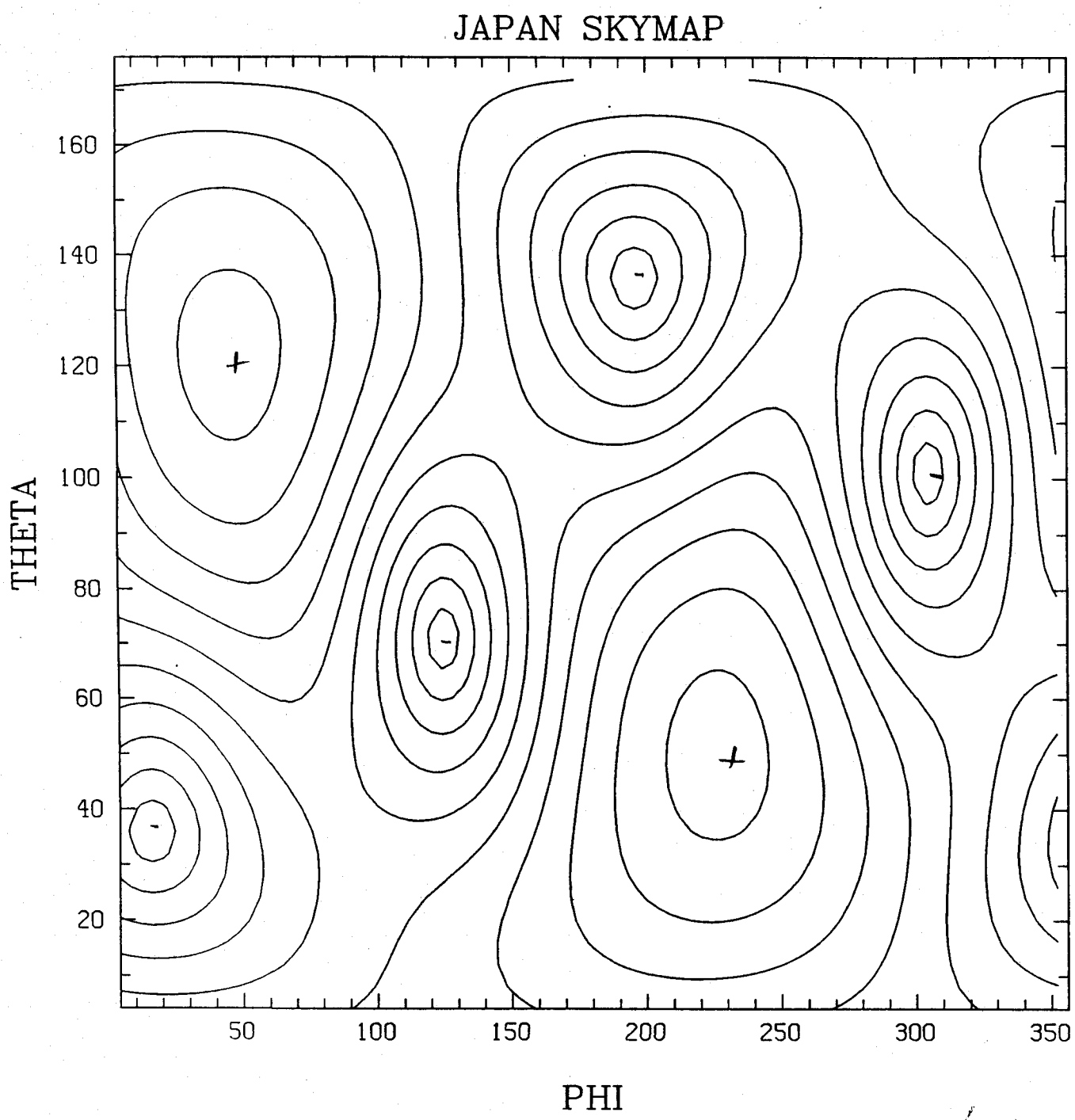

GEOMETRICAL

$h_+ = h_\times$

Fig. 12(a)

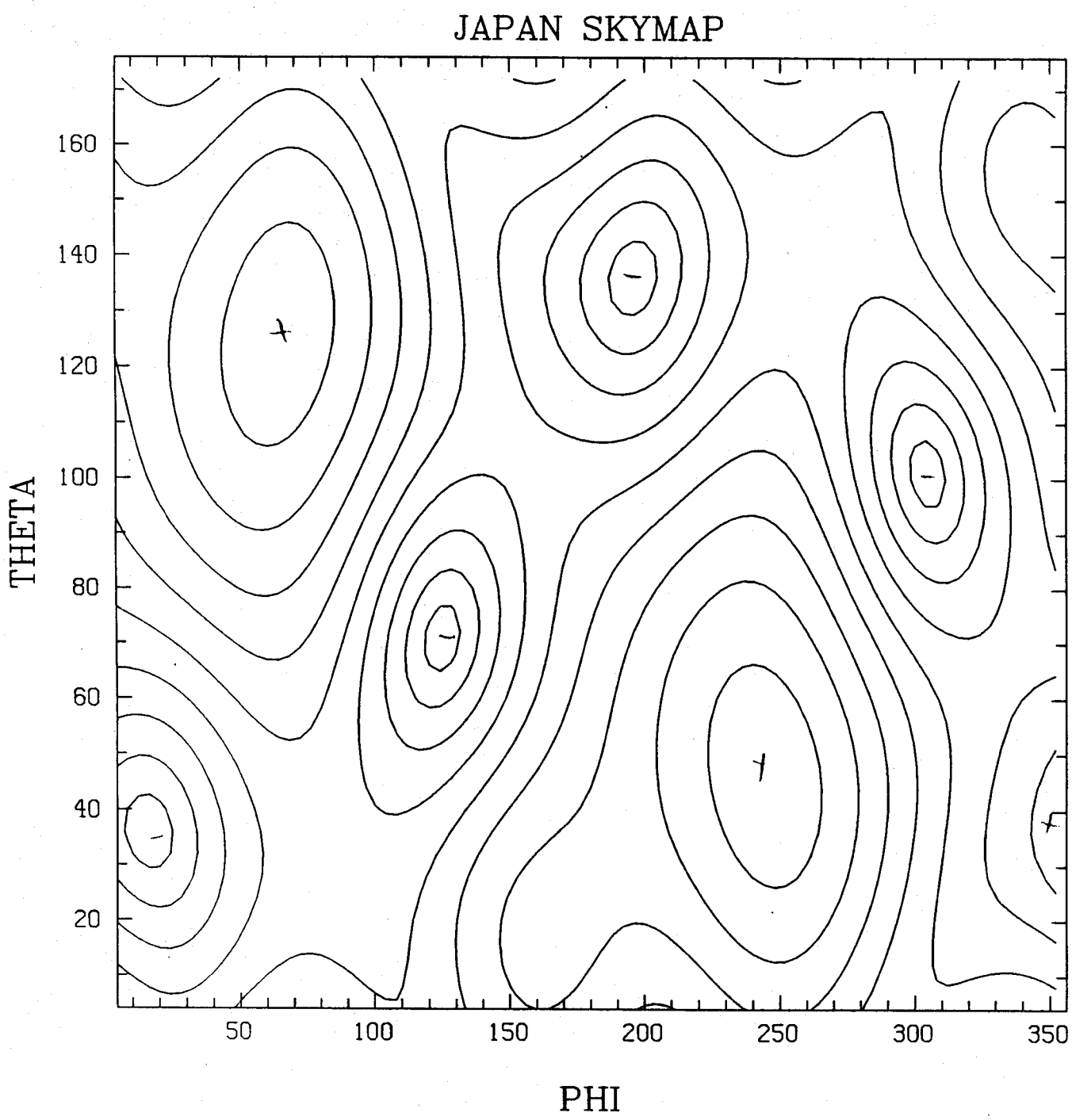

GEOMETRICAL

$l/x = 0.8\ l/t$.

Fig. (1)

GEOMETRICAL

hx=0.5ht.

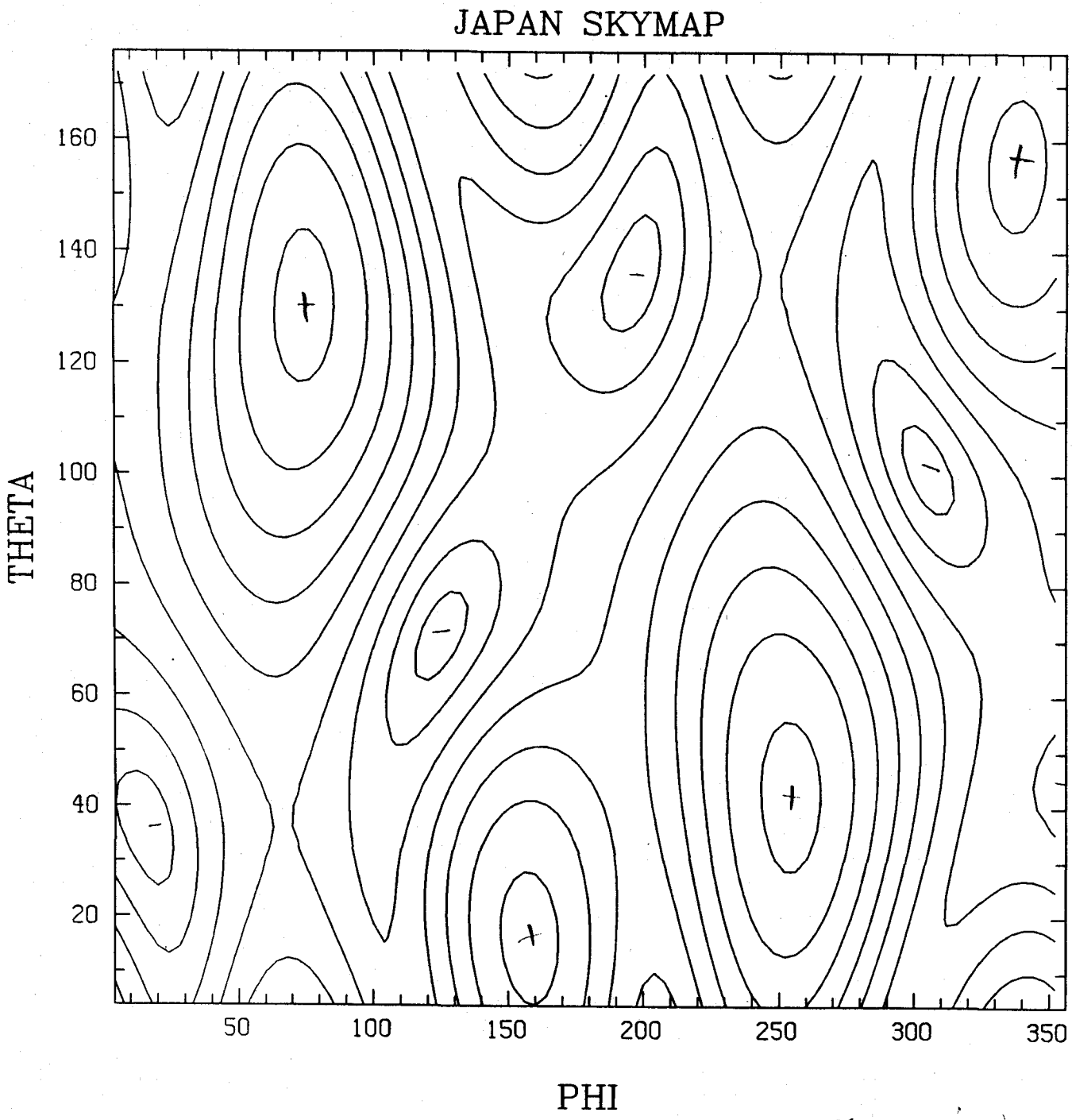

Figure 1

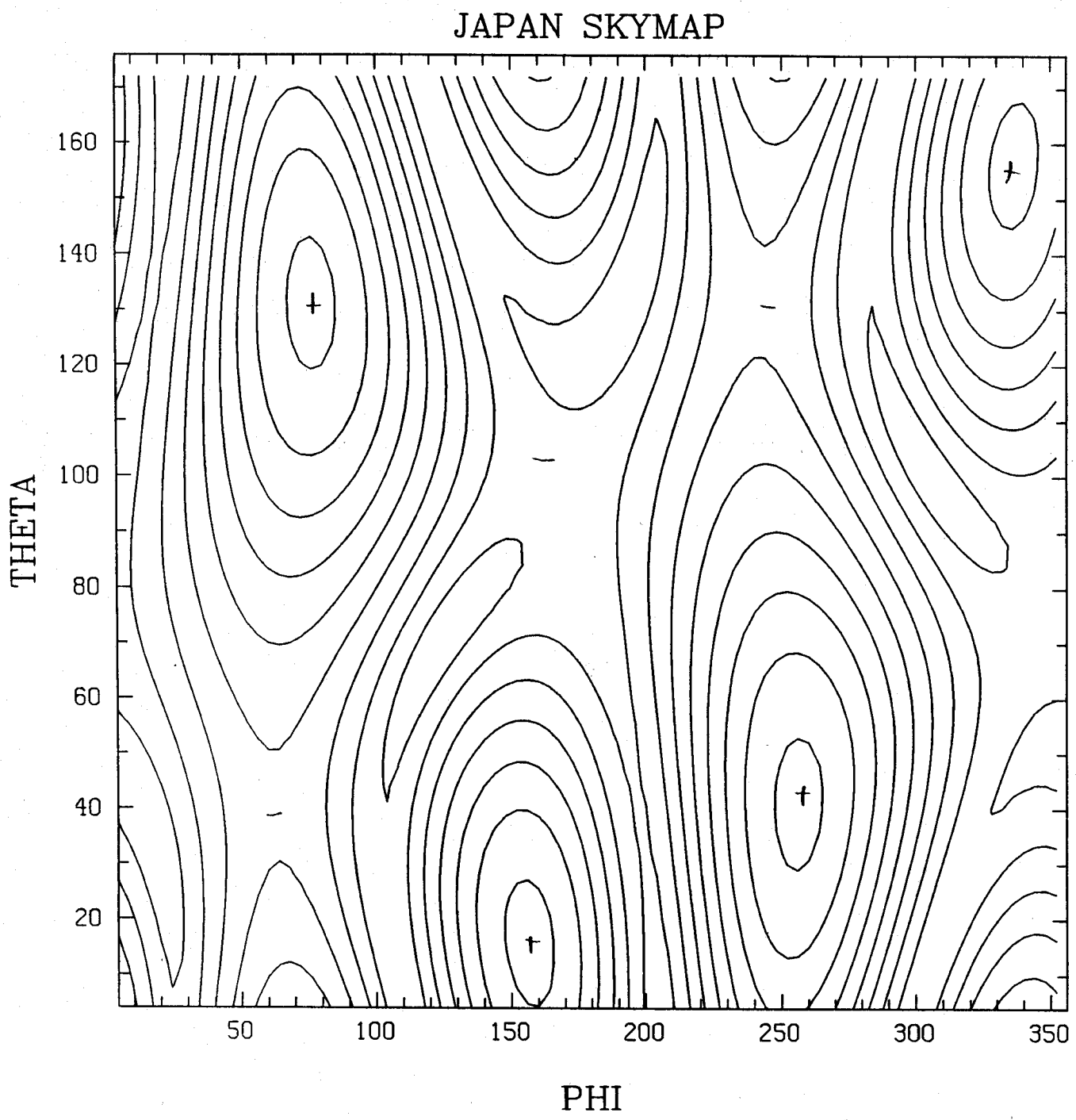

GEOMETRICAL

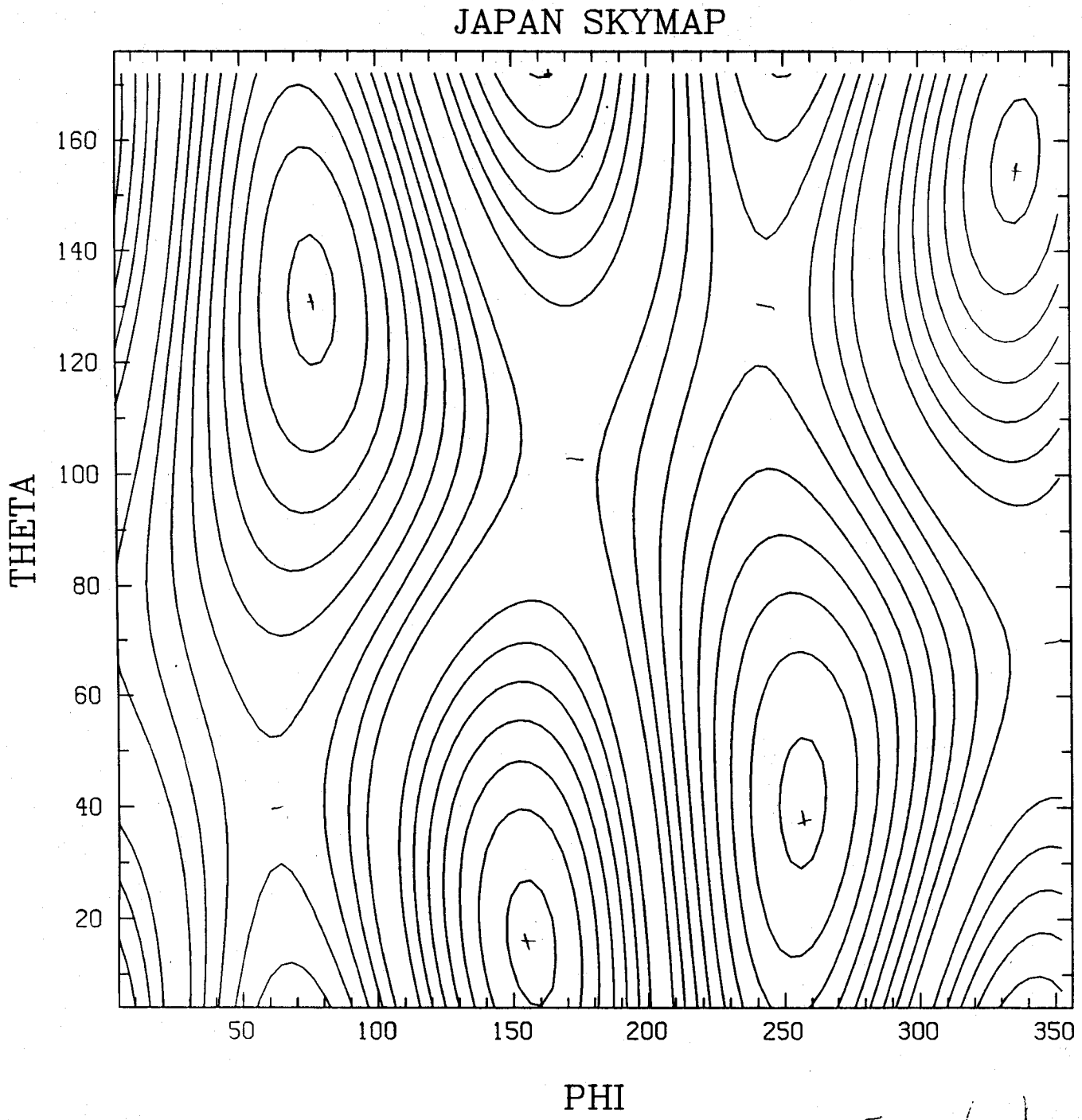

JAPAN

$h_x = 0$

Fig 12(e)

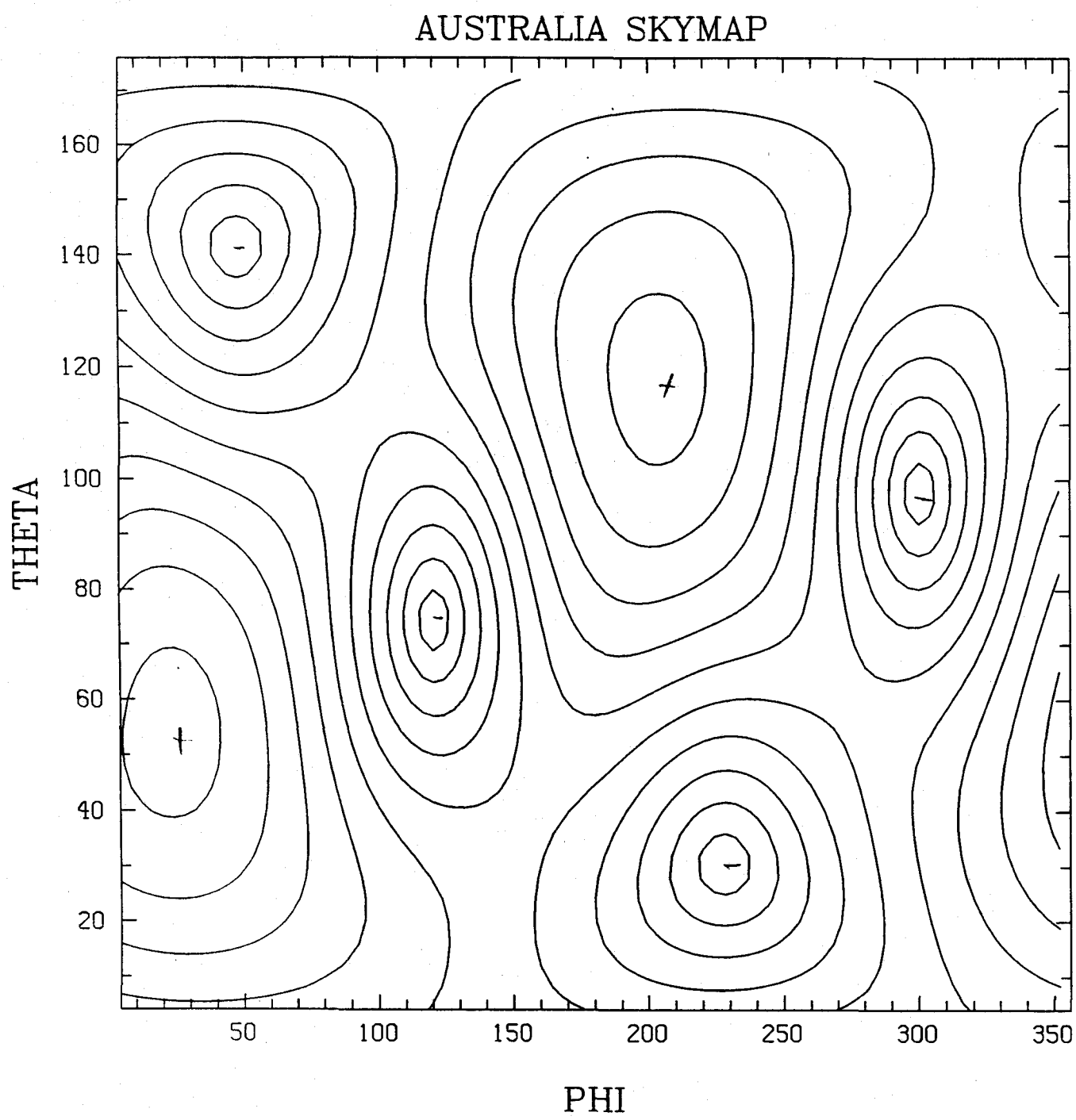

GEOMETRICAL
$h_+ = h_\times$.

GEOMETRICAL

$k_x = 0.8 k_+$

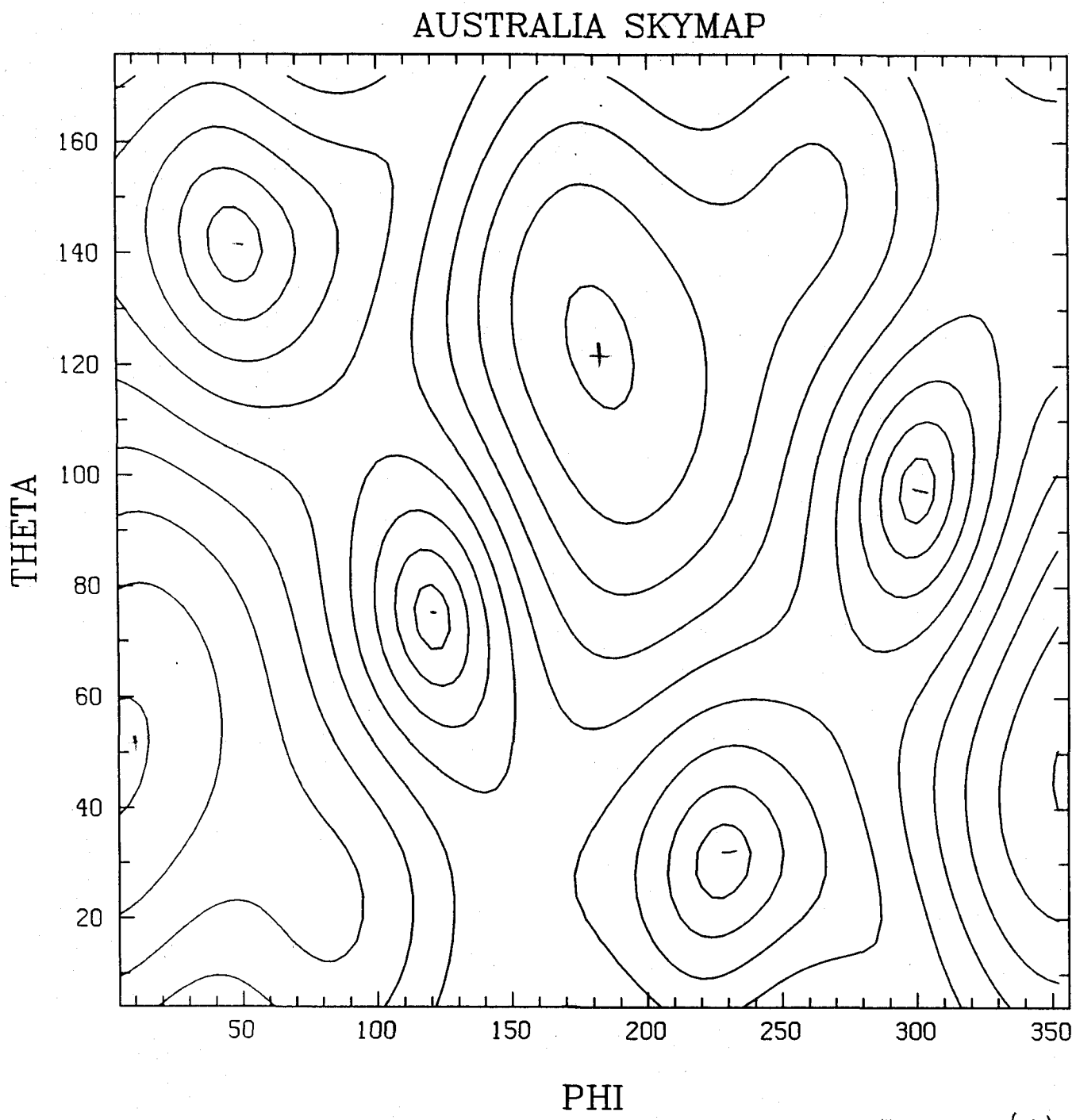

Fig. 13(1)

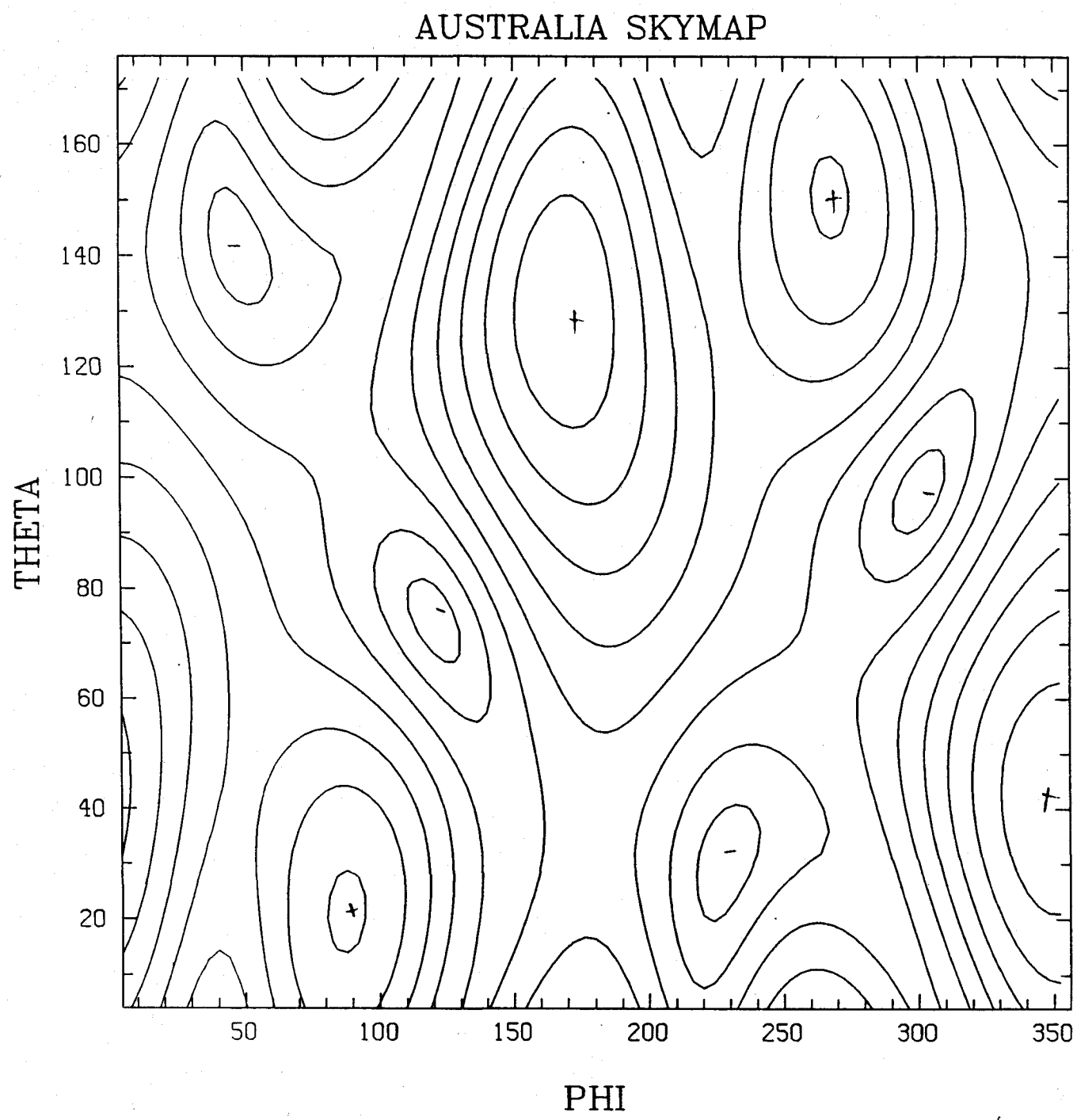

GEOMETRICAL

$\mu_{X=0} = \mu_+$

Fig. 12(c)

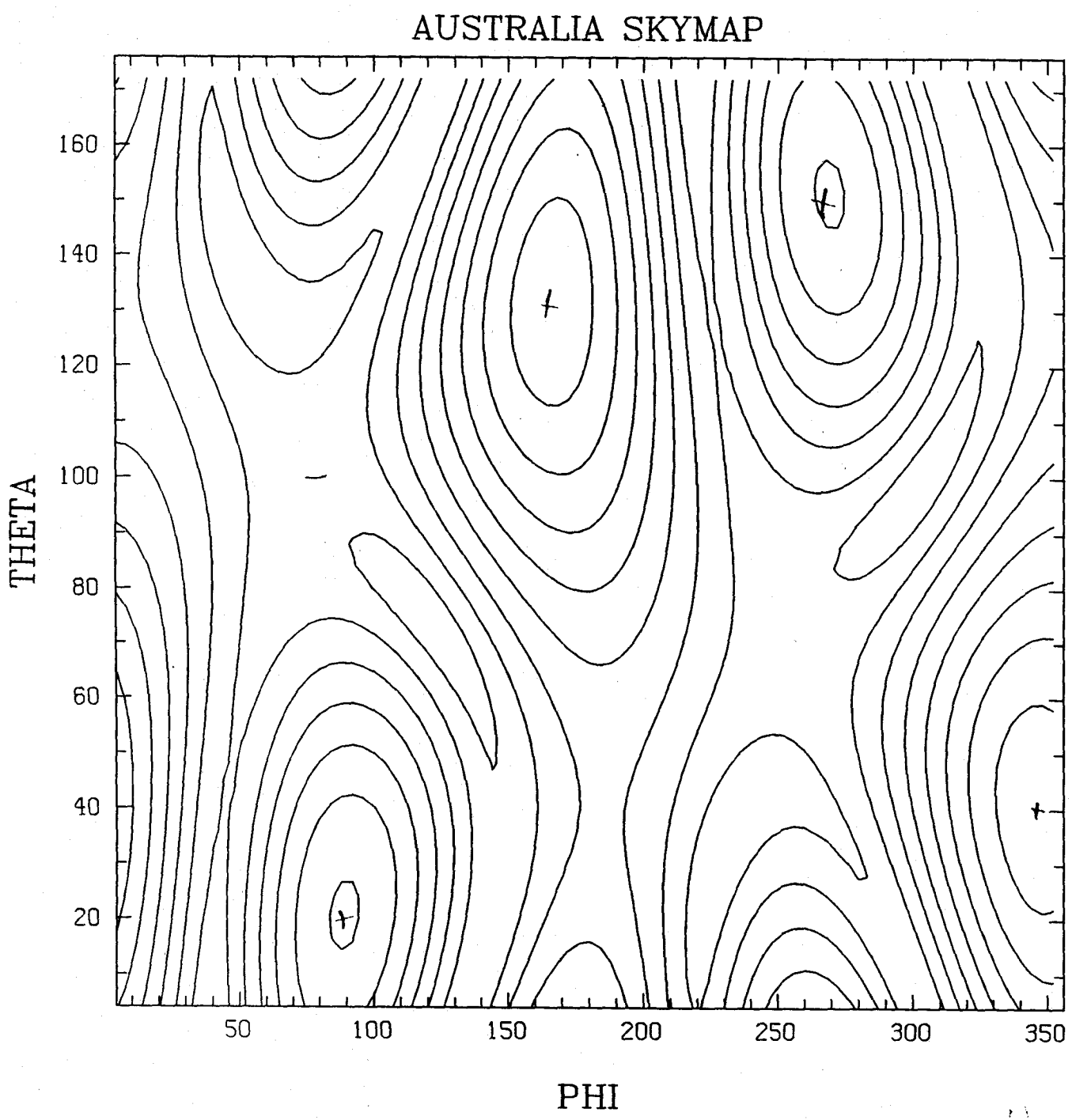

GEOMETRICAL

$h_x = 0.2\,h_t$

Fig. 12(d)

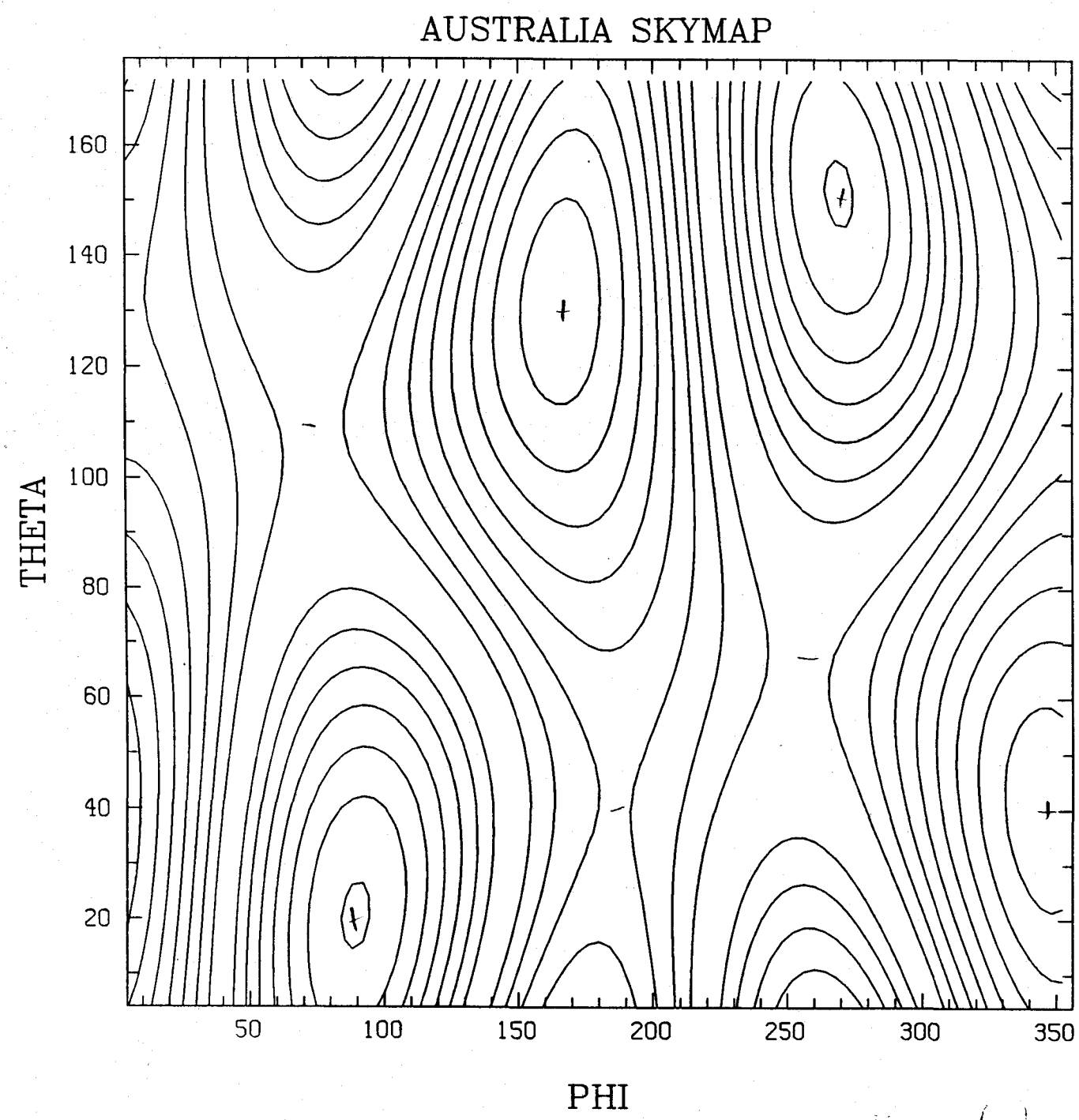

GEOMETRICAL

$h_x = 0$

Figure 1

CALIF

Variex = ON

hr = hx

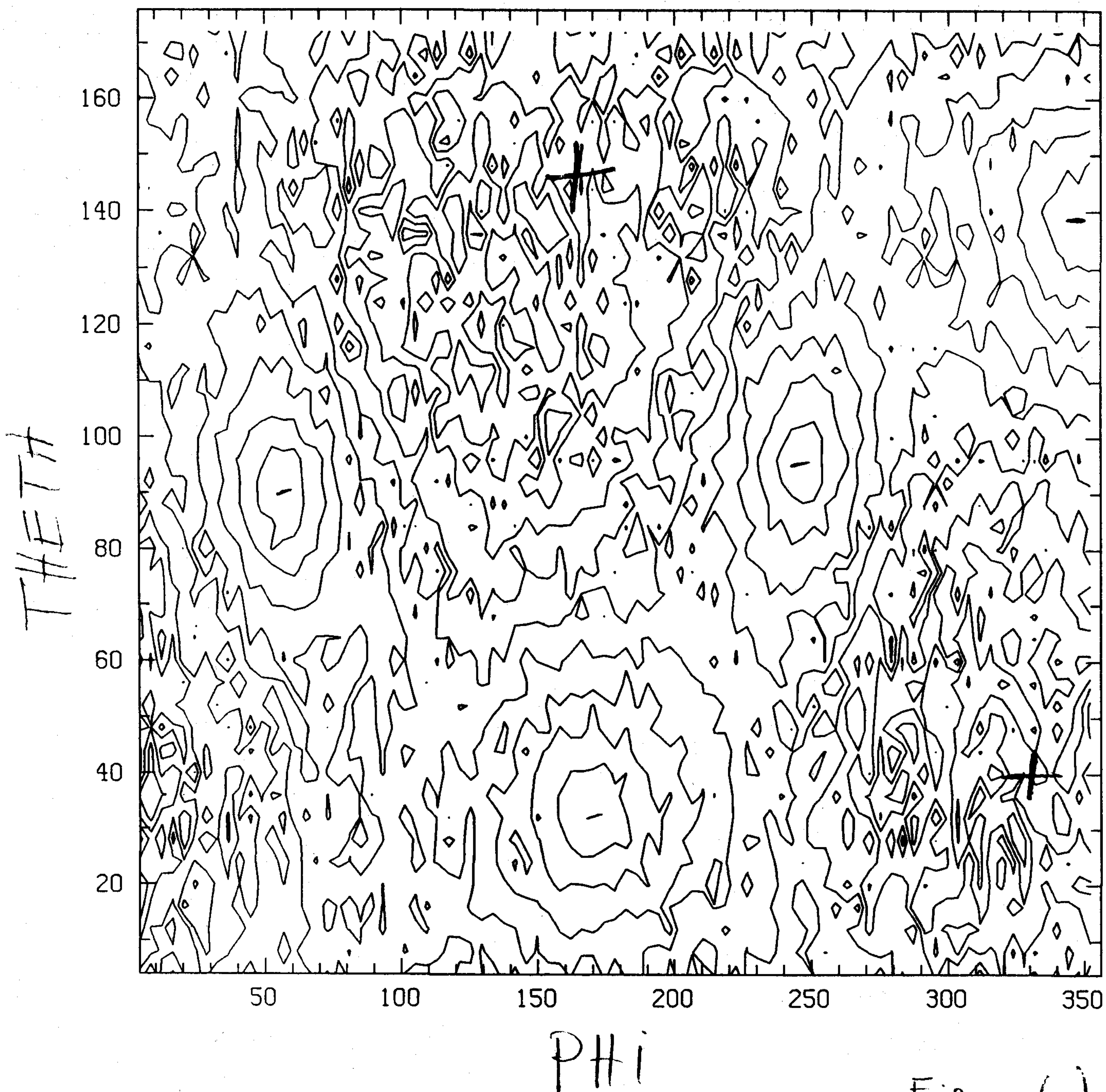

Fig 14(a)

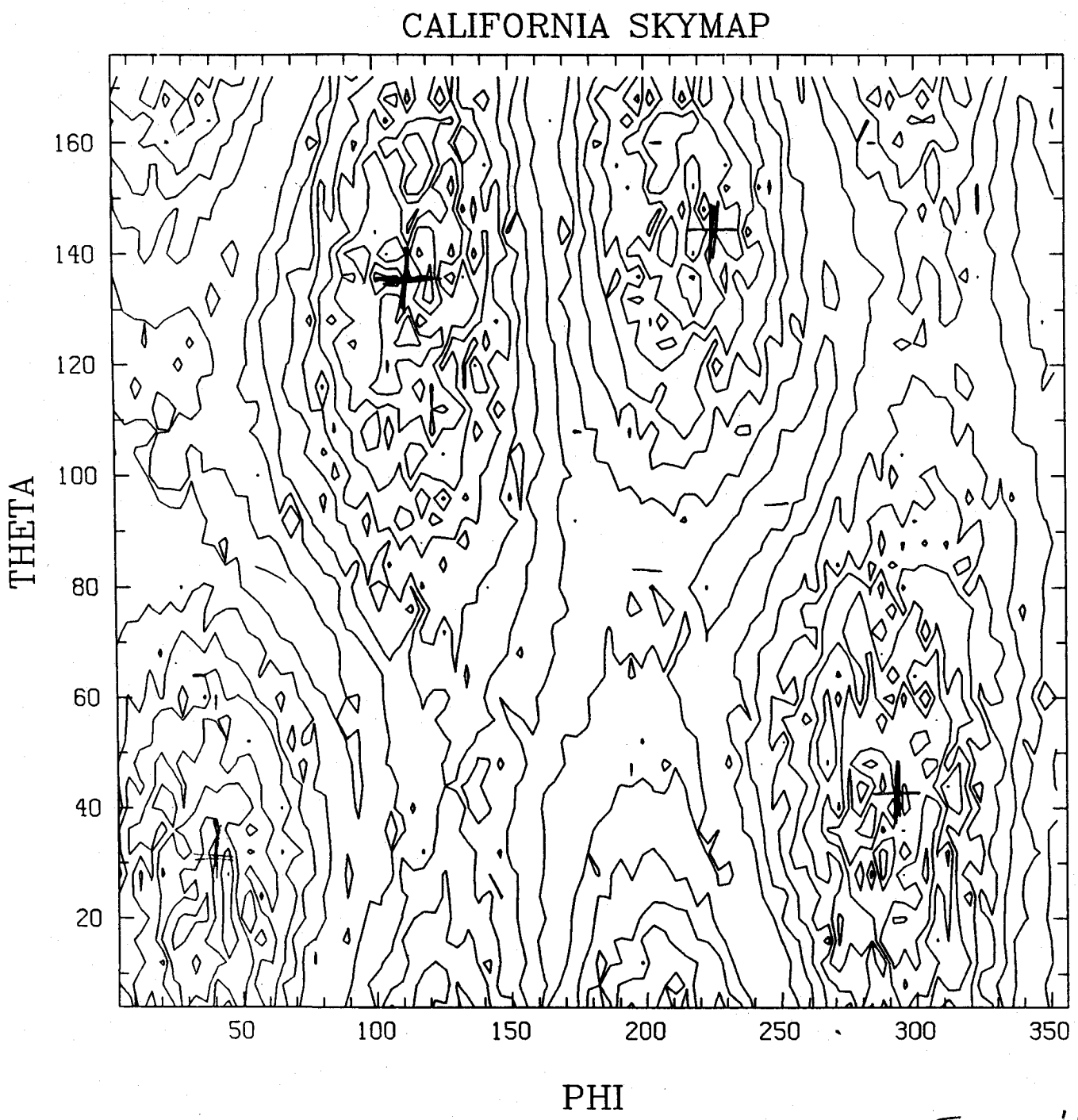
CALIFORNIA SKYMAP
THETA
PHI
160
140
120
100
80
60
40
20
50
100
150
200
250
300
350

Fig. 14(b)

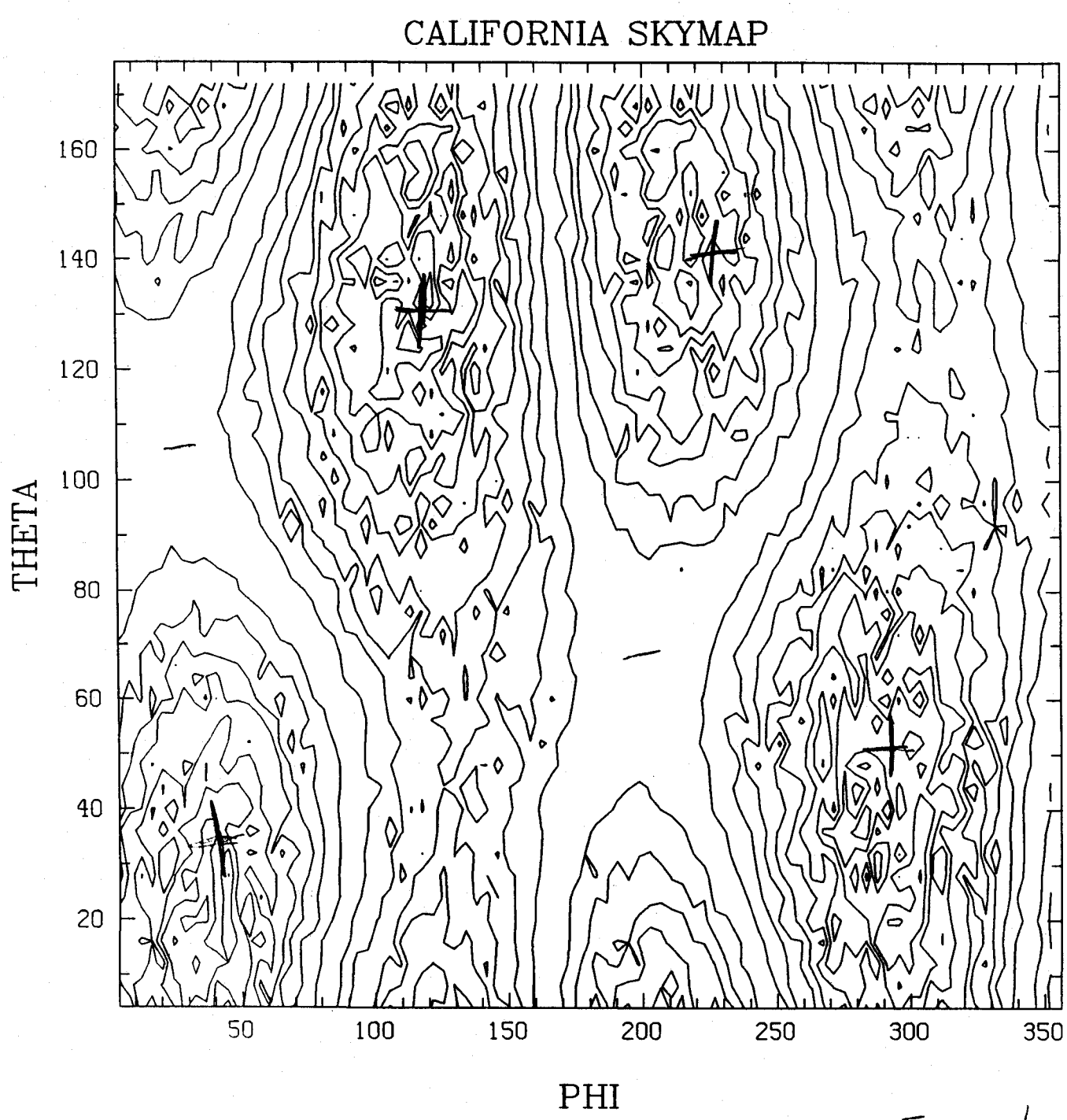
CALIFORNIA SKYMAP
THETA
PHI
160
140
120
100
80
60
40
20
50
100
150
200
250
300
350

Fig. 14(c)

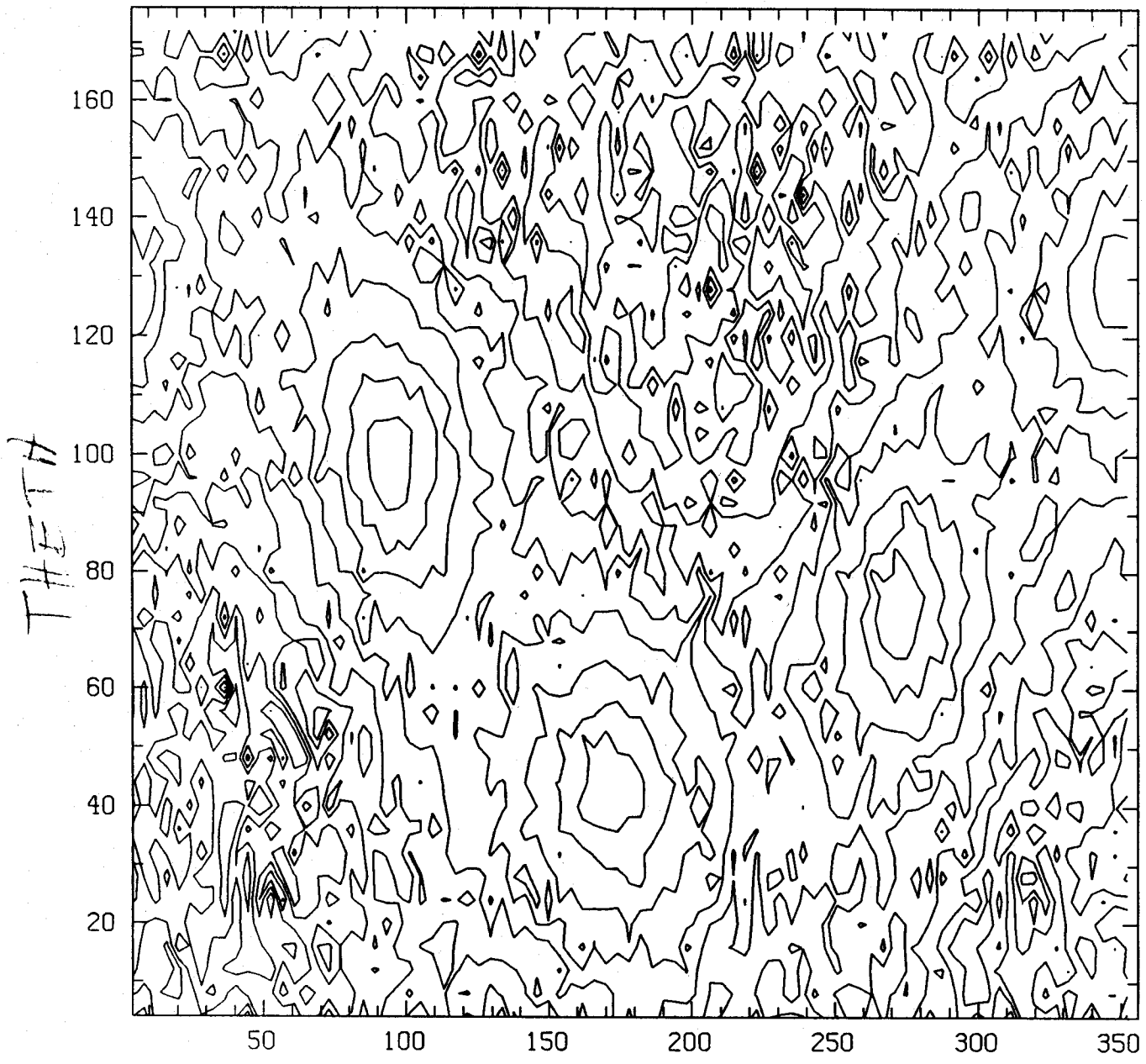

Fig. 15(a)

NOISE = ON

hx = 0.2

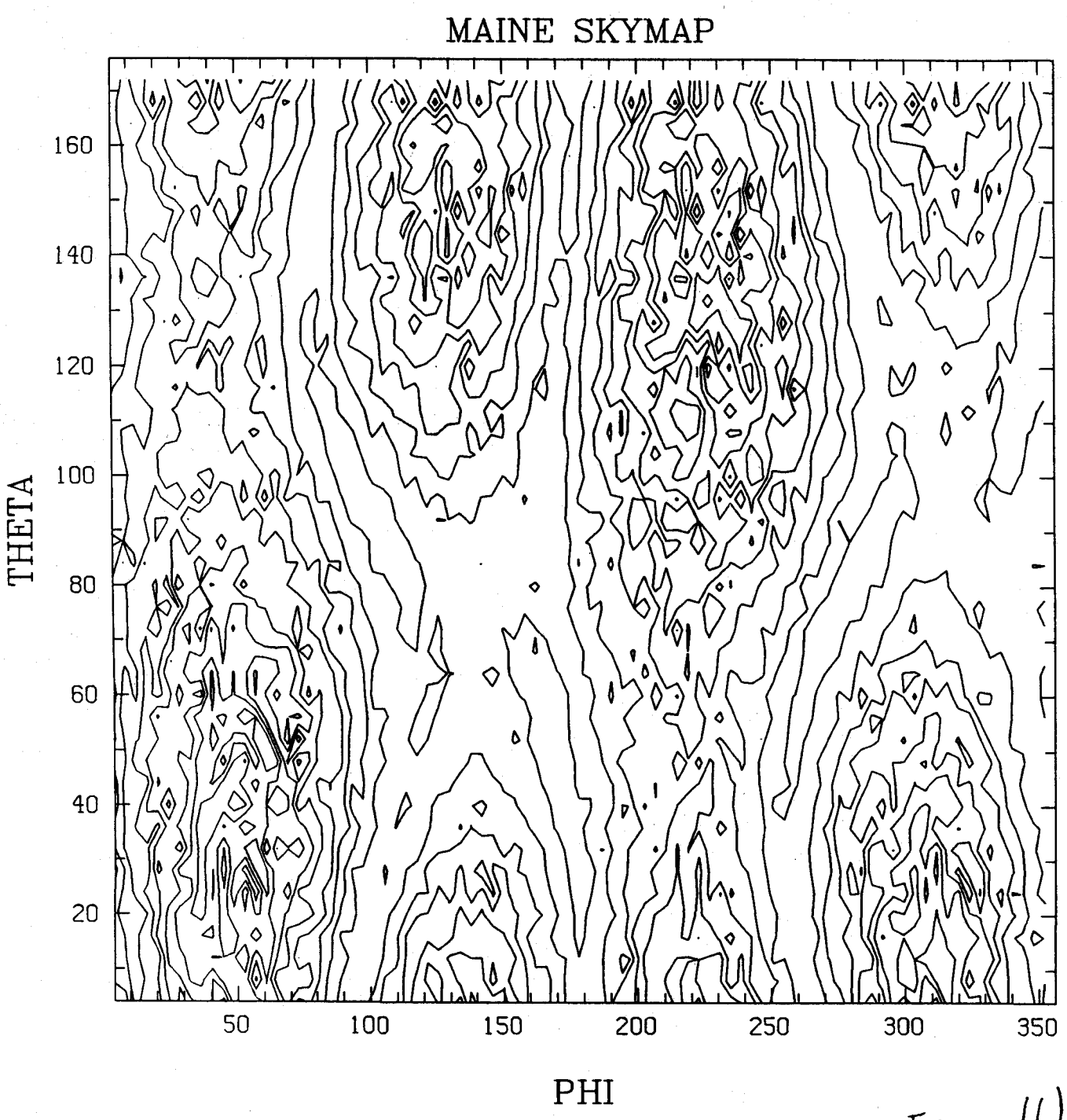

Fig. 15(b)

Noise = on

hx = 0

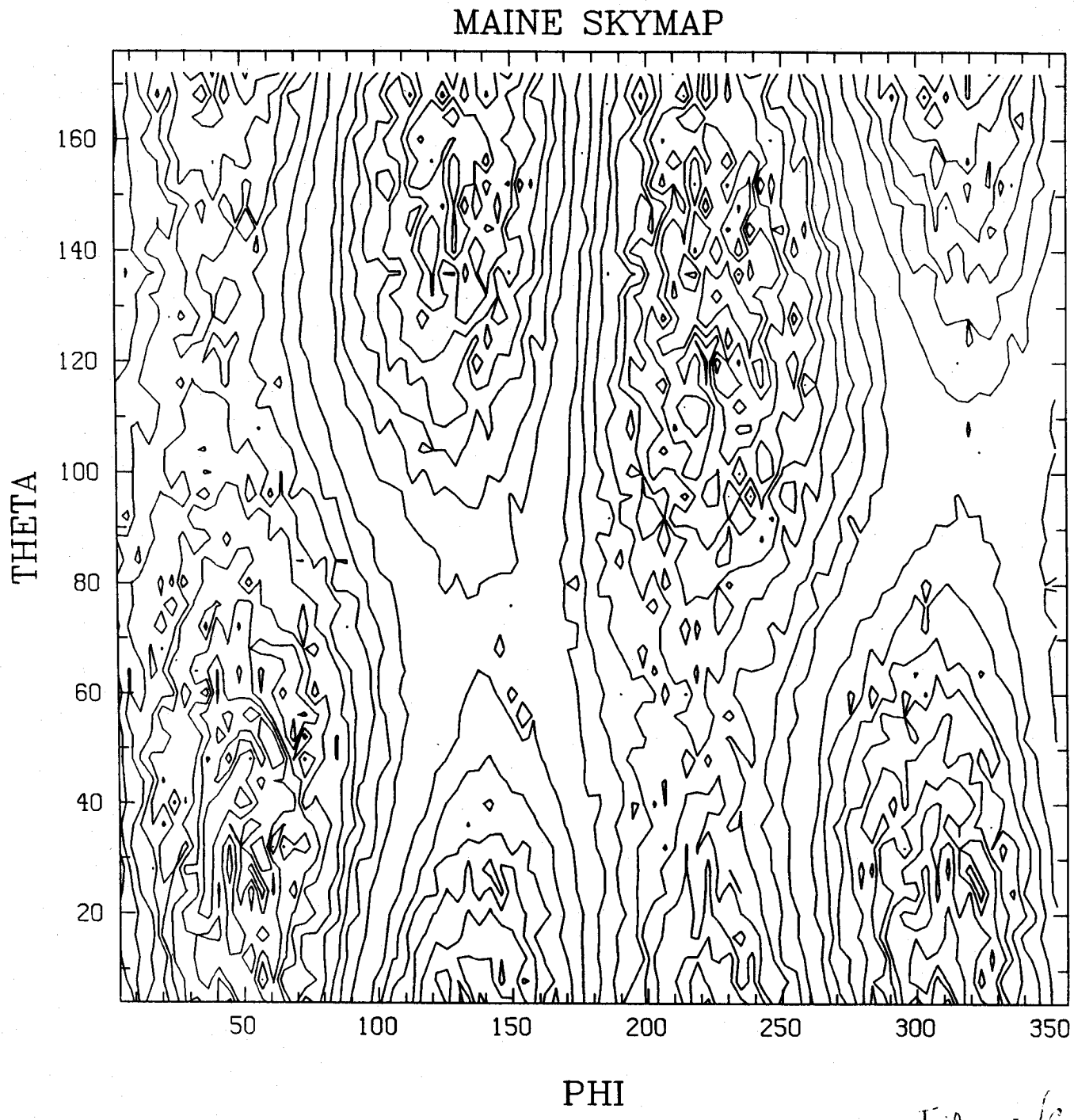

Fig. 15 (a)

GERM

Noise = on

h+ = h x

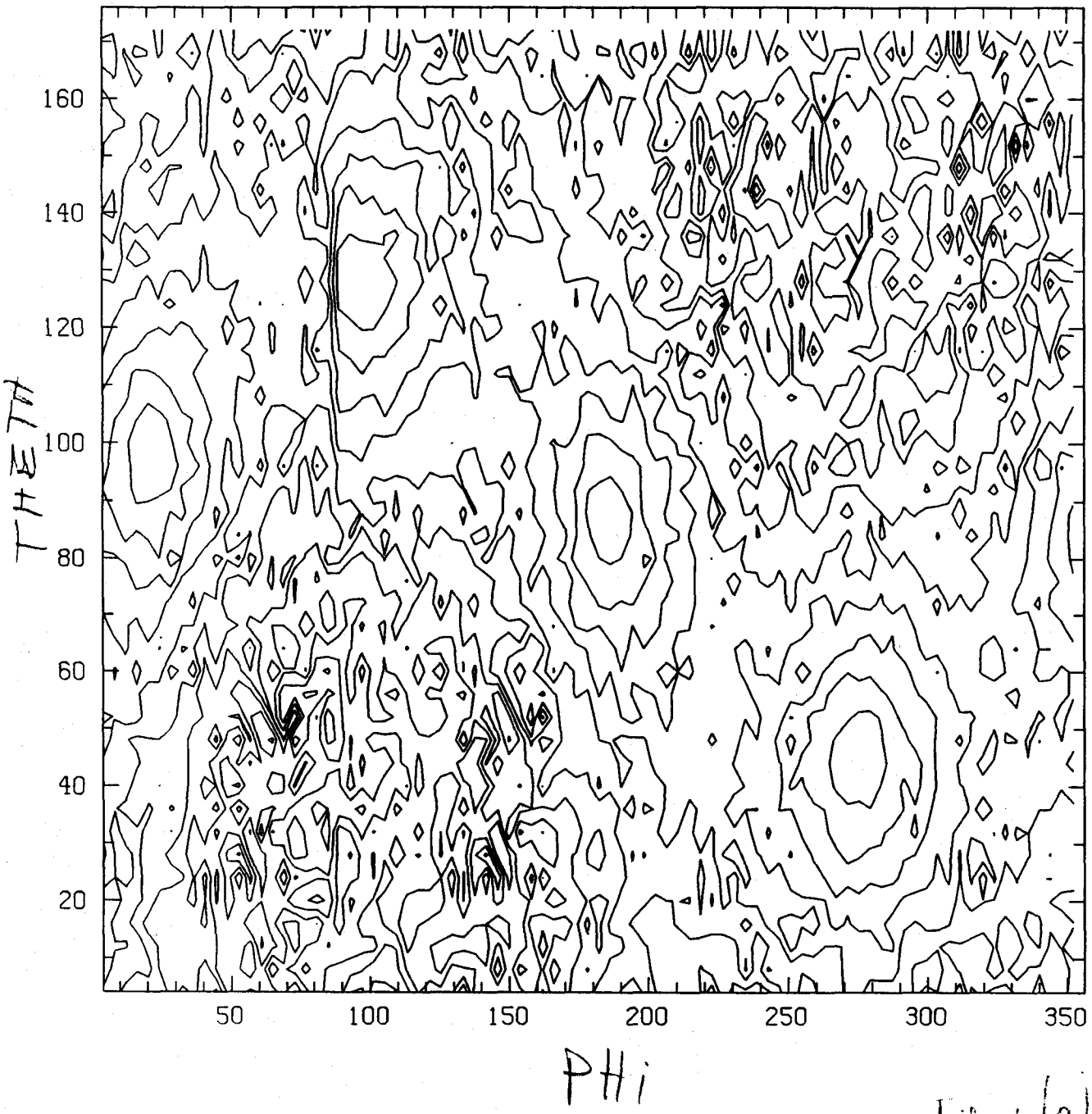

Fig. 16(a)

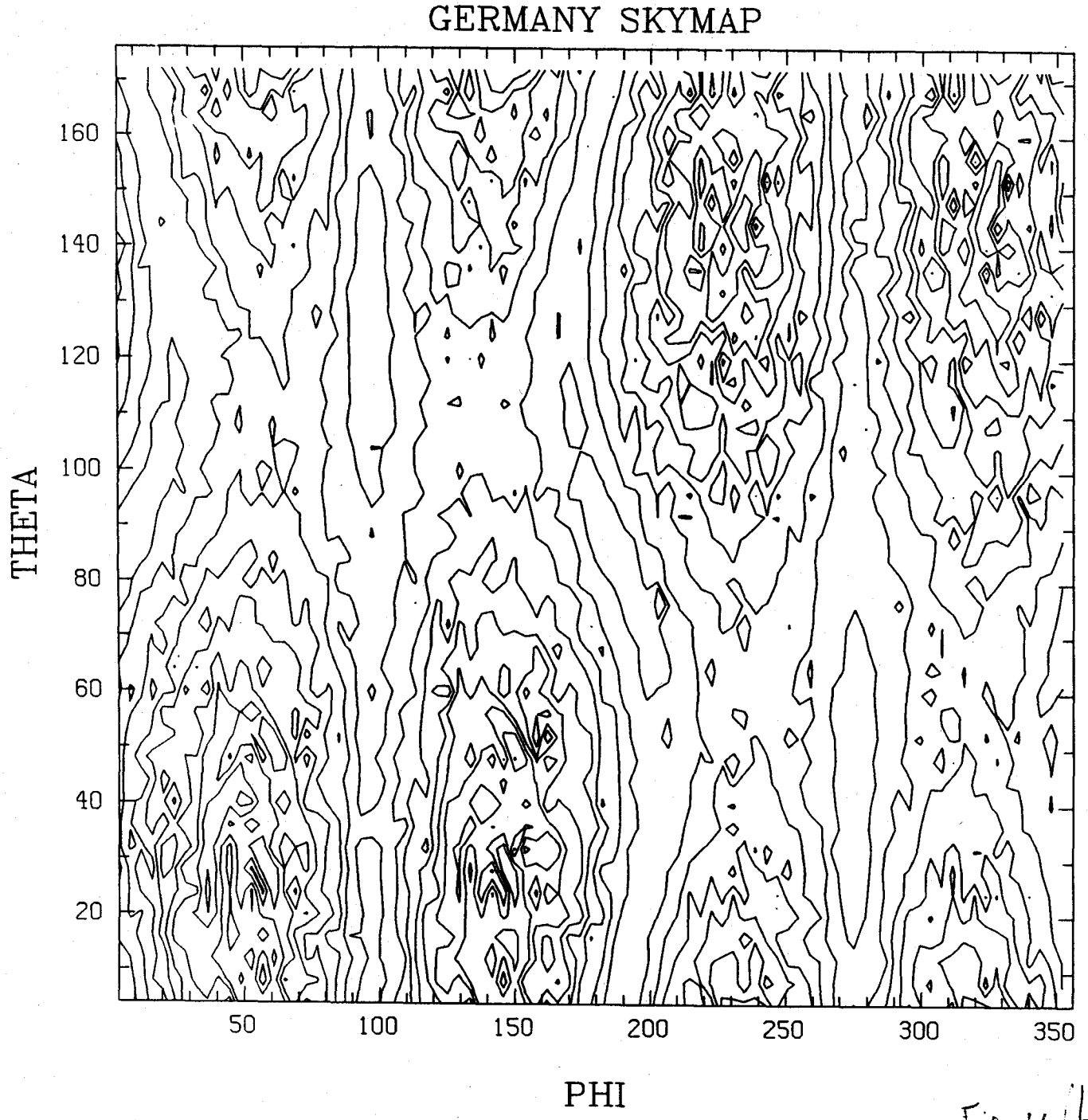
GERMANY SKYMAP
THETA
160
140
120
100
80
60
40
20
50
100
150
200
250
300
350
PHI

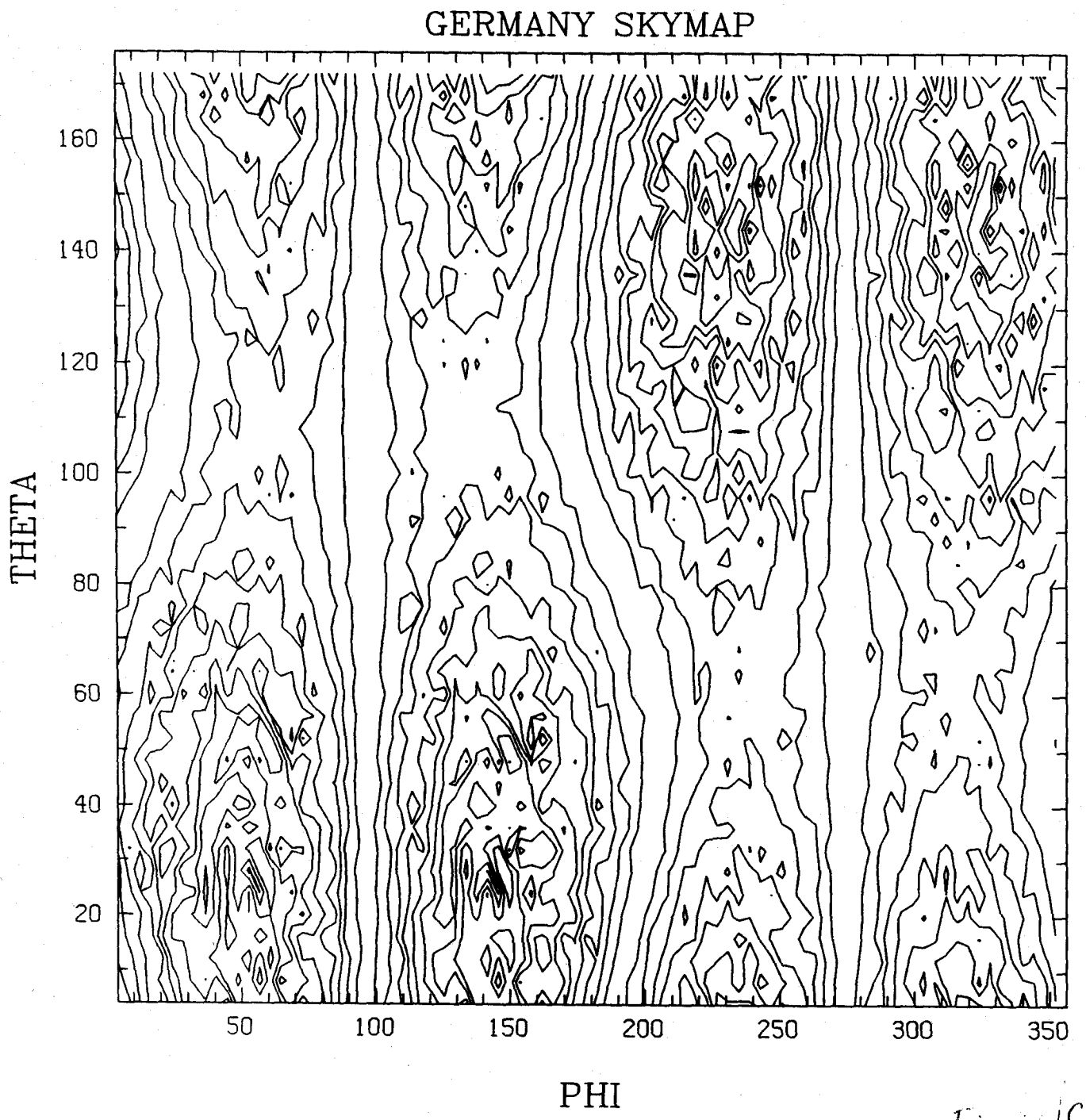
GERMANY SKYMAP
THETA
160
140
120
100
80
60
40
20
50
100
150
200
250
300
350
PHI

NOISE = ON

Ux = 0

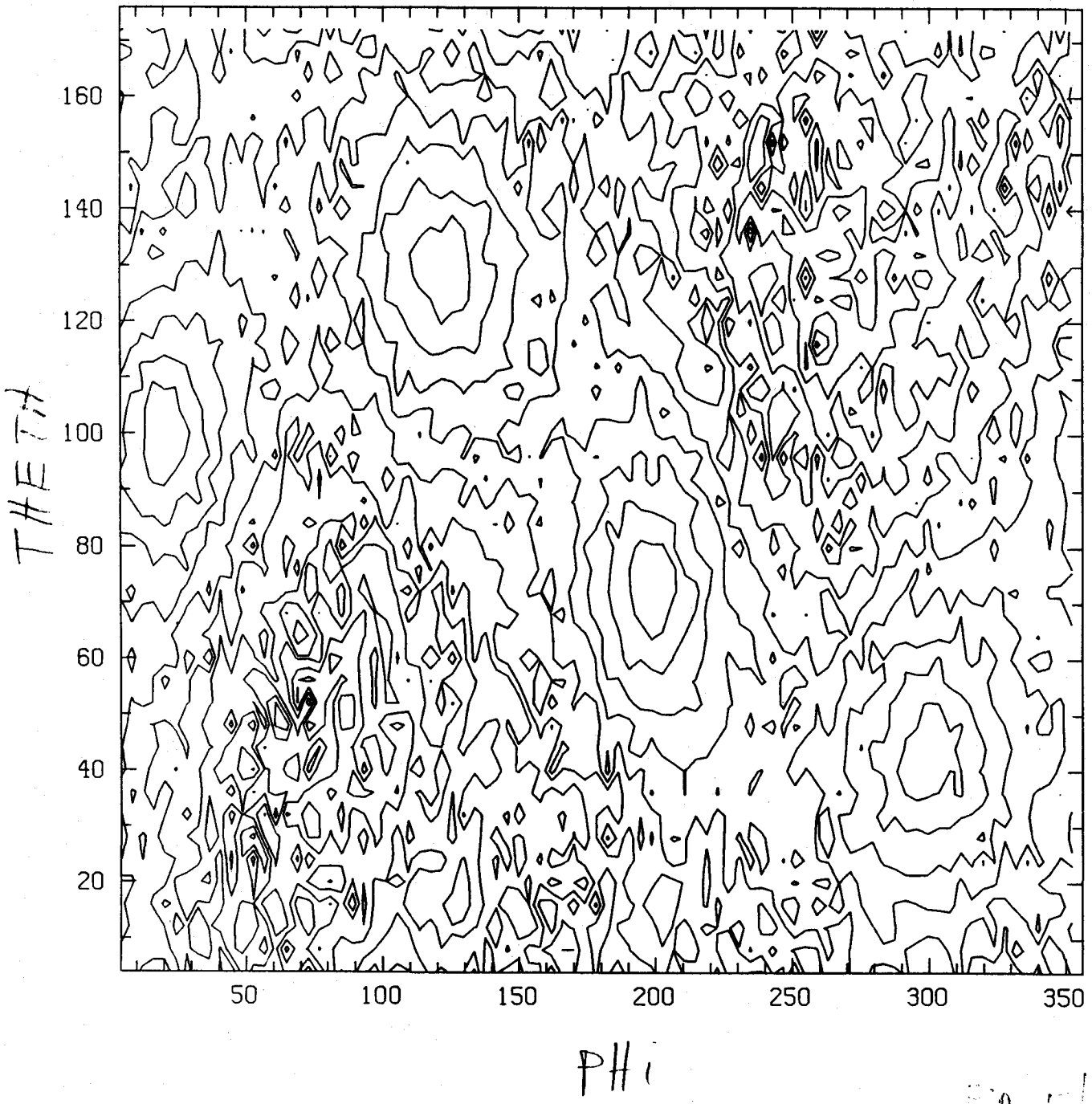

ITALY

NOISE = ON

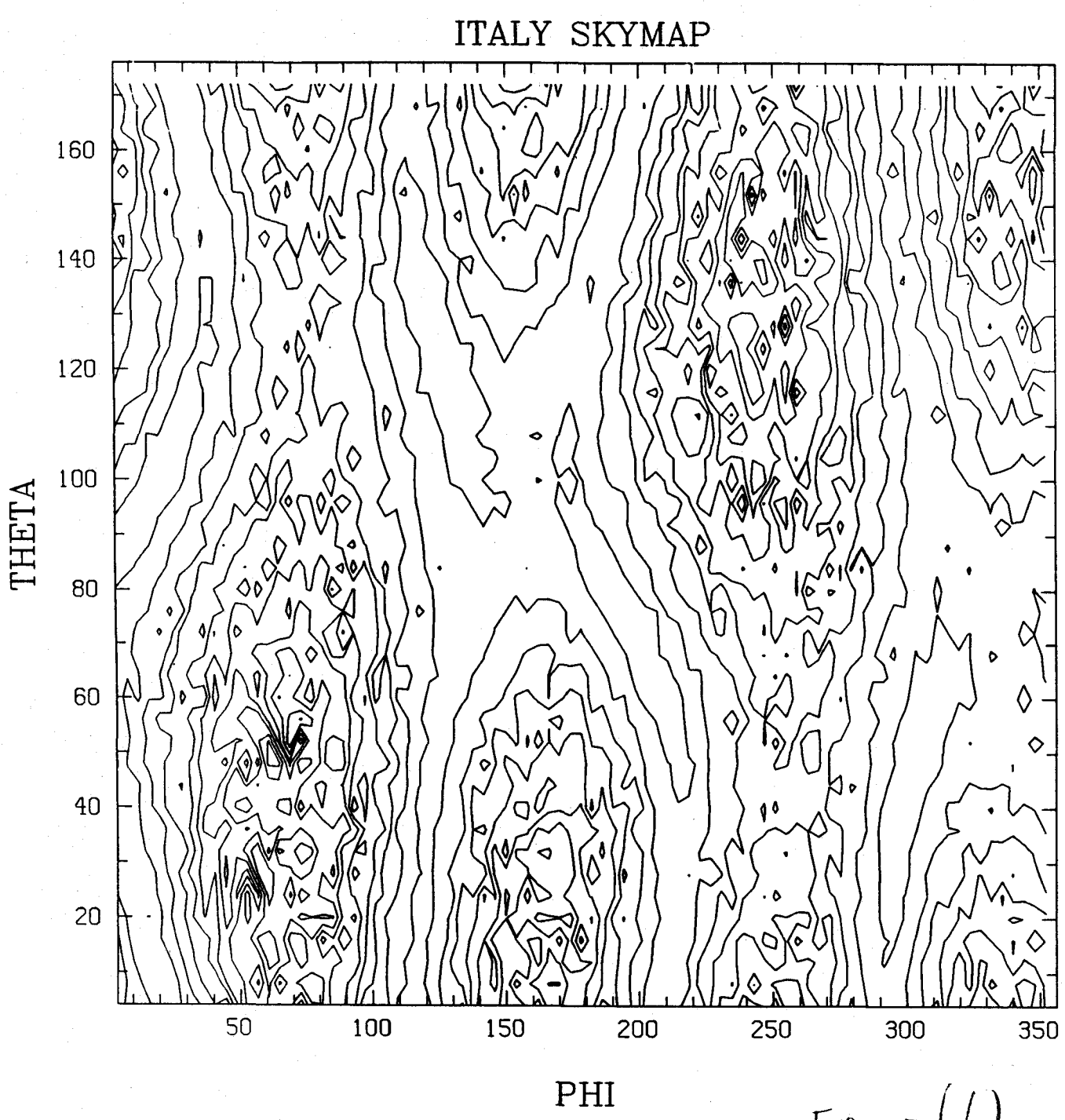

Noise = 0 V

Fig. 17 (5)

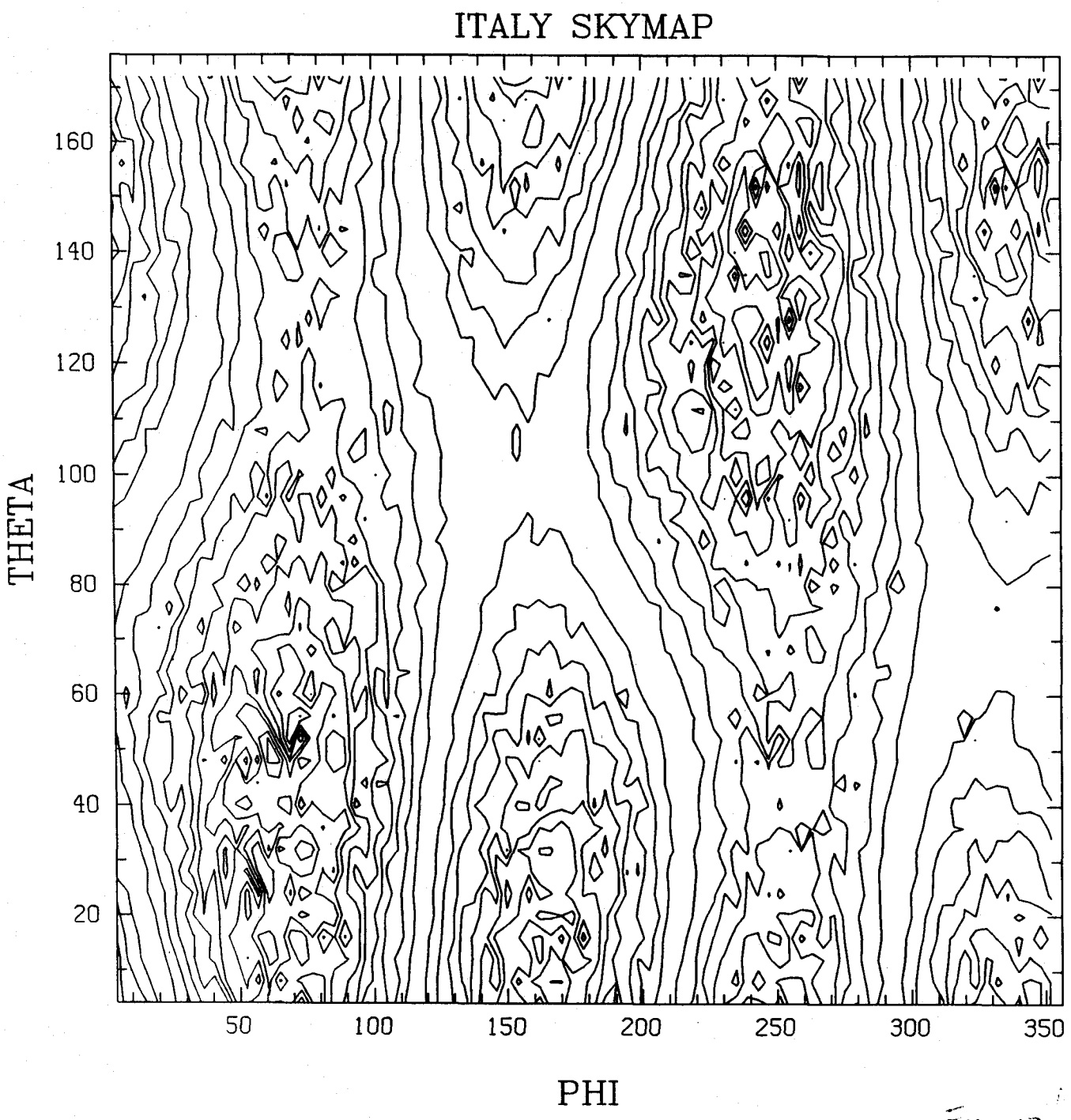
ITALY SKYMAP
THETA
160
140
120
100
80
60
40
20
50
100
150
200
250
300
350
PHI

JAPAN

Noise - on

$h_+ - h_\times$

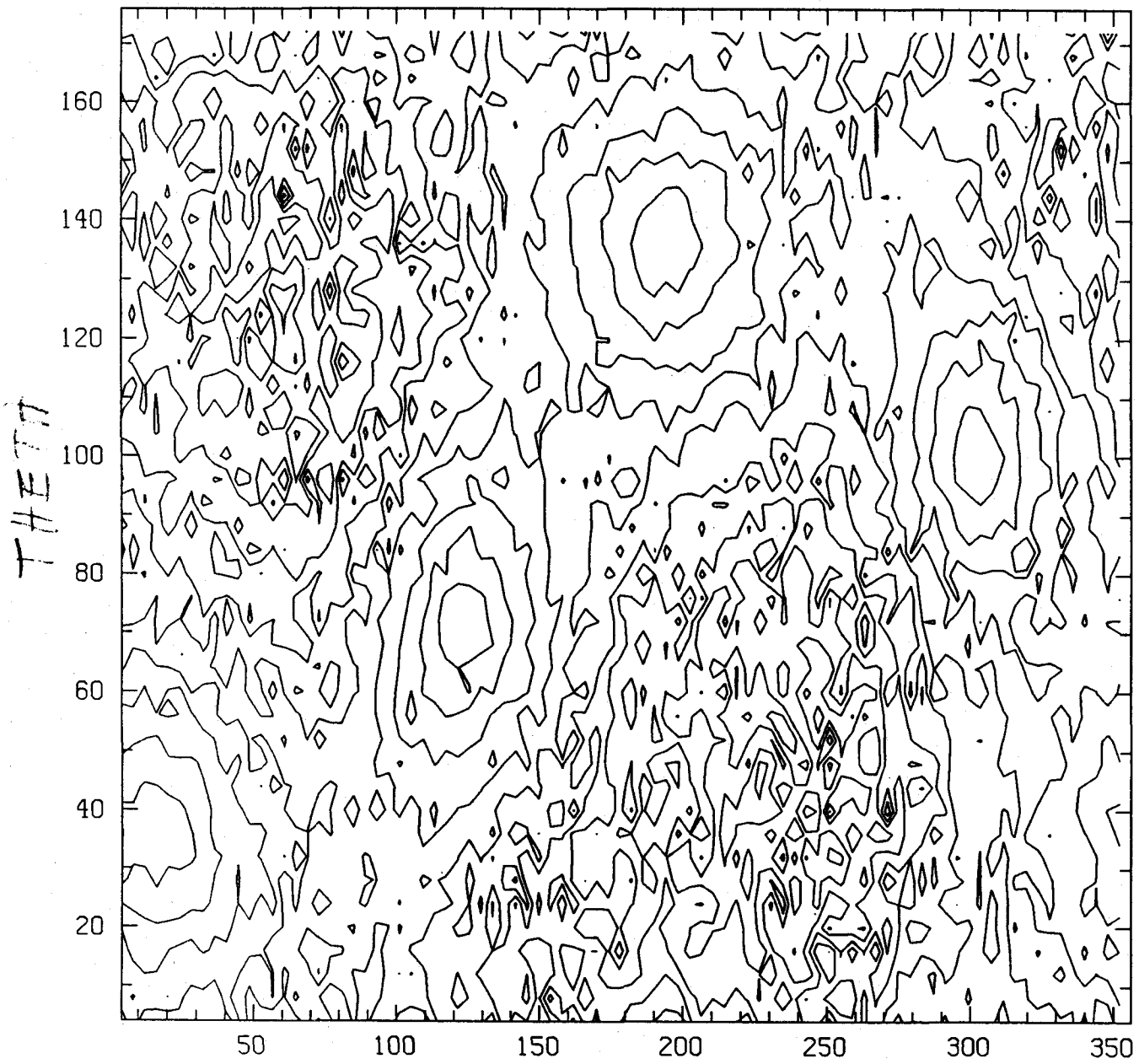

Fig. 1p/o)

Noise=ON

Hx=0.2 Hz

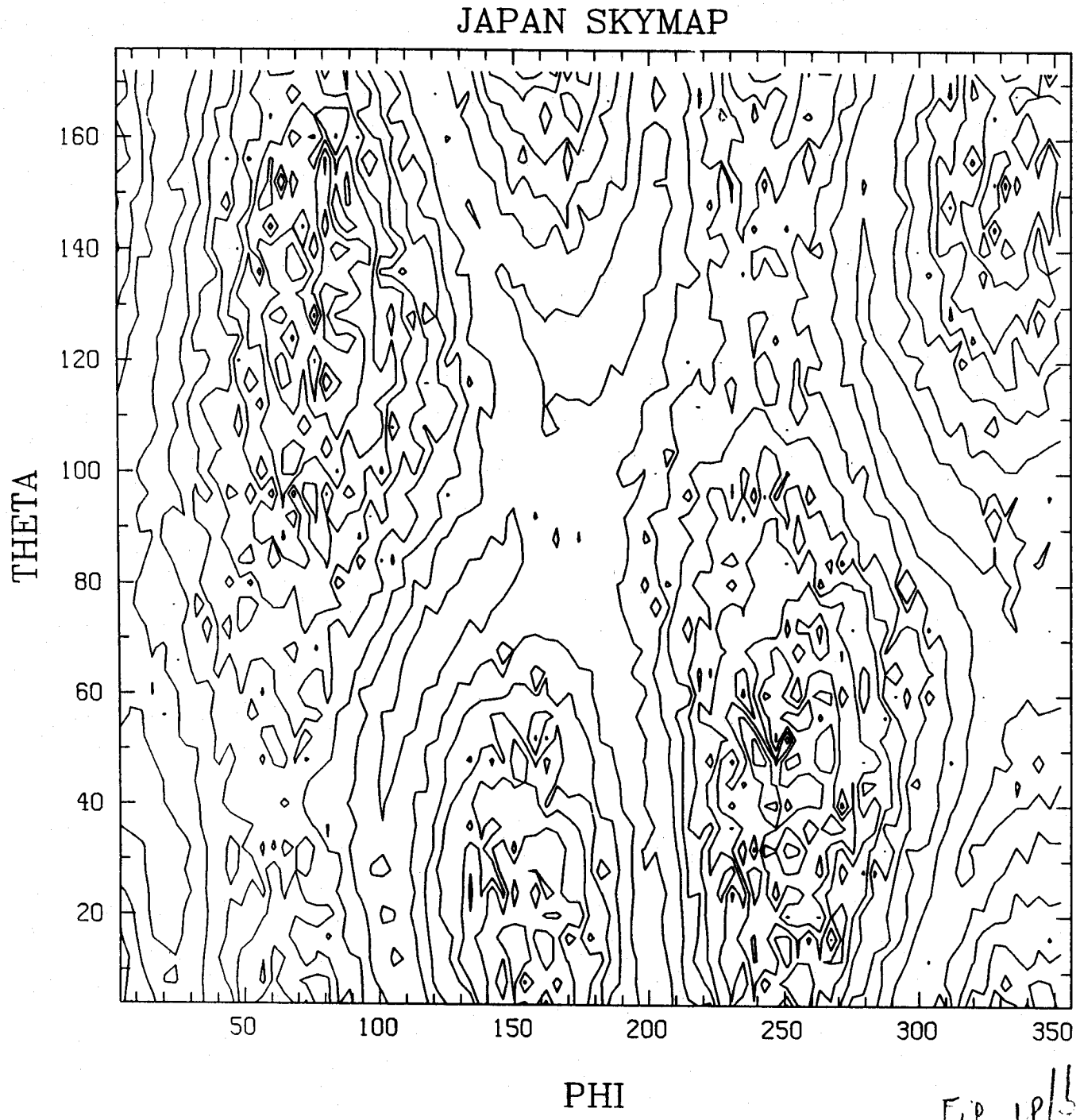

Fig. 18(b)

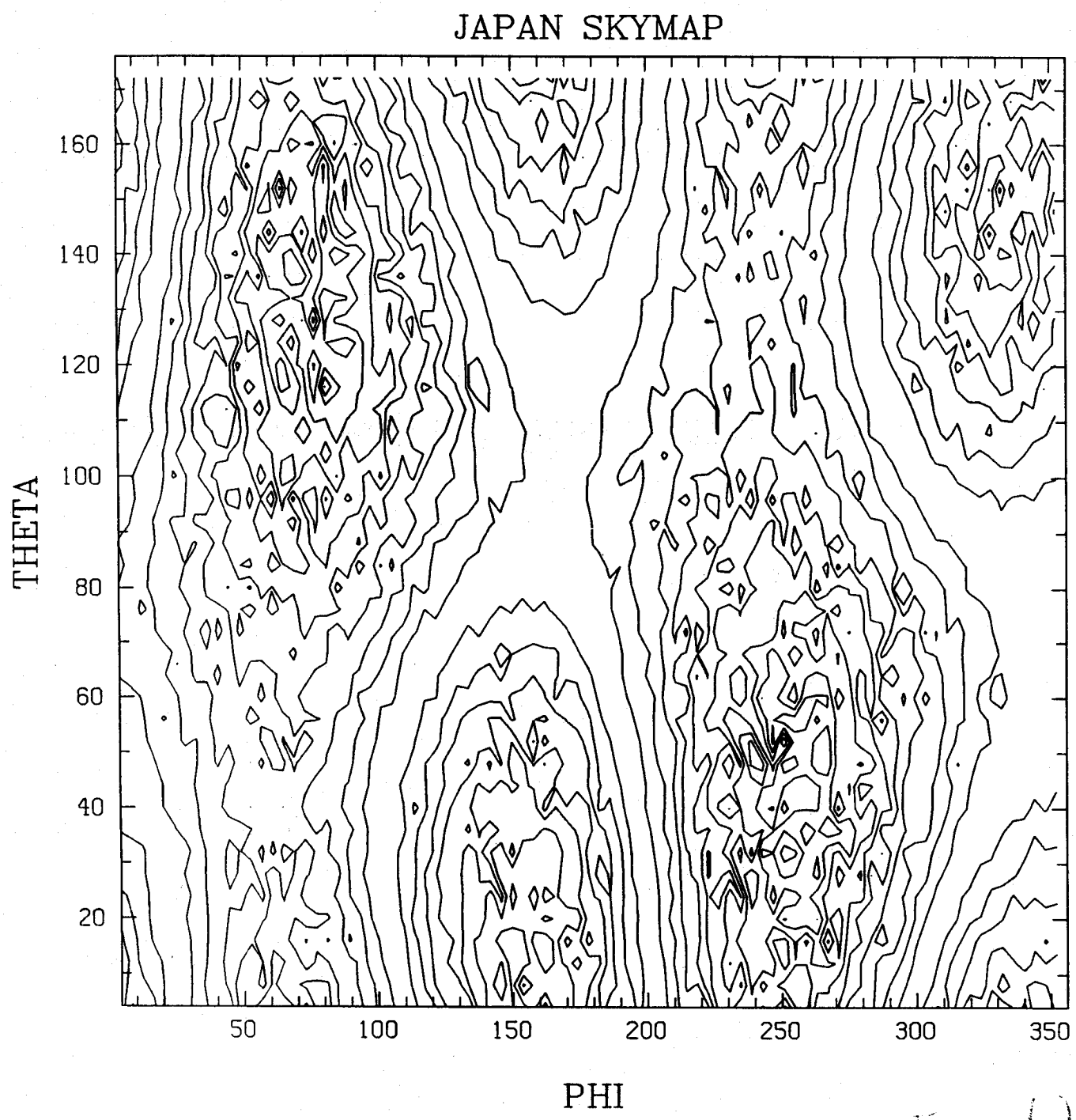
JAPAN SKYMAP
THETA
PHI
160
140
120
100
80
60
40
20
50
100
150
200
250
300
350

AUSTR.

Noise = on

$h_+ = h_\times$

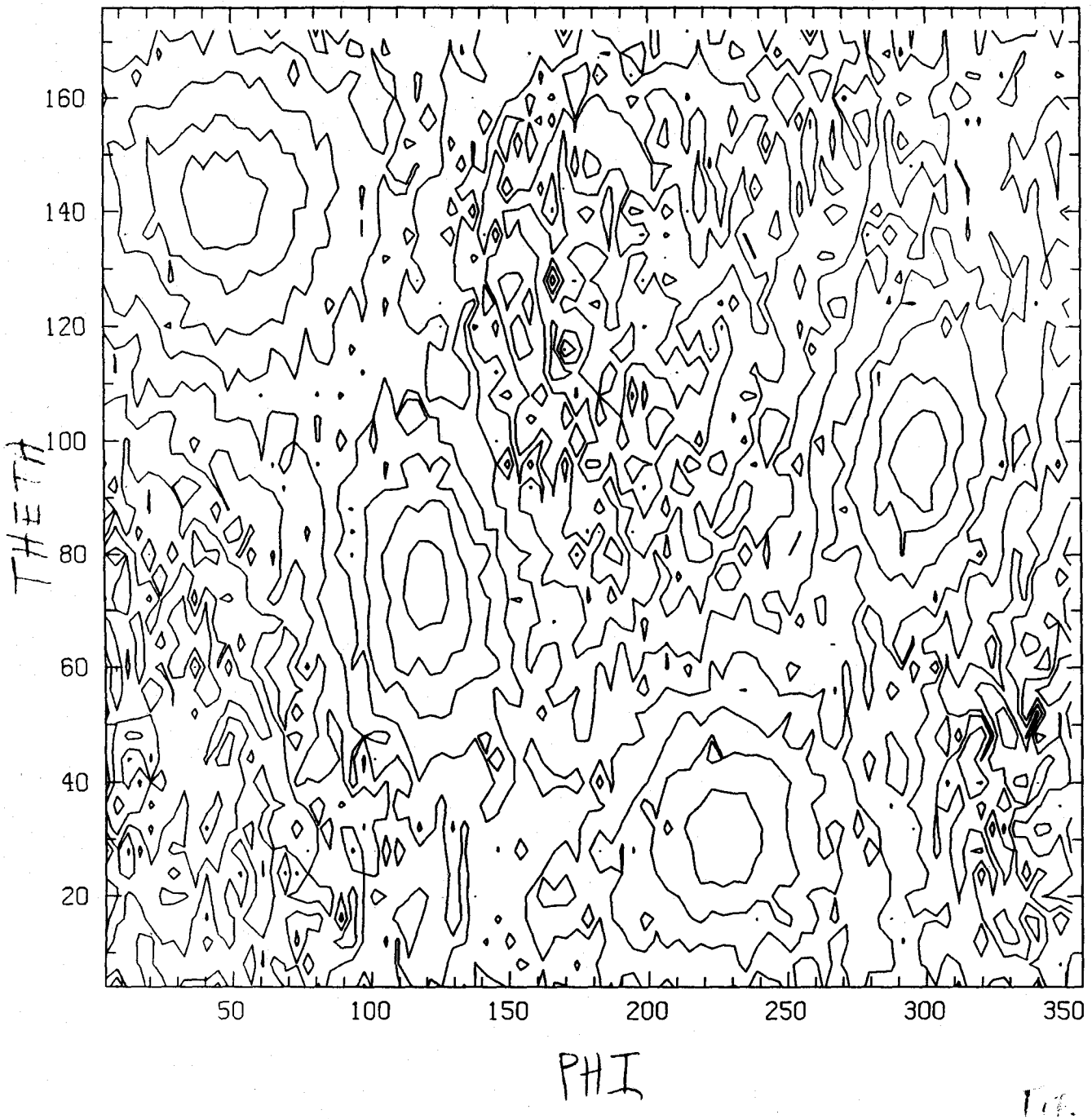

Fig. 19(a)

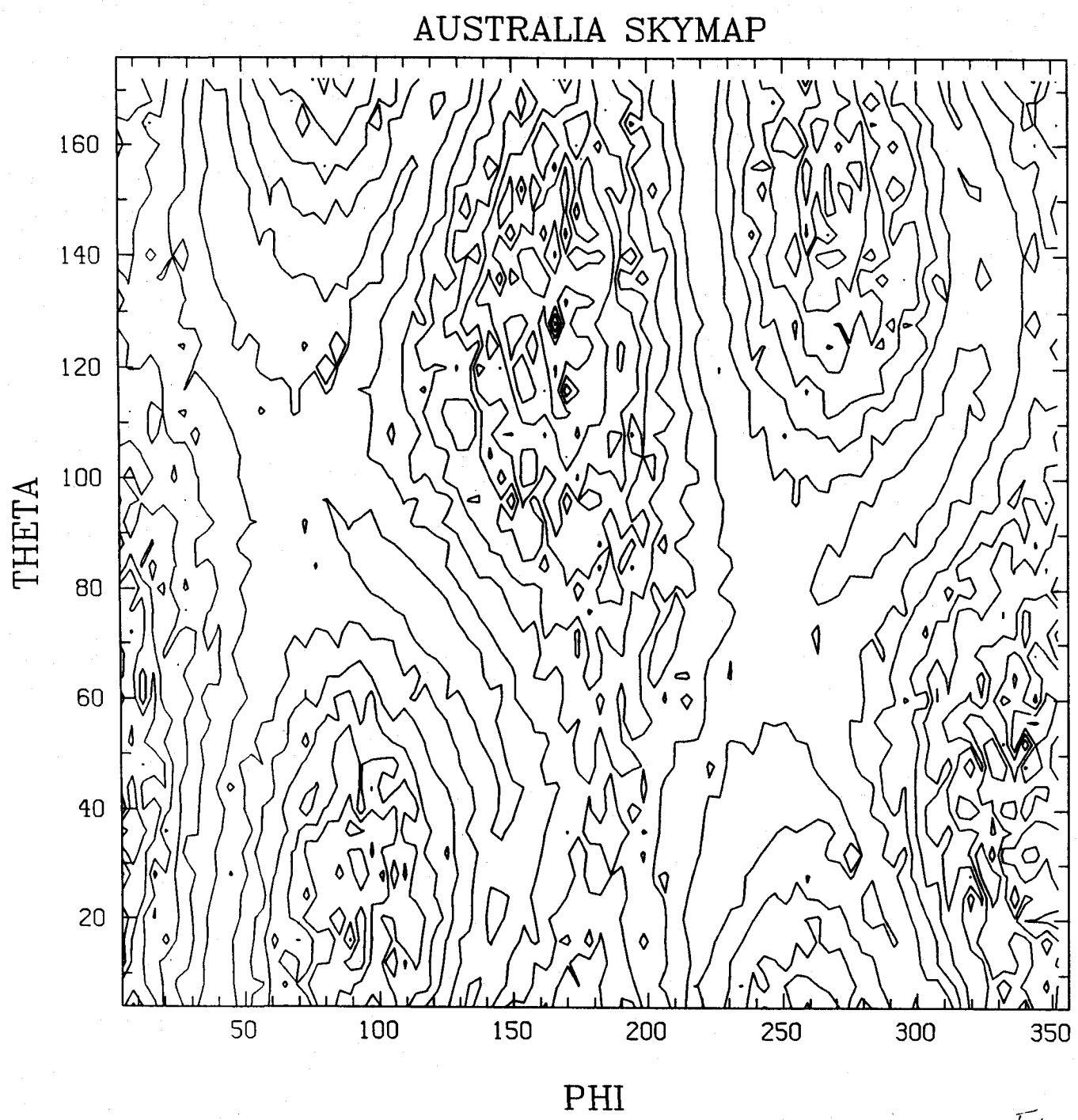
AUSTRALIA SKYMAP
THETA
PHI
160
140
120
100
80
60
40
20
50
100
150
200
250
300
350

Fig. 19(b)

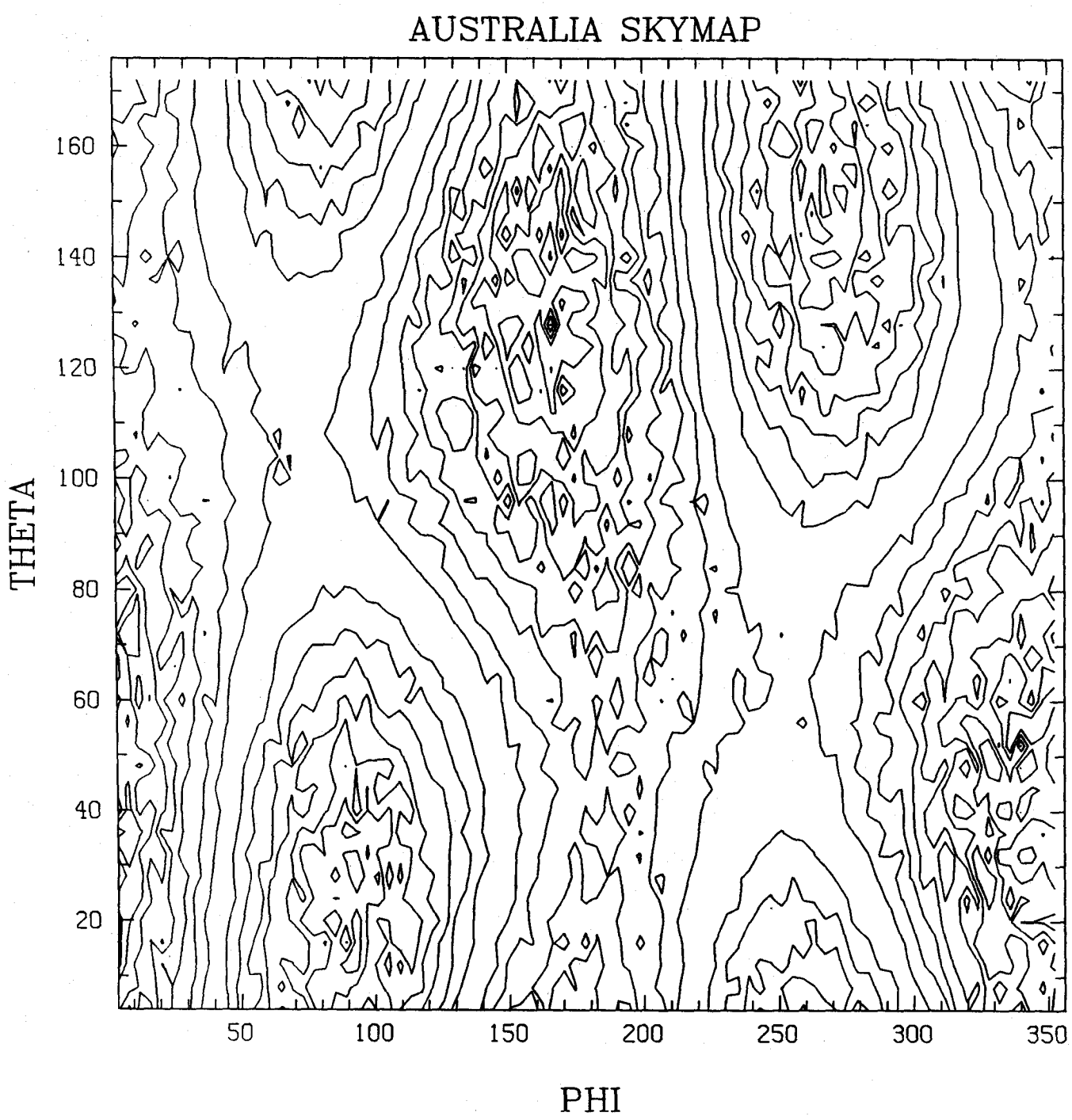

NOISE - ON

1/X - 0

Fig. 19(c)

ADDENDUM TO THE MEMORANDUM TITLED "ORIENTATION OF LIGO RECEIVERS"

WRITTEN BY: Yekta Gürsel and Massimo Tinto January 8, 1989

I. Introduction

In the memorandum titled "ORIENTATION OF LIGO RECEIVERS" we did not include the mean coincidence probability plots and the skymaps for a receiver located on the Virginia site. In this addendum we present these plots for two different orientations of a receiver placed on this site.

II. Mean Coincidence Probabilities

In figure 20, we plot the mean coincidence probability as a function of the orientations of two receivers located on the California and Virginia sites respectively for sources located in the Virgo cluster of galaxies. The contours are labeled by the percentage values of the probability. In figure 21, we gave a similar plot for a random distribution of sources in the sky.

III. Geometric Skymaps

In sets of figures 22 and 23 we give the geometric skymaps for a receiver located on the Virginia site optimally oriented with a receiver on the California site and oriented 45 degrees away from the optimal orientation respectively. In each set, the figures (a) to (e) show skymaps for different values of instantaneous polarizations of the wave amplitudes. As we go from figure (a) to figure (e) the polarization changes form "circular" to "linear" as in the previous memorandum.

MEAN COINCIDENCE PROBABILITY (VIRGO)

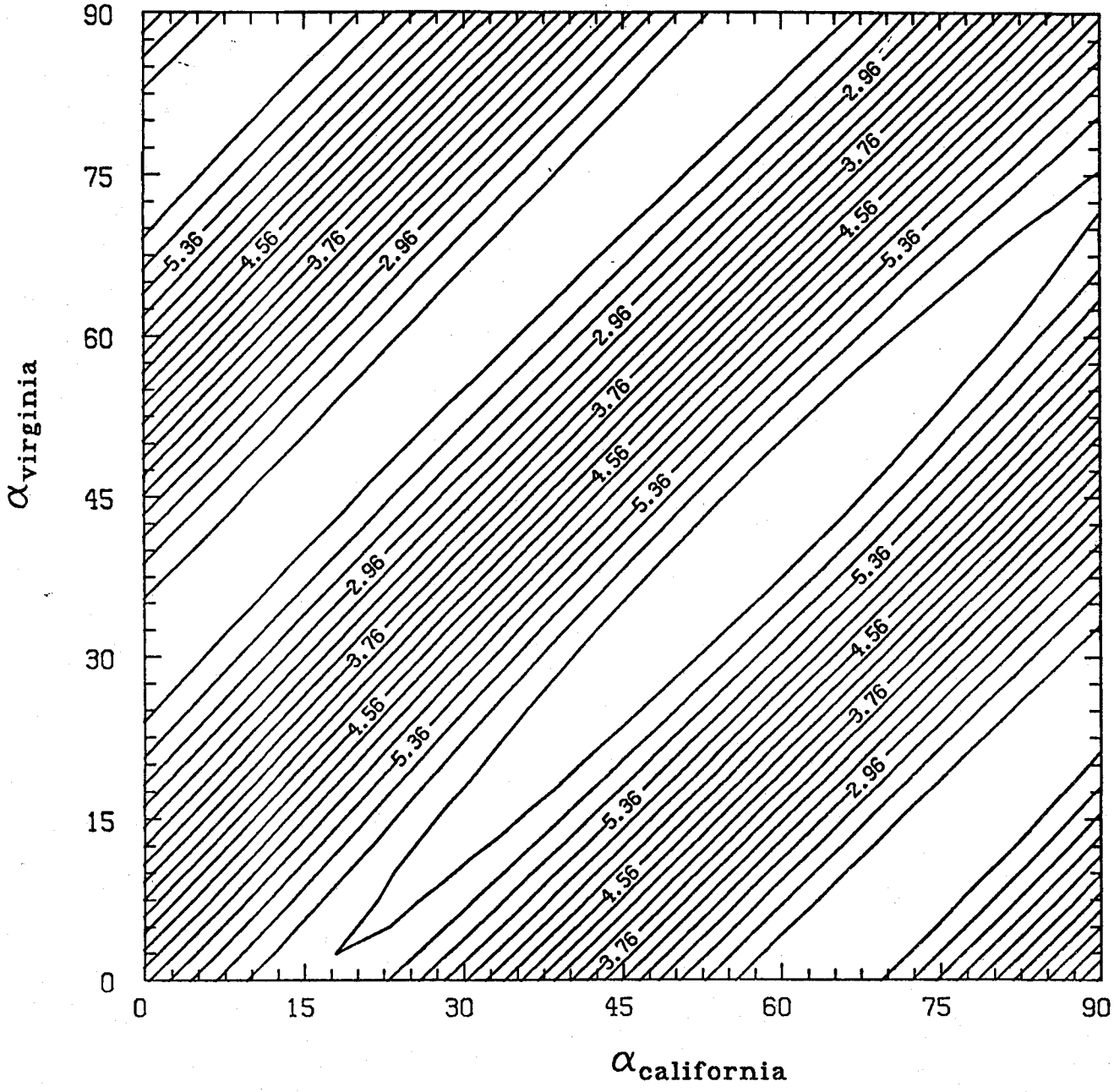

Fig. 20

CØNTØUR FRØM 2.1600 TØ 5.9600 CØNTØUR INTERVAL [illegible]0.20000 PT(3.3)= 4.9200

MEAN COINCIDENCE PROBABILITY (RANDOM)

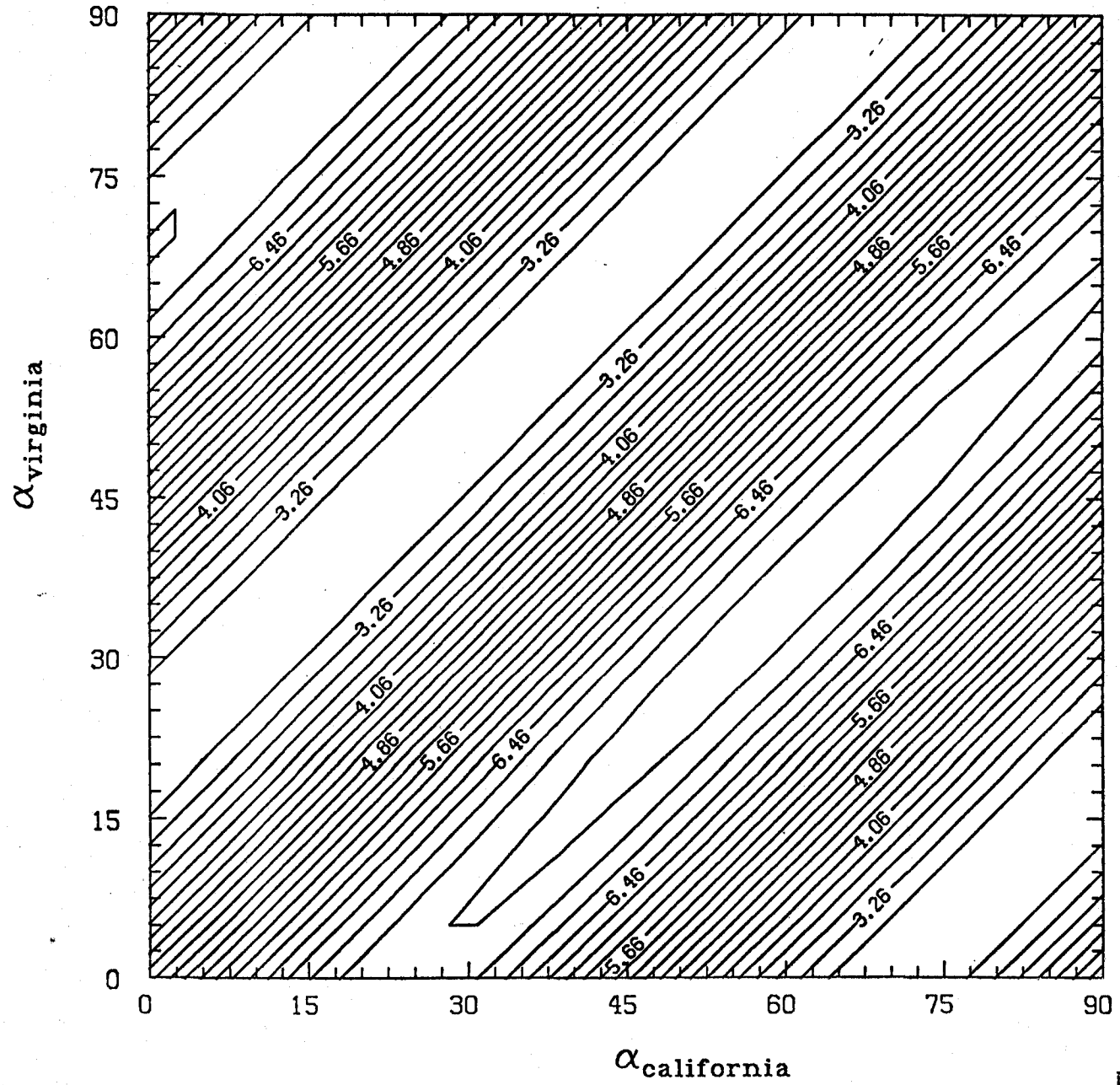

CØNTØUR FRØM 2.8600 TØ 7.0600 CØNTØUR INTERVAL 0.20000 PT(3.3)= 4.7800

Fig. 21

VIRGINIA SKYMAP ($h_x = 1.0\ h_+$, $\alpha = 85°$)

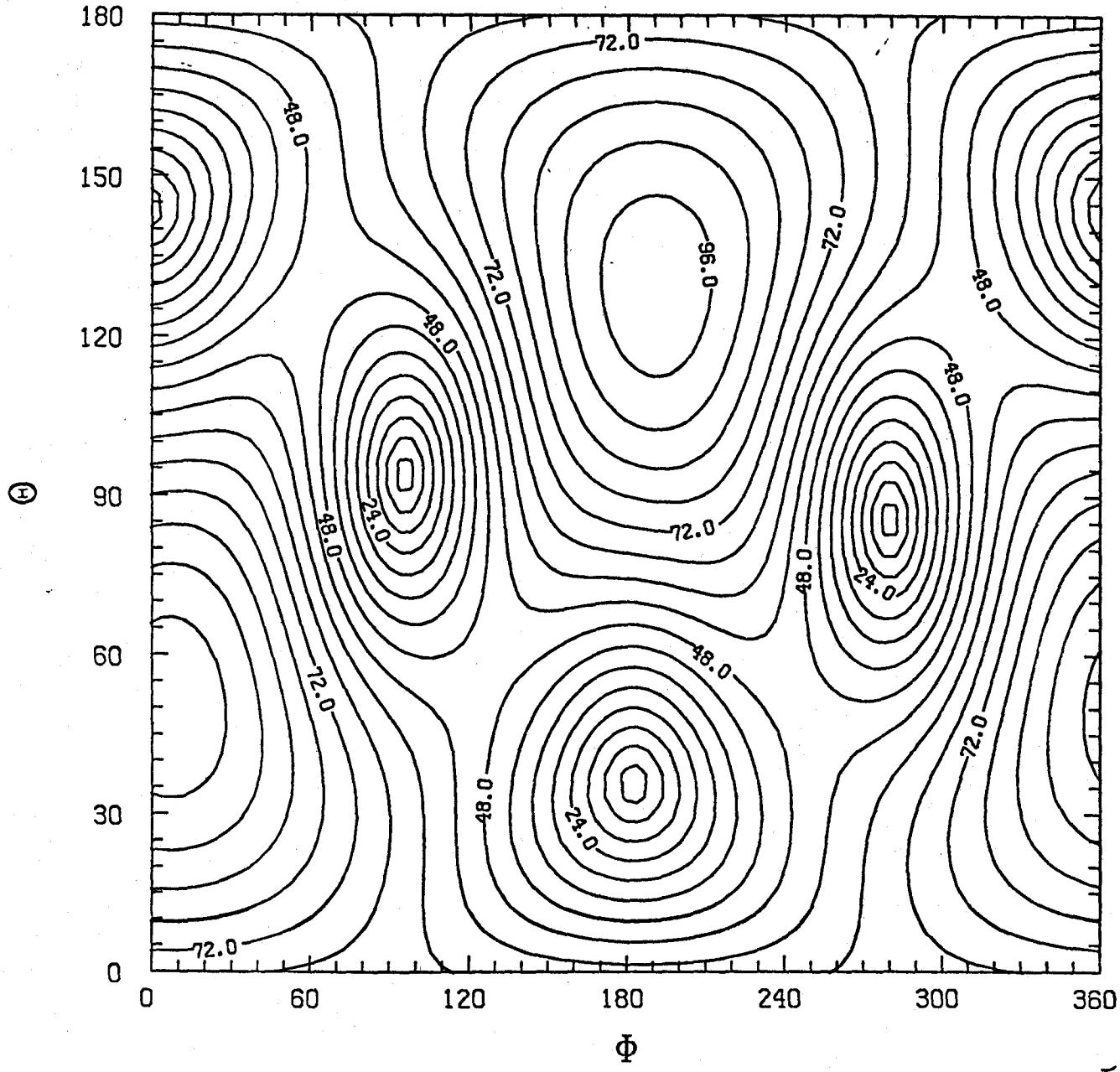

CØNTØUR FRØM 0. TØ 96.000 CØNTØUR INTERVAL 6.0000 PT(3,3)= 76.700

Fig. 27(a)

VIRGINIA SKYMAP ($h_x = 0.8\ h_+$, $\alpha = 85°$)

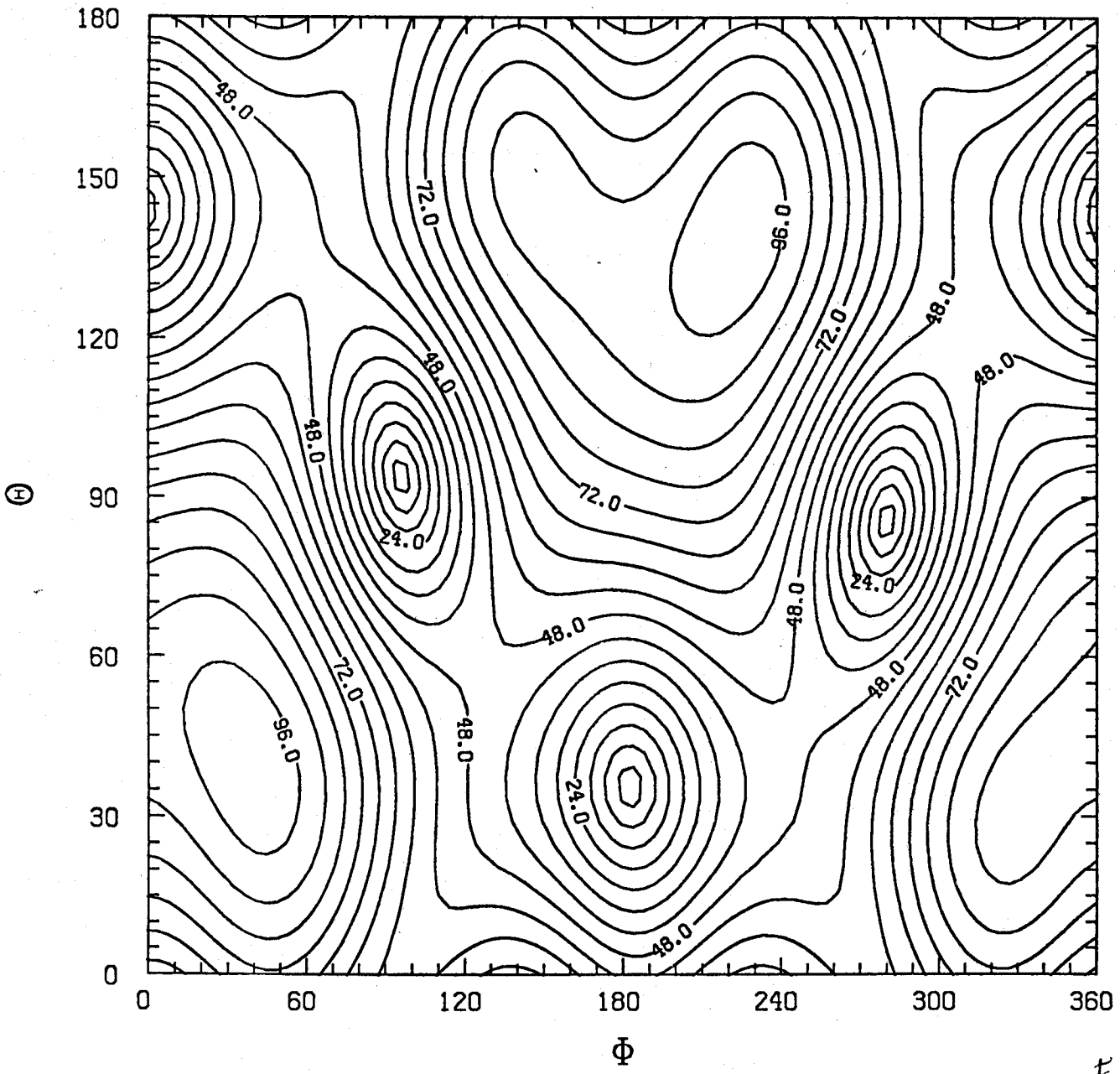

CØNTØUR FRØM 0. TØ 96.000 CØNTØUR INTERVAL 6.0000 PT(3.3)= 72.900

Fig 22(1)

VIRGINIA SKYMAP ($h_x = 0.5\ h_+$, $\alpha = 85°$)

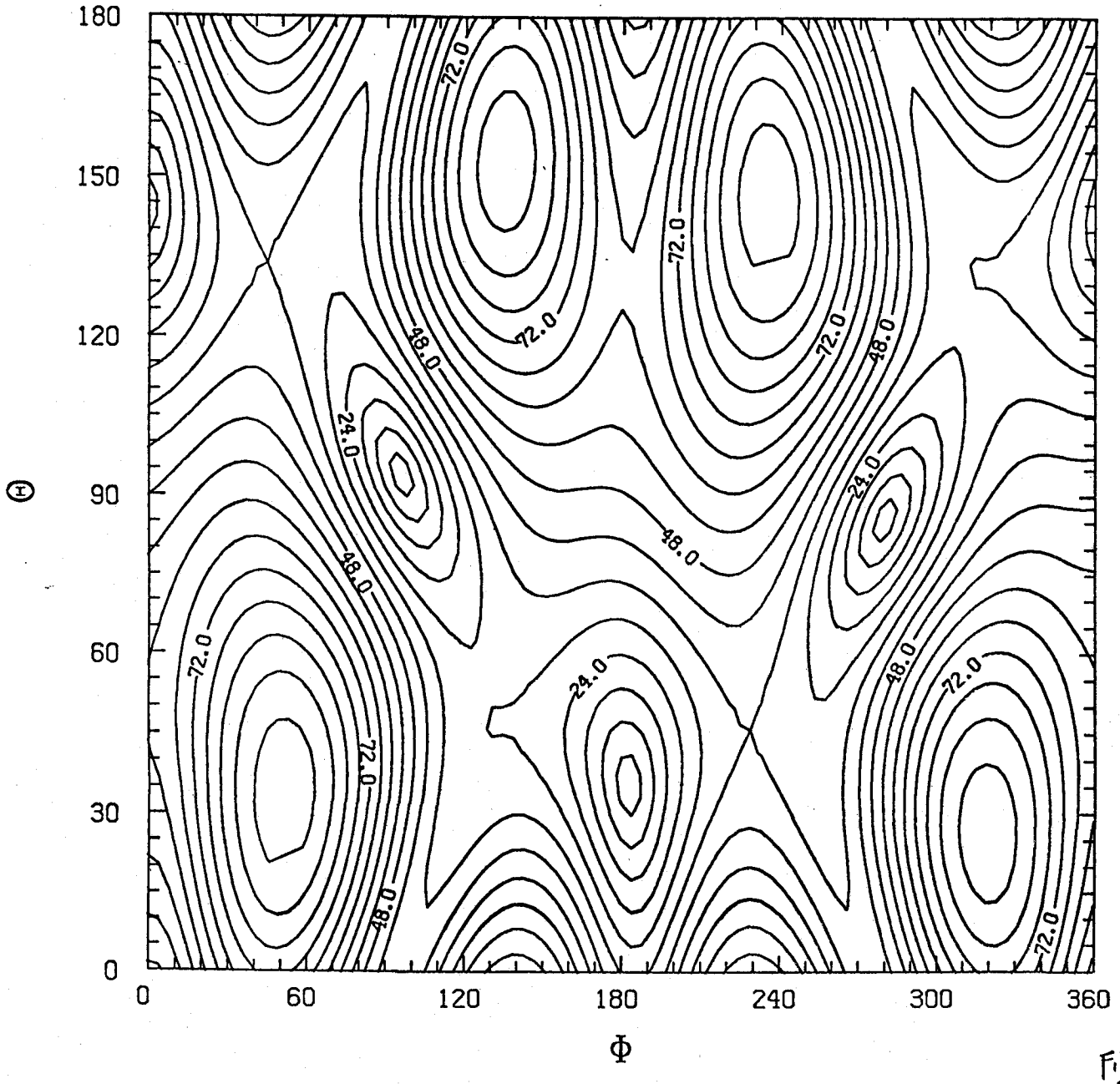

Fig. 22 (c)

CØNTØUR FRØM 0. TØ 96.000 CØNTØUR INTERVAL 6.0000 PT(3,3)= 49.500

VIRGINIA SKYMAP ($h_x = 0.2\ h_+$, $\alpha = 85°$)

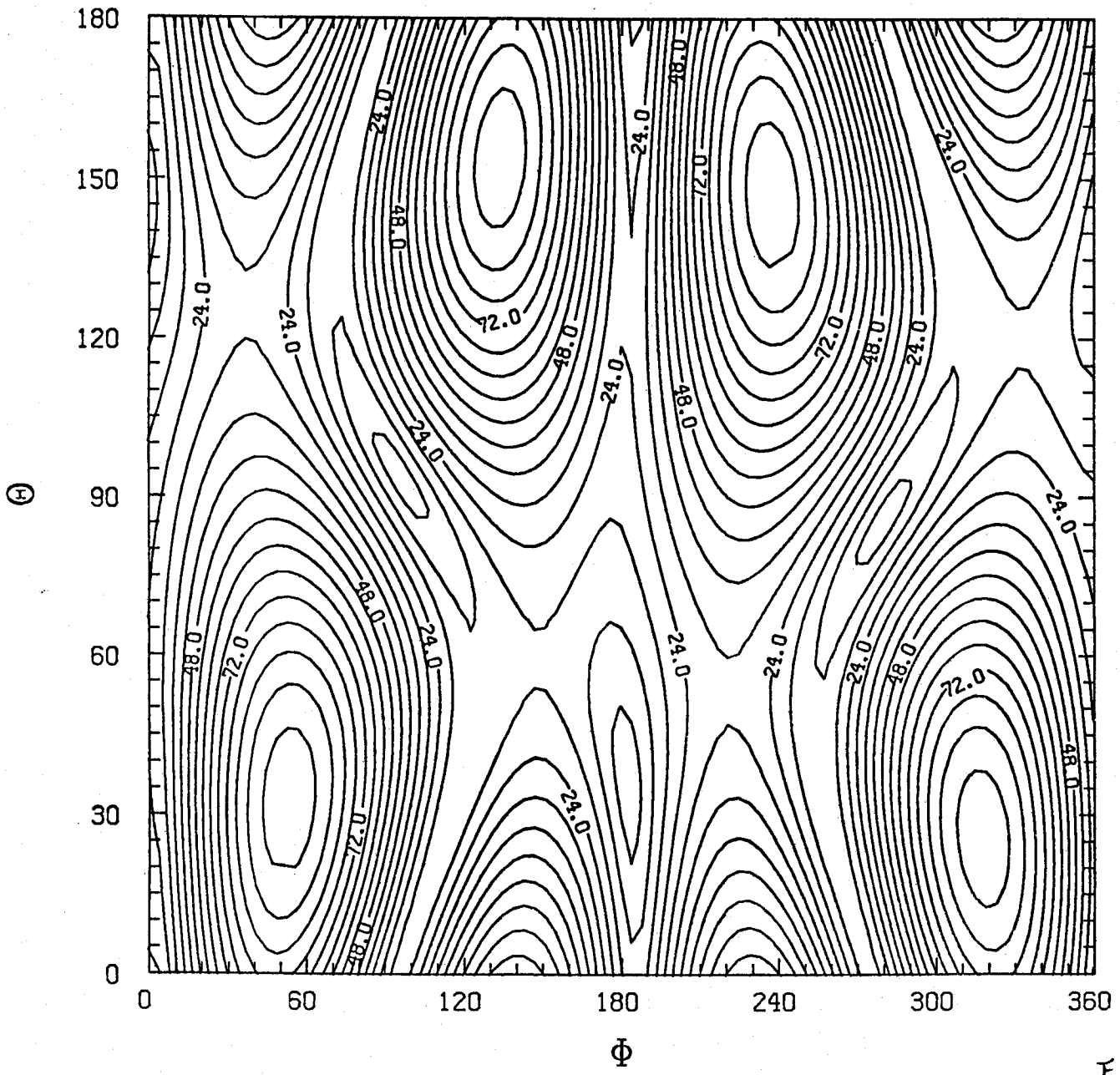

Fig. 22(d)

CØNTØUR FRØM 0. TØ 96.000 CØNTØUR INTERVAL 6.0000 PT(3,3)= 26.900

VIRGINIA SKYMAP (h_x= 0.0 h_+ , α = 85°)

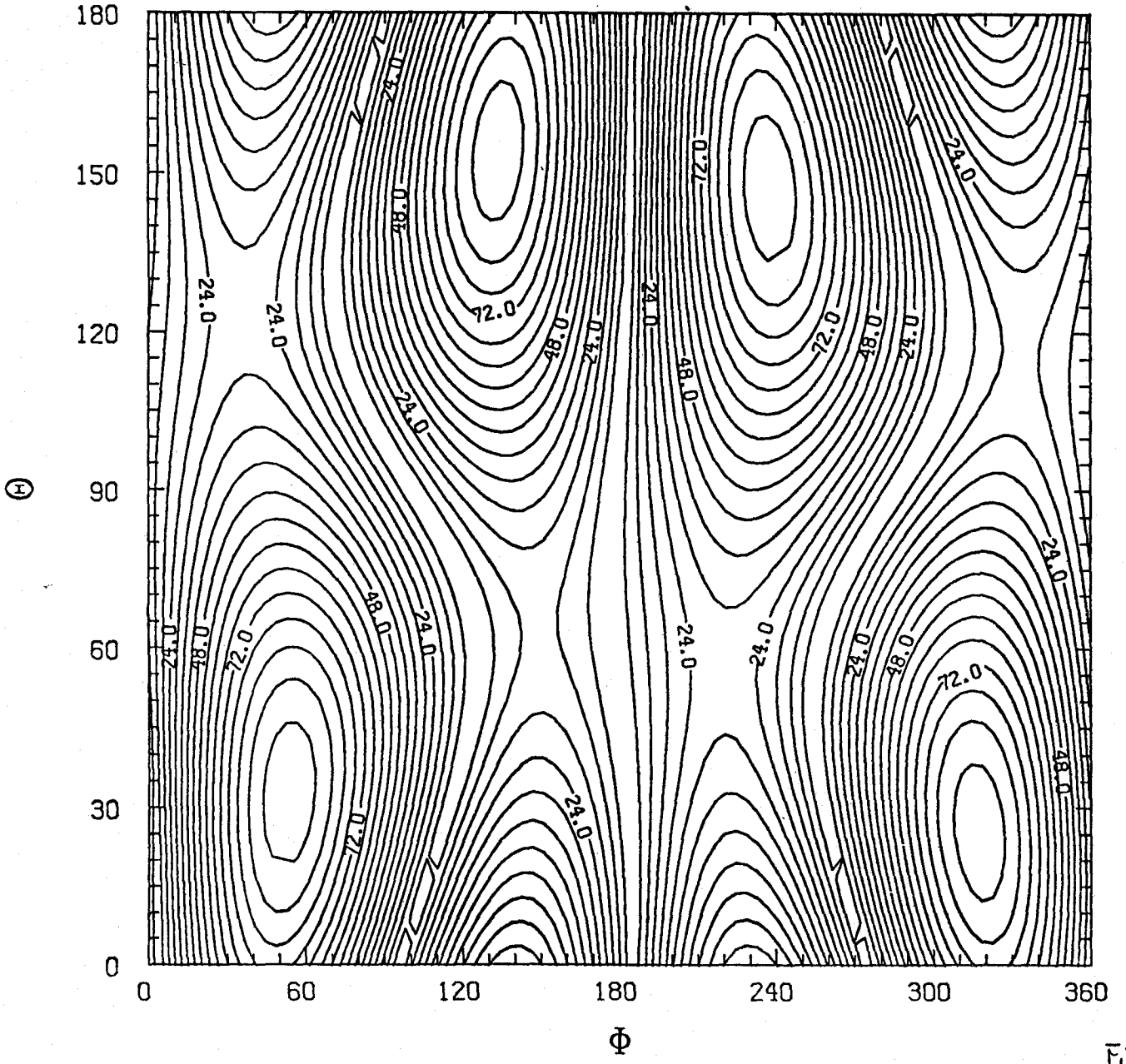

Fig. 22(e)

CØNTØUR FRØM 0. TØ 96.000 CØNTØUR INTERVAL 6.0000 PT(3,3)= 19.700

VIRGINIA SKYMAP ($h_x = 1.0\ h_+$, $\alpha = 40°$)

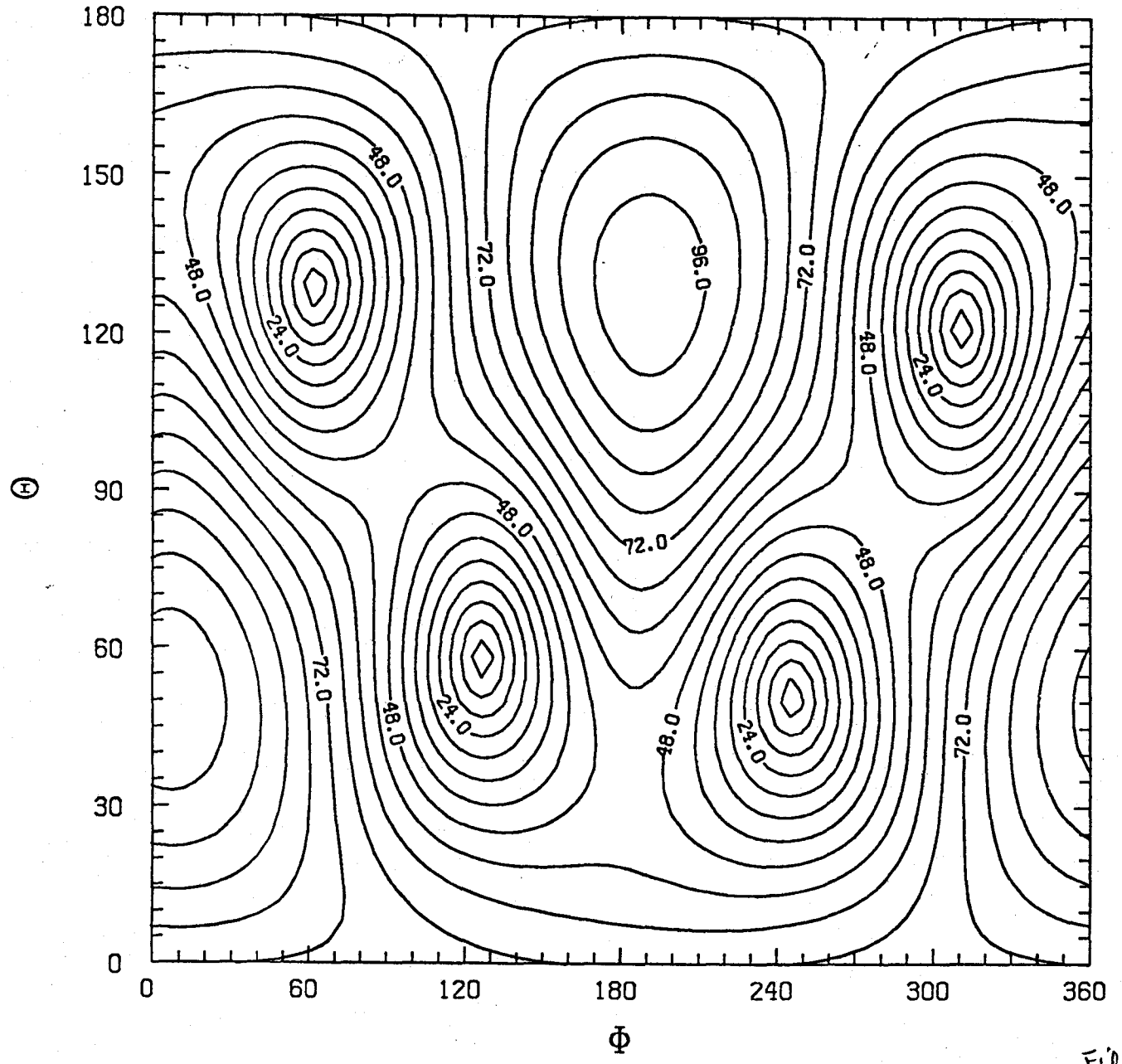

Fig. 23(a)

CØNTØUR FRØM 0. TØ 96.000 CØNTØUR INTERVAL 6.0000 PT(3,3)= 79.300

VIRGINIA SKYMAP ($h_x = 0.8\ h_+$, $\alpha = 40^\circ$)

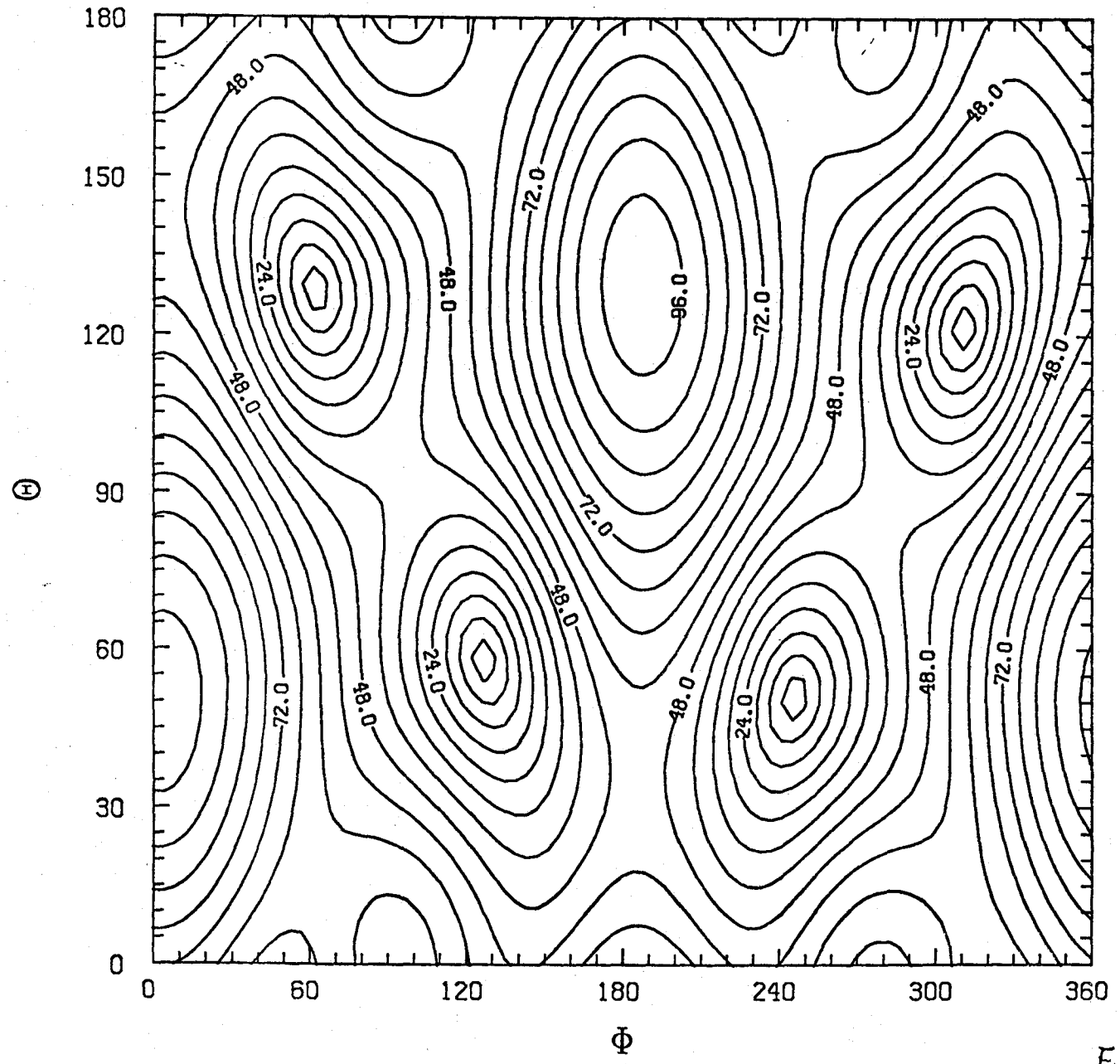

Fig 13(5)

CØNTØUR FRØM 0. TØ 96.000 CØNTØUR INTERVAL 6.0000 PT(3.3)= 78.900

VIRGINIA SKYMAP ($h_x = 0.5\ h_+$, $\alpha = 40°$)

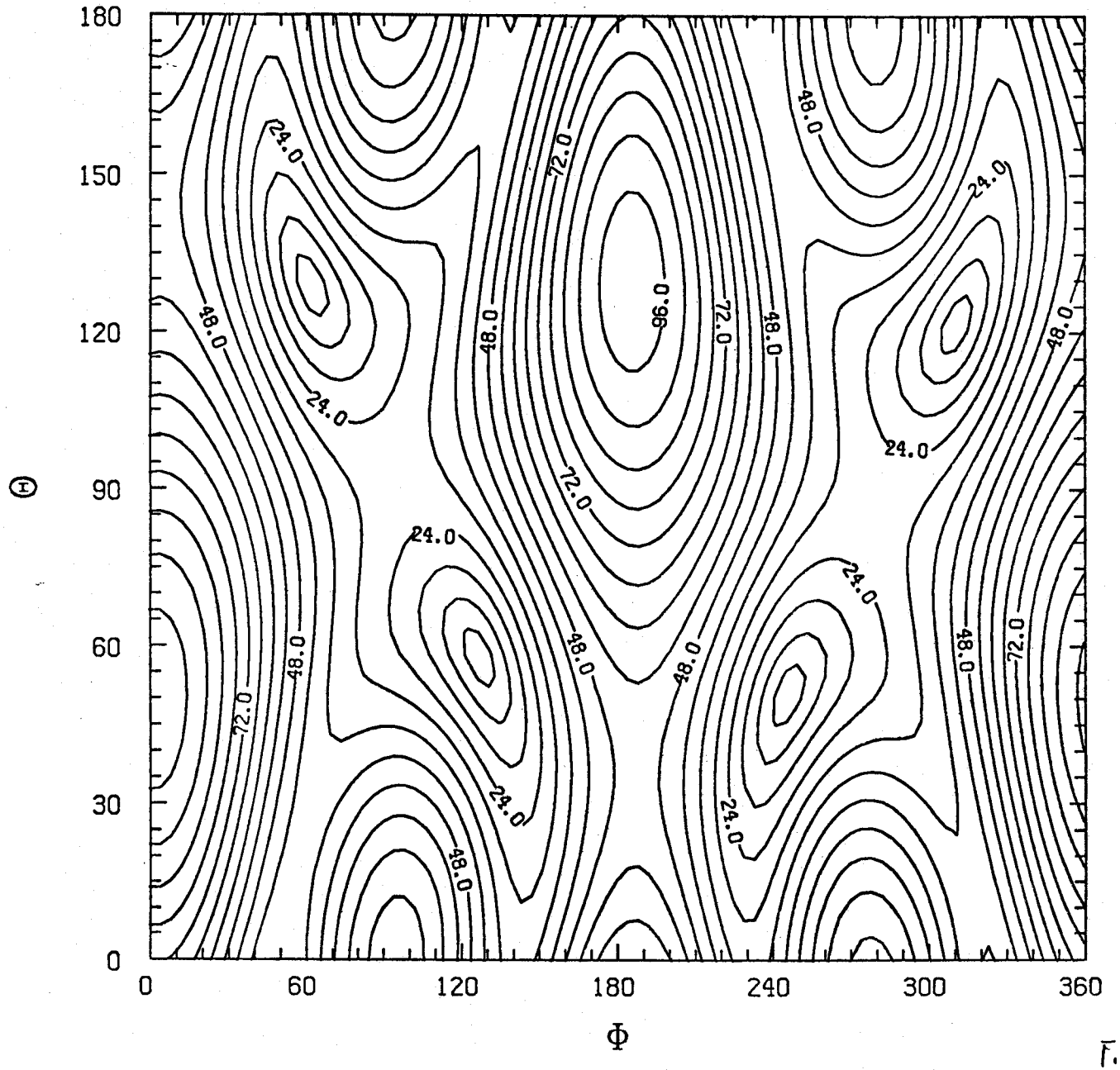

Fig 23(c)

CØNTØUR FRØM 0. TØ 96.000 CØNTØUR INTERVAL 6.0000 PT(3,3)= 78.500

VIRGINIA SKYMAP ($h_x = 0.2\ h_+$, $\alpha = 40°$)

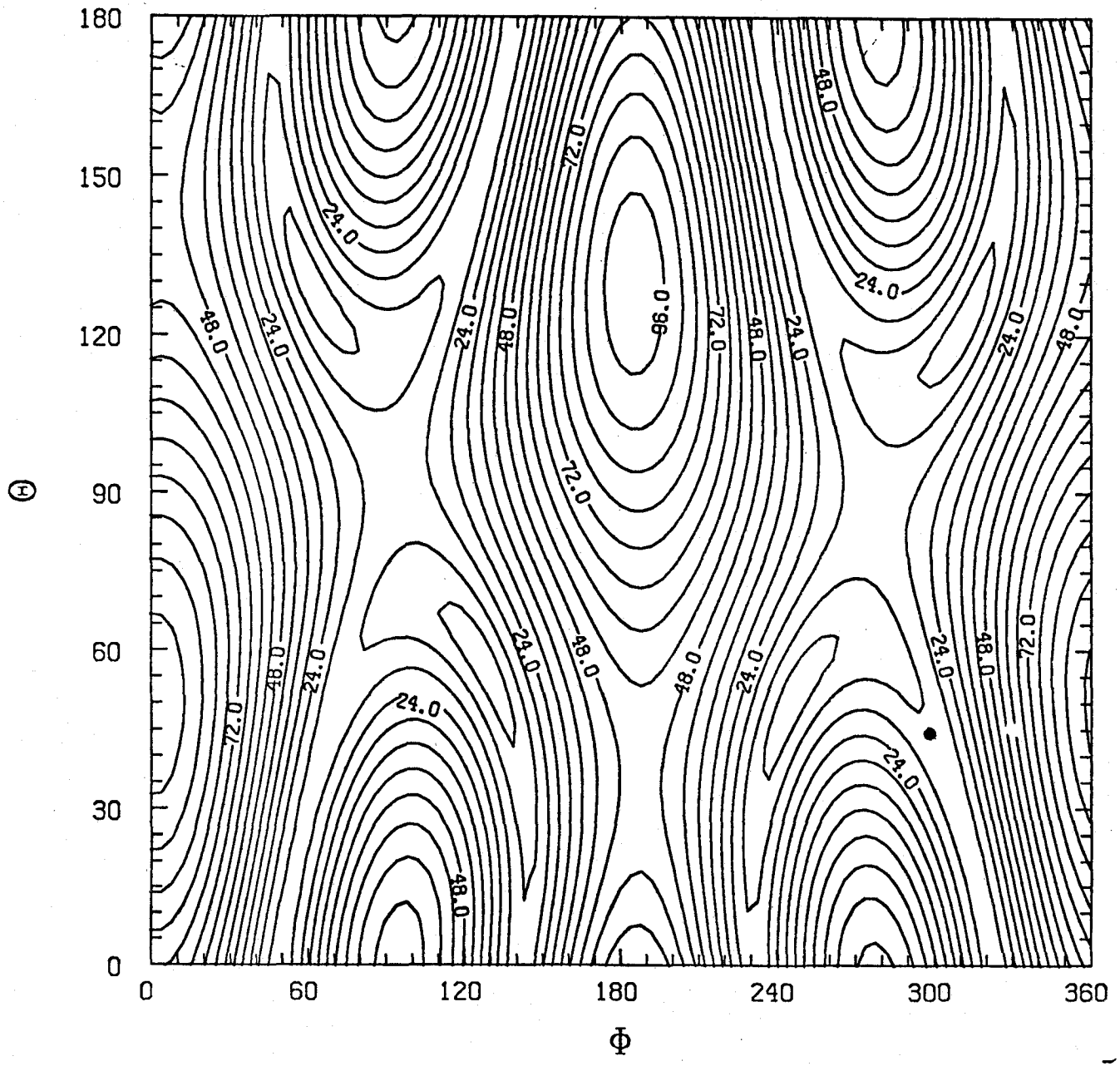

CØNTØUR FRØM 0. TØ 96.000 CØNTØUR INTERVAL 6.0000 PT(3.3)= 78.100

Fig 23(01)

VIRGINIA SKYMAP (h_x= 0.0 h_+ , α = 40°)

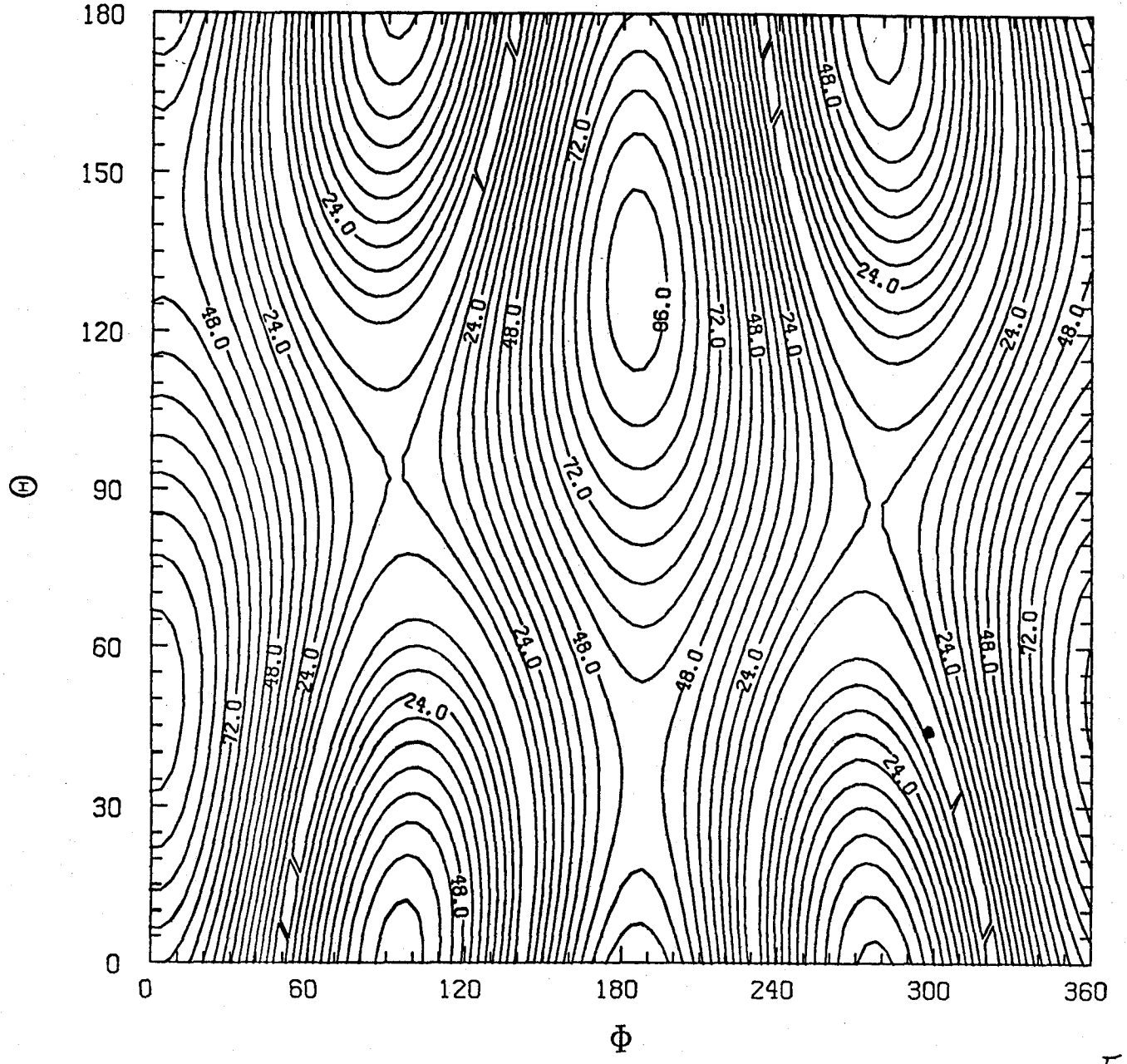

CØNTØUR FRØM 0. TØ 96.000 CØNTØUR INTERVAL 6.0000 PT(3,3)= 78.100

Fig. 22(e)

ADDENDUM II TO THE MEMORANDUM TITLED "ORIENTATION OF LIGO RECEIVERS"

WRITTEN BY: Yekta Gürsel and Massimo Tinto **January 10, 1989**

I. Geometric Skymaps

In this addendum we present skymaps for another orientation of a receiver on the Virginia site. This receiver is optimally aligned with a receiver on the California site with an orientation of the bisector 85 degrees North of East. The set 24 includes the skymaps for this receiver for a similar set of polarizations considered in the previous memoranda.

VIRGINIA SKYMAP (h_x= 1.0 h_+ , α = 10°)

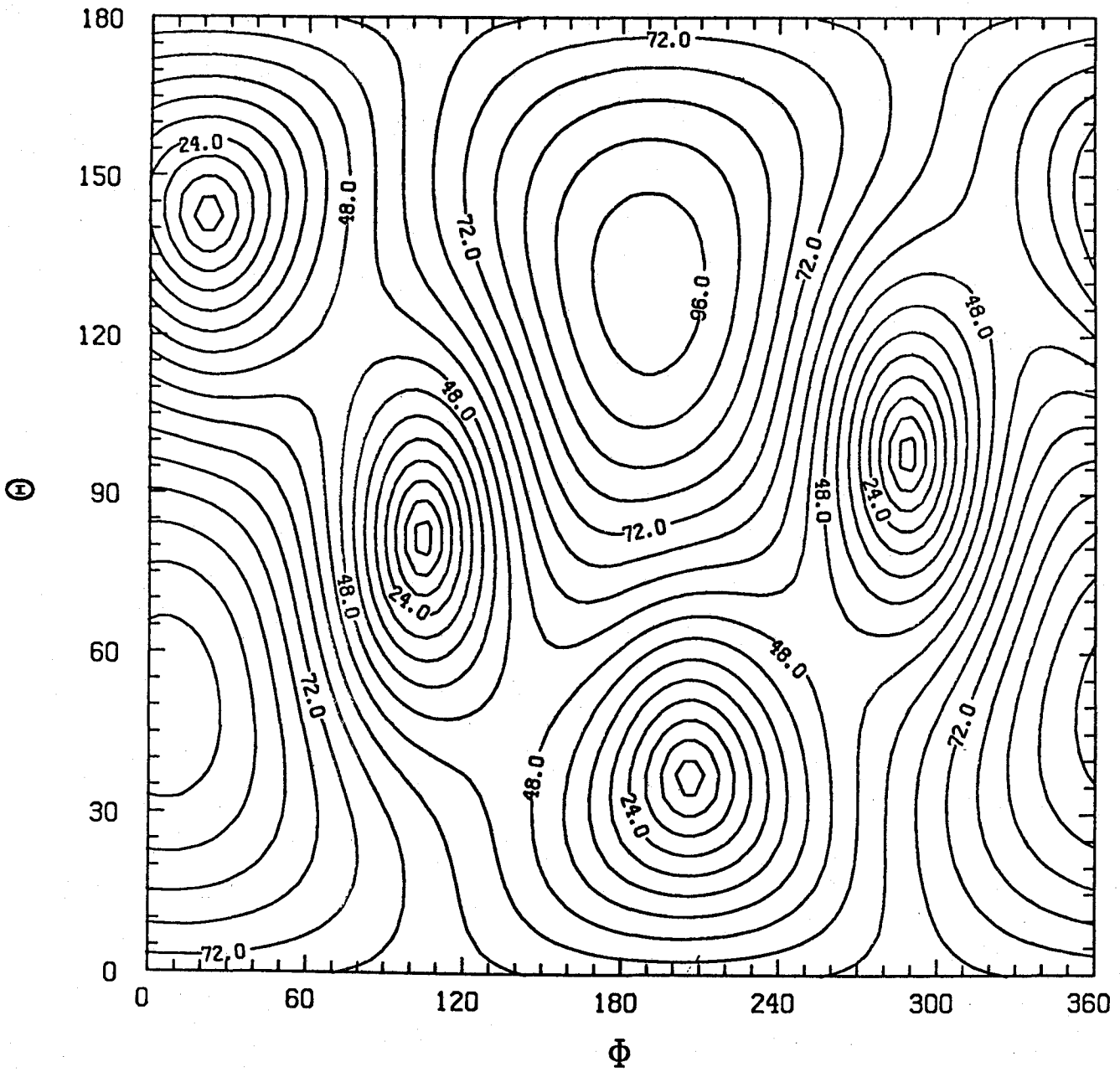

CØNTØUR FRØM 0. TØ 96.000 CØNTØUR INTERVAL ØF 6.0000 PT(3,3)= 77.400

Fig 24(a)

VIRGINIA SKYMAP ($h_x = 0.8\ h_+$, $\alpha = 10°$)

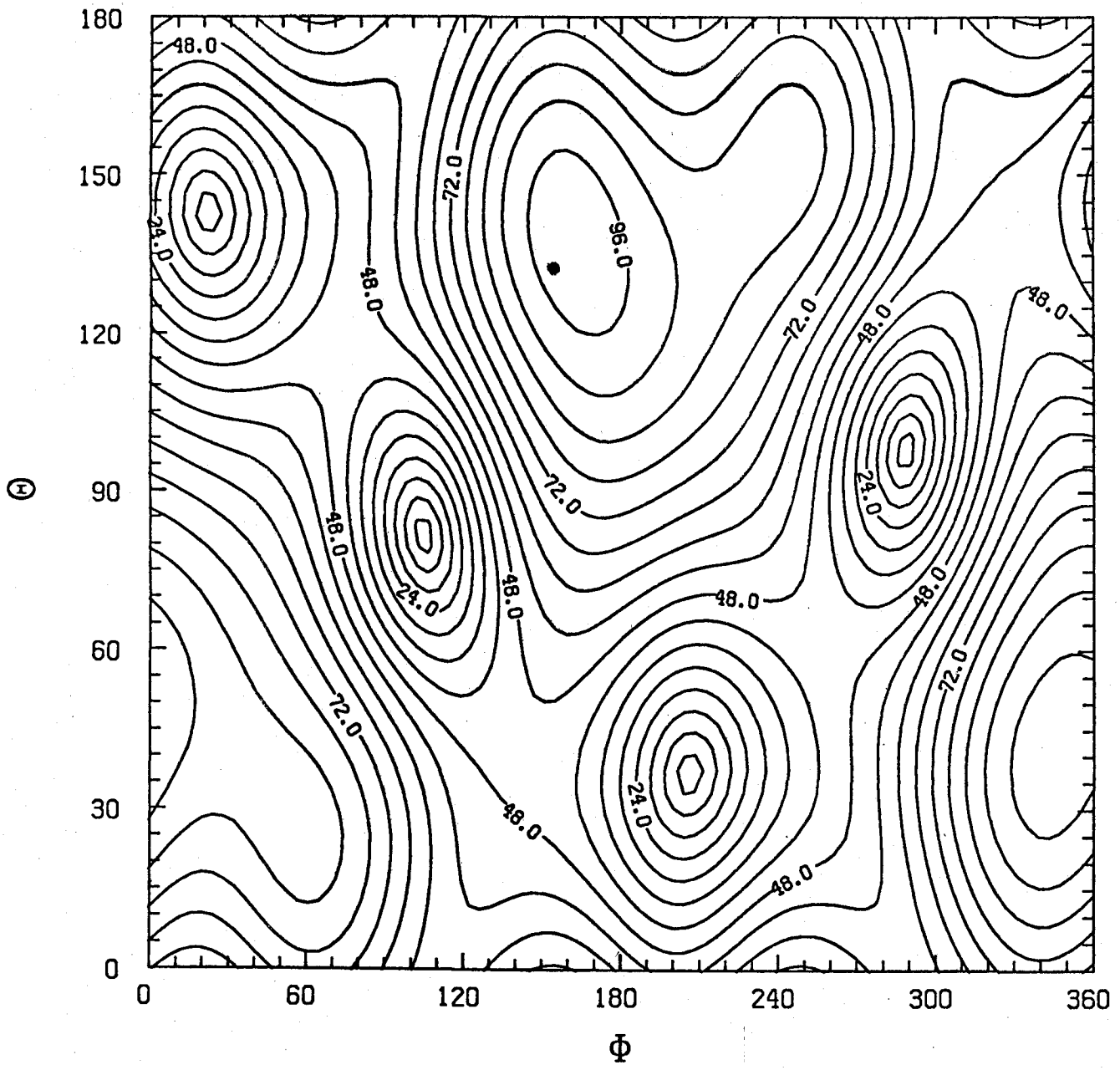

CØNTØUR FRØM 0. TØ 96.000 CØNTØUR INTERVAL ØF 6.0000 PT(3,3)= 71.900

Fig. 24(5)

VIRGINIA SKYMAP ($h_x = 0.5\ h_+$, $\alpha = 10°$)

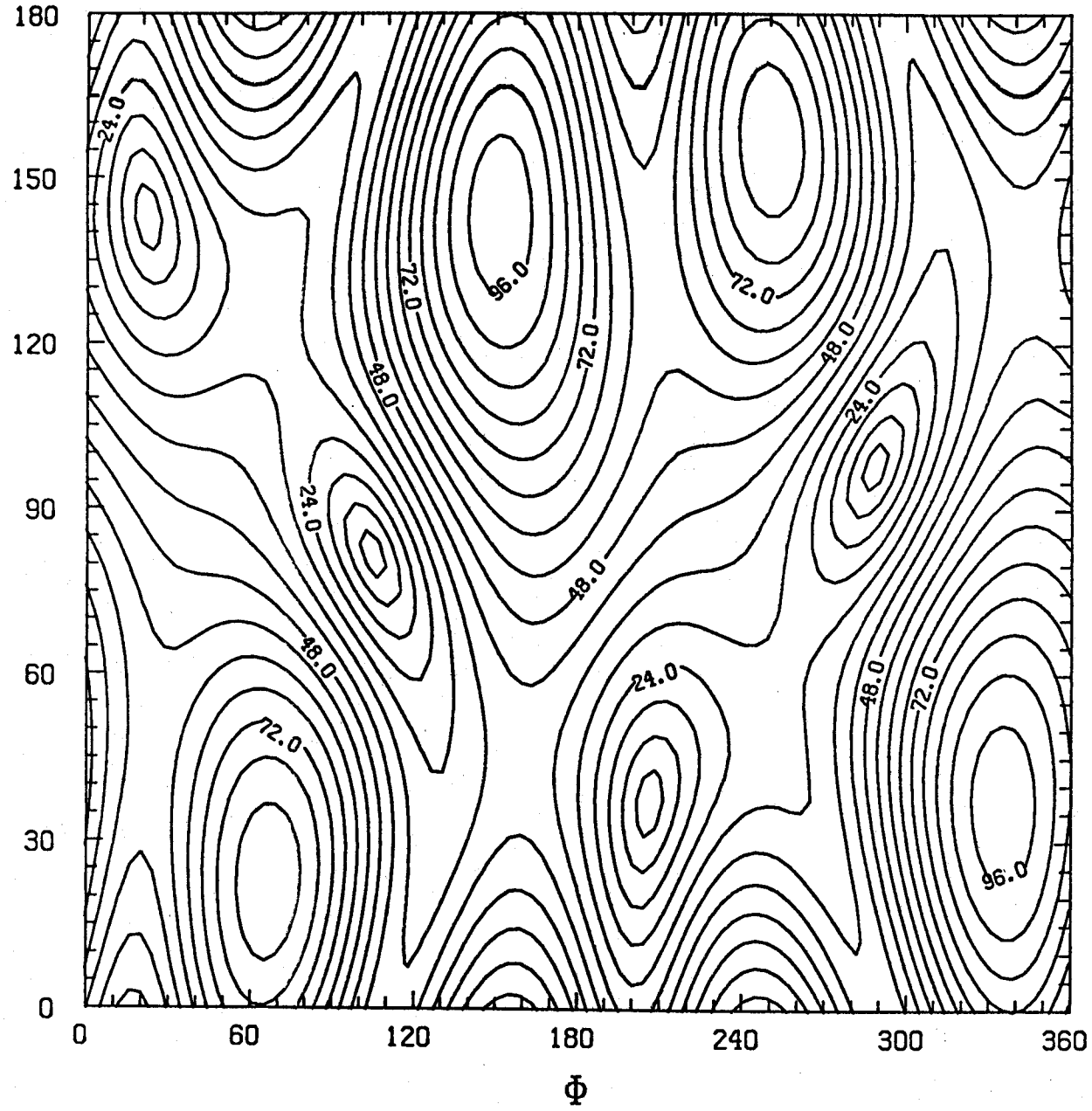

CØNTØUR FRØM 0. TØ 96.000 CØNTØUR INTERVAL ØF 6.0000 PT(3,3)= 50.900

Fig. 24(c)

VIRGINIA SKYMAP ($h_x = 0.2\ h_+$, $\alpha = 10°$)

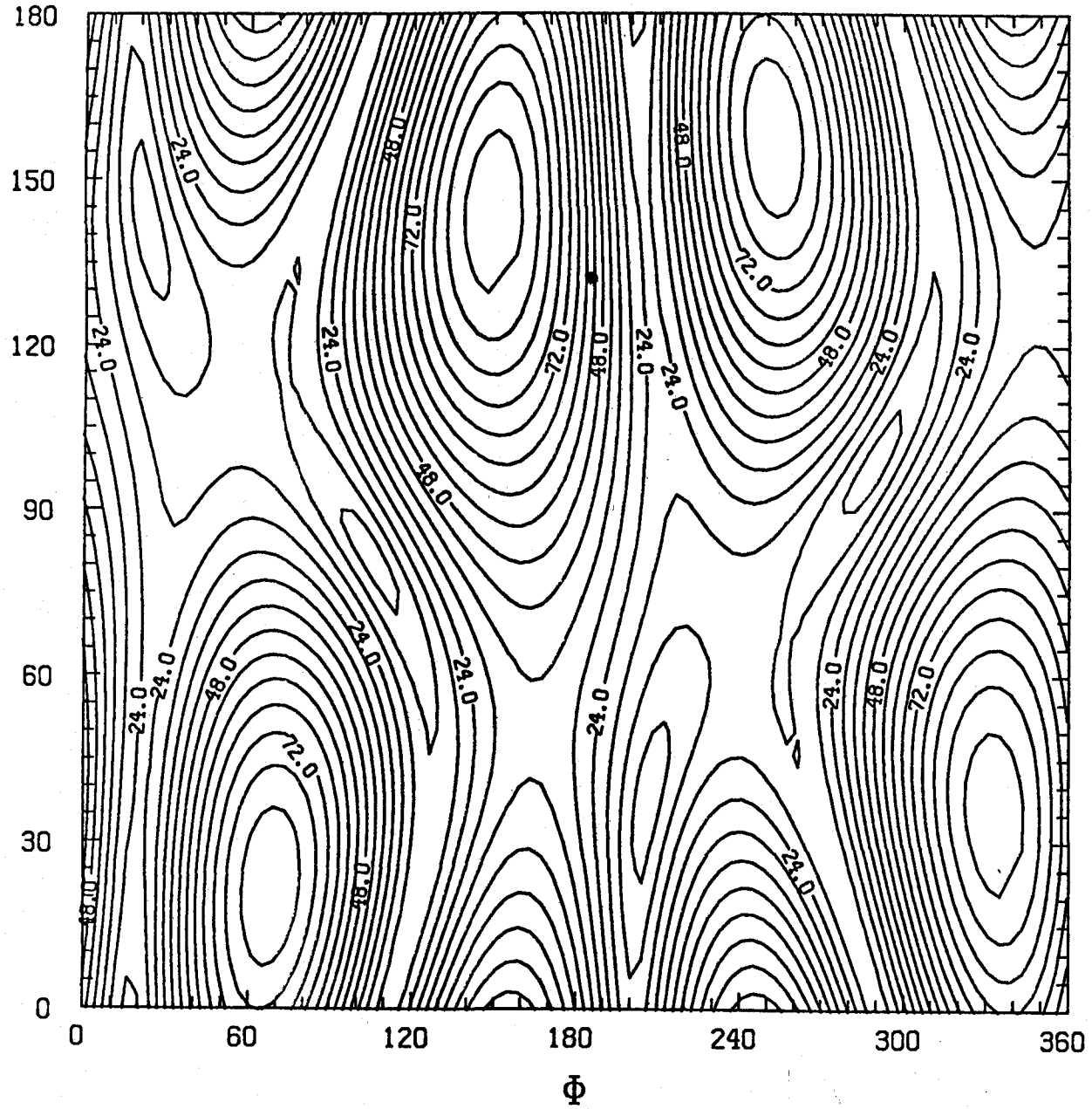

Fig. 24(d)

VIRGINIA SKYMAP (h_x= 0.0 h_+ , α = 10°)

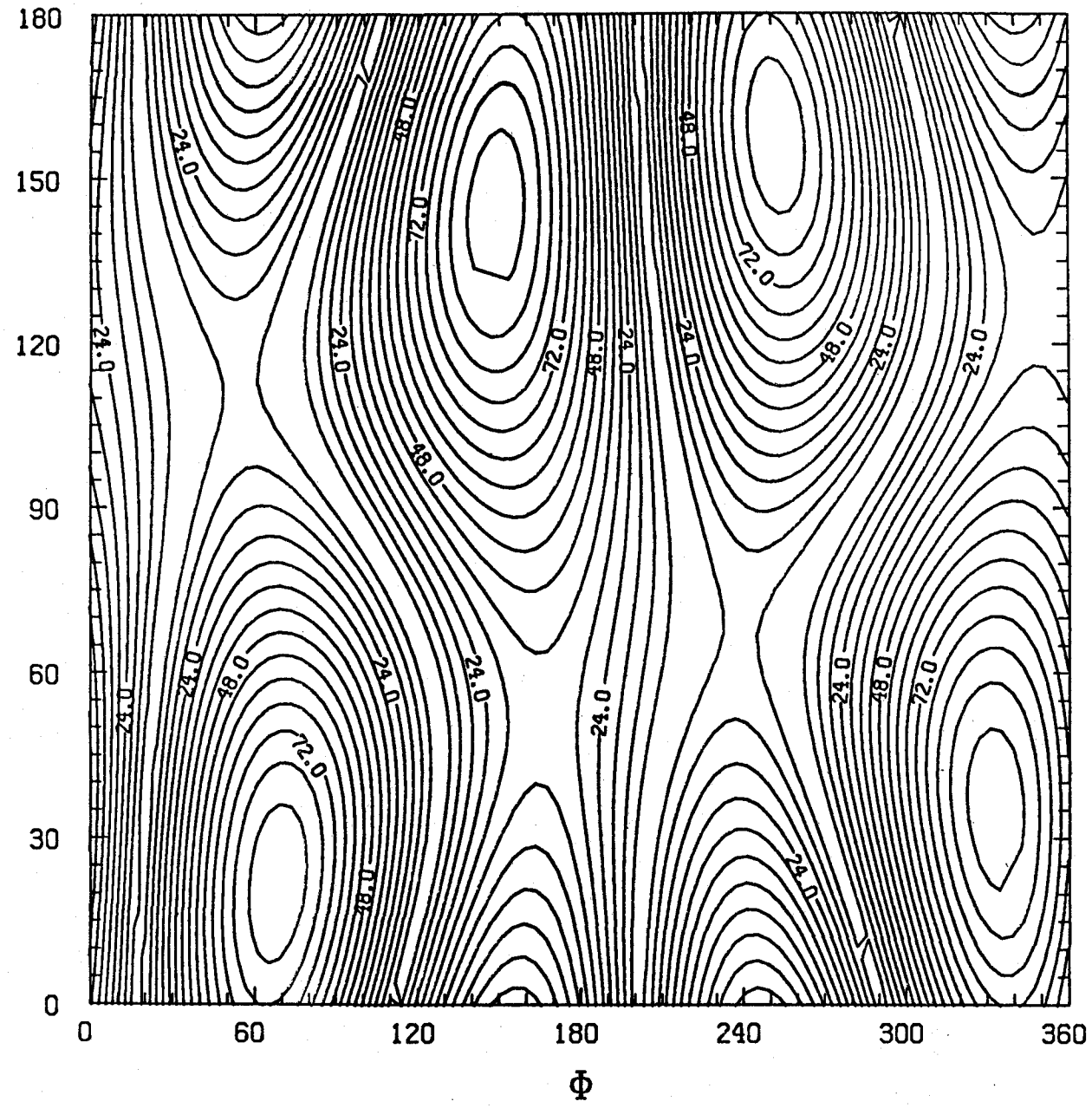

CØNTØUR FRØM 0. TØ 96.000 CØNTØUR INTERVAL ØF 6.0000 PT(3,3)= 27.300

Fig. 24(e)